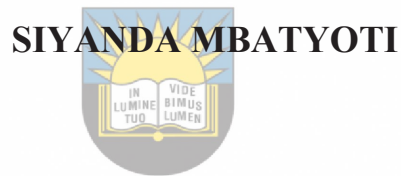




**Assessment of soil erosion based on clustered
geoinformatics approaches: a case study of
Tyume River Catchment,
Eastern Cape,
South Africa**



University of Fort Hare

A mini-dissertation submitted in partial fulfilment of the requirements for the degree of
Masters of Philosophy in Environmental Studies

SUPERVISOR: Professor P.D. Sumner

**In the
Department of Geography and Environmental Science
Faculty of Science and Agriculture
University of Fort Hare**

2022

DECLARATION

This dissertation is my work and has not previously been submitted in fulfillment of the requirement of another degree or to another university.

Signature



.....



University of Fort Hare
Together in Excellence

18/03/2022

DECLARATION ON PLAGIARISM

I, Siyanda Mbatyoti, student number 200701212, hereby declare that I am fully aware of the University of Fort Hare's policy on plagiarism, and I have taken every precaution to comply with the regulations.

Signature

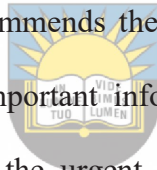


University of Fort Hare
Together in Excellence

ABSTRACT

This research centres on the holistic assessments of spatial and temporal dimensions of soil erosion zones based on the parameters of geomorphometry, hydro-statistics, and land use/cover dynamics. The study used a case study approach based on a clustered framework model of soil erosion parameters in the Tyume River basin in Eastern Cape, South Africa. The methods adopted for the investigation are, namely; non-parametric time-series assessment of streamflow dataset, semi-decadal assessment of land use/cover (LU/C) dynamics, geospatial analysis of geomorphometric variables, vulnerability analysis of soil erosion zones, regression analysis of determination coefficient, and Receiver Operating Characteristic Curve (ROC). The delineation of soil erosion zones was based on the integrated analysis of the parameters of geomorphometry, geology, hydrology, and land use/ cover. The result of the hydro-statistical analysis of the Tyume River reports a major decline in the inter-annual regime frequency of storm flow based on the Mann-Kendall (MK) test and Sen's slope assessment in 1992 (p -value = 0.031), 1997 (p -value = 0.045), 2003 (p -value = 0.021), 2008 (p -value = 0.003), and 2016 (p -value = 0.002). The MK test depicted a recurrence of peak streamflow acceleration in every three years based on low-flow and high-flow transition. The sensitivity of LU/C to temporal dynamics of streamflow trends shown by the coefficient of correlation of trends of the LU/C water bodies with streamflow semi-decadal acceleration indicates a moderately relevant relationship, $R = 0.76$. The temporal analysis of LU/C and hydro-statistical analysis shows that the Tyume basin was highly vulnerable to soil erosion by water in 1999, 2009, and 2019. The vulnerability of the Tyume River basin in 2019 is exceptional and this is due to the conversion of forested area (woodland) into a built-up environment and farmland, with a high vulnerability in 2019 due to the slump in the rate of change of woodland and precipitation, and the increase in the rate of built-up and agricultural activities. The soil erosion

vulnerability mapping divides the river basin into the critical high, high, moderate, low, non-vulnerable zones that cover 40 km², 135 km², 209 km², and 186 km² respectively. Regression analysis shows that the areas of soil erosion in the Tyume basin are moderately represented by the model ($R^2 = 56$) while the model performance assessment based on success rate and prediction rate estimation from the area under the ROC curve shows that the model is good, Area Under Curve of the ROC = 0.899, and 0.897. The analysis suggests that soil erosion is driven by the impact of land use/land cover change, particularly in areas of high drainage density. Significantly, high vegetation density played a vital role in lowering high-flow on the hill-slope and low topographic wetness area as well as in areas with erodible geologic properties. The study, therefore, recommends the advocacy of crop rotation method of agricultural practice in the highly critical areas of soil erosion and recommends the development of riparian forests around the Tyume River. The study provides important information for environmental stakeholders on degradable areas which may require the urgent implementation of sustainable development measures.



University of Fort Hare
Together in Excellence

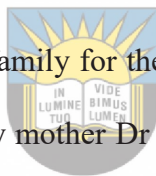
Keywords: Morphometric analysis; Land use/land cover; Hydro-statistics; River Basin; Topographic Position Index; Topographic Wetness Index; Terrain Ruggedness Index; Vector Ruggedness Measure

ACKNOWLEDGMENT

I am grateful to the Almighty God, for the grace and intellect that made me begin and see the MPhil programme to this very final stage.

My utmost gratitude goes to my supervisors, Prof. Paul Sumner and Dr Ahmed Kalumba, whose persistent encouragement, dedication, and patience made this work a possibility. Their consistent academic, moral, and logistical support throughout every stage of the programme was the major synergy that brought me this far in the work. I like to thank the entire staff of the Department of Geography and Environmental Science, for their moral and technical contribution to my advancement.

My heartfelt appreciation goes to my family for their sacrificial love and endurance through the academic journey. I am indebted to my mother Dr P Mbatyoti who invested greatly in spiritual, emotional, and financial terms into who I am today.



University of Fort Hare
Together in Excellence

I am grateful to have shared the Postgraduate experience with several other postgraduate students in the Department of Geography and Environmental Sciences, University of Fort Hare. I am particularly thankful to Dr Solomon Owolabi for his advice. I am thankful to my colleagues Lungisile Mzanywa, Noluvuyo Mzini, and Sibulele Bongoza for their encouragement during our time together in the Postgraduate laboratory. I am thankful for their moral support, assistance, and friendship.

I would like to thank the ERM and Govan Mbeki Research and Development Centre for their financial assistance.

TABLE OF CONTENTS

DECLARATION	ii
DECLARATION ON PLAGIARISM	iii
ACKNOWLEDGMENT	vi
TABLE OF CONTENTS	vii
Chapter 1: Introduction	1
1.1 Background	1
1.2 Rationale	6
1.3 Research questions	8
1.4 Specific Aim	8
1.5 Objectives	9
1.6 Research Justification and Significance	9
1.7 Dissertation structure	10
Chapter 2: A literature review	12
2.1 Introduction	12
2.2 Stages of soil erosion	13
2.3 Effects of soil erosion	15
2.4 Quantification of soil erodibility	17
2.5 Elements of soil erosion modeling	18




University of Fort Hare
Together in Excellence

2.5.1	<i>Rainfall and runoff</i>	18
2.5.2	<i>Vegetation cover</i>	19
2.5.3	<i>Agricultural practices</i>	19
2.5.4	<i>Slope gradient and Length</i>	21
2.5.5	<i>Rock-type</i>	22
2.6	Soil erosion in South Africa.....	23
2.7	Approaches for monitoring/evaluating soil erosion.....	30
2.7.1	<i>Field-based methods:</i>	30
2.7.2	<i>Computer-based method</i>	31
2.7.3	<i>Emerging computer-based approach for soil erosion vulnerability assessment</i>	34
2.7.3.1	Morphometric parameters	34
3.1	Introduction.....	40
3.2	Study area.....	40
3.3	Materials	43
3.4	Methods and Techniques adopted.....	43
3.4.1	<i>Streamflow variability assessment</i>	44
3.4.1.1	Man-Kendall test computation	45
3.4.1.2	Theil-Sen rate of change computation.....	46
3.4.2	<i>Assessment of Land use land cover change dynamics</i>	47
3.4.3	<i>Vulnerability mapping of soil erosion zones</i>	51
3.4.3.1	Geology and LU/C maps.....	52
3.4.3.2	Geomorpho-metric analysis.....	52
3.5	Overlay analysis.....	57
3.6	Validation of soil erosion vulnerability map	58
Chapter 4: Results.....		62
4.1	Introduction.....	62



University of Fort Hare
Together in Excellence

4.2	Streamflow variability trend assessment	62
4.3	Land use/land cover change dynamics	65
4.3.1	<i>The axial changes in land use/land cover spatial density</i>	65
4.3.2	<i>Rate of change across the land use/land cover spatial features</i>	67
4.3.3	<i>Land use/land cover feature trend analysis</i>	70
4.4	Vulnerability analysis of zones of soil erosion by water	71
4.4.1	<i>Hydrological characterization of Tyume River Basin</i>	72
4.4.1.1	Drainage density	72
4.4.1.2	Topographic wetness index	73
4.4.2	<i>Terrain characterization</i>	75
4.4.2.1	Topographic position index.....	75
4.4.2.2	Terrain roughness index.....	76
4.4.2.3	Vector ruggedness measure.....	77
4.4.3	<i>Geology characteristics</i>	78
4.5	Soil erosion by water vulnerability zoning	79
4.6	Validation of soil erosion vulnerability map	81
 University of Fort Hare <i>Together in Excellence</i>		
Chapter 5: Discussion		89
5.1	Introduction.....	89
5.2	Temporal variability that impacts soil erosion.....	89
5.3	Spatial variability of soil erosion	90
Chapter 6: Conclusion and Recommendations		95
References.....		100

Chapter 1: Introduction

1.1 Background

Land and water resources in South Africa have been increasingly threatened by soil erosion over the years. Not only has the ecological productivity of the soil been washed away, but the lands are also left degraded, while the hydrological functions of the soil are disrupted (Le Roux, 2015; Msadala and Basson, 2017). Research on soil erosion has been one of the core interests of the Department of Environmental Affairs and the Department of Water and Sanitation, South Africa, due to ongoing siltation of streams, streamflow reduction, pollution of water resources, and the abatement of water infrastructure functionality (Compton et al., 2010, DEA, 2015; DWS, 2017). For example, some of the major dams in South Africa such as the Welbedacht Dam, Massingir Dam, Nooitgedacht Dam, Vaalkop Dam, Olifantsnek Dam, and Mzhelele Dam have declined in capacity within the last 50 years due to sedimentation (DWS, 2017; Msadala and Basson, 2017). The sedimentation results from the process of soil erosion by water, movement of sediments, its deposition, and consolidation in reservoirs such as dams, lakes, waterways (Schellenberg et al., 2017). Soil erosion by water, therefore, impacts negatively on water security, sustainable development of the environment, and may hamper future economic development. The loss of soil fertility through soil erosion constitutes a threat to global food production. Soil erosion causes loss of important soil quality and reduces the suitability of the land for agricultural purposes and subsequently causes abandonment of the land (Pimentel, 2010). On this note, this study undertakes the integrated assessment of land degradation by soil erosion driven by water at a catchment scale.

Soil erosion is a major problem globally as it affects environmental sustainability, ecological services, and natural resource conservation (Rahman et al., 2009). Maintenance of soil profile disrupted by soil erosion is a significant aspect of environmental sustainability due to its importance to soil fertility preservation and the habitation of biodiversity. The topsoil layer accounts for 99.7% of human food production, while 0.3% comes from the ocean (Pimentel and Burgess, 2013). The rate of soil loss was noted to be twice the rate of soil formation annually (Parwada and Van Tol, 2016). Consequently, the erosion of the soil layer is a serious environmental issue.

Human interaction with environmental resources and climatic oscillation influencing the acceleration of the hydrologic cycle are the two major promoters of environmental modification (Reitsma et al., 2015). Urbanization, industrialization, and agricultural development bring out major changes in natural vegetation settings and recreation of the cultural landscape. Forest and rangeland are converted as a result of communities immigrating and rapid expansion of socio-economic activities, residential use of landscape, increase in construction activities, and the impervious area which further intensifies runoff generation (Zare et al., 2017; Gholami et al., 2019). The major challenge is that human impacts resulting in land degradation are difficult to trace on a short-term temporal and a regional scale due to the heterogeneity of topography and vegetation and obscurity by soil geologic differences. However, human impacts resulting in the stripping of vegetation paved the way for land degradation inflicted by high rainfall intensities and strong winds.

Globally, climatic cycles of events have been associated with El-Nino/Sothern Oscillation (ENSO), Arctic Oscillation, and Multi-Decadal Oscillation, among others (Meehl et al., 2016). Particularly, the entwined behaviour of atmospheric and oceanic ENSO and its association

with other climate systems, such as temperature, precipitation, and wind force, has been noted to drive the seasonal and inter-annual climate variability especially within the Mediterranean climate zone (Ashok et al., 2007; Yuan and Yang, 2012; Yang and Jiang, 2014; Capotondi et al., 2015; Wang et al., 2017; Yang et al., 2018). Empirical analysis has revealed that the semi-arid environments of developing countries are the most vulnerable to these cycles of events (Piguet et al., 2011). The long-term variability pattern of rainfall in Southern Africa has been indicated to be influenced by ENSO (Anyamba et al., 2002; Owolabi et al., 2021). Knowledge of ENSO timing, frequency, and hotspots is crucial to the understanding of the extremity of the climatic elements, such as wind and rain energy, driving land degradation.

Droplets of rain dislodge exposed soil particles from the topsoil assemblage through combined gravitational energy and hydraulic action to cause rain-splash, which is the first stage of soil erosion (Oldeman, 1997). The accumulation of the rain droplets, rain-splash, combined with sheet wash produces a rain wash phenomenon referred to as sheet erosion (Shen et al., 2016). The severity of erosion is greater with the steepness of the topographic slope, soil/geologic type, and increased extent of change of land use/cover (Pimentel, 2010). These factors highlight the reason why South African lands are vulnerable to soil erosion, considering the extremity of slope erosion across the landscape during heavy storms.

The United Nations Convention to Combat Desertification (UNCCD) noted that more than 250 million people have been directly affected by land degradation while more than one billion people are left vulnerable to this (UNCCD, 2007; Salami and Adepoju, 2012; Smith et al., 2020). About 75 billion tons of topsoil were washed away by soil erosion annually in the 1990s. More than 80,000 km² of cultivated land have lost topsoil at the rate of about 10 to 40 tons/hectare as a result of land degradation and soil erosion in the recent decade (Pimentel,

2010; Wang et al., 2016; Hladky et al., 2017). Sun et al. (2014) noted that about one-third of croplands had been eroded in the 40 years before 2012. The extent of soil erosion is more severe in a semi-arid and arid climate such as South Africa (Blair et al., 2018; Vos et al., 2019).

In South Africa, 10.9 million hectares of grazing land and 6.1 million hectares of cultivatable land have been affected by soil erosion by water in recent times (Lal et al., 1989; Boardman et al., 2017). Of the portion of the cultivatable land affected by soil erosion, 48% of it was considered by remedial, 37% of it can be terraced for other land use purposes while 15% is severely damaged and ultimately lost beyond sustainability (Lentsoane, 2006; Russell and Ward, 2016). South Africa launched a LandCare program to address the problem of unsustainable land-use practices and improve the management of natural resources (Nabben and Nduli, 2000). Landcare projects which focused on sustainable land management practices were developed through the program. The program also developed a campaign that sensitized land and environment stakeholders and farmers at the community level on the factors and practices that triggers soil erosion at a local and regional scale (Lentsoane, 2006). To ensure the success of the program, participatory monitoring, and evaluation (PM&E) processes were engaged. The effectiveness of the PM&E depends on the aptness, resolution, and simulation accuracy of the erosion model being used and the field assessment method being adopted (Hoffman and Tod, 2000). Several essential factors that must be incorporated into the approaches and models for soil erosion by water assessment are documented in the following chapter. Many of the methods developed over time for soil erosion by water modeling were either socio-economically biased or climate-insensitive.

Many climate-sensitive models based on the inclusion of hydro-meteorological parameters such as rainfall have been developed. The models include: European Soil Erosion Model

(EUROSEM) (Morgan et al., 1998; Takahashi and Das, 2014), Soil and Water Assessment Tool (SWAT) (Arnold et al., 1998; Modi et al., 2021), Universal Soil Loss Equation (USLE) (Wischmeier and Smith, 1978; Hosseini and Khaleghi, 2020), and Water Erosion Prediction Project (WEPP) (Flanagan and Nearing, 1995). USLE application is a process-oriented model for assessing soil erosion, specifically in hilly terrains. However, it was modified by improving the precision of estimation of land cover management, soil erodibility, conservation practice factor, rainfall erosivity, and the soil erosion process (Renard et al., 1991) and then referred to as the Revised Universal Soil Loss Equation (RUSLE). RUSLE has also been modified to develop the Sediment Assessment Tool for Effective Erosion Control (SATEEC) to enable the estimation of sediment deposition based on the infusion of spatial analysts for disturbed sediment delivery ratios. The development of SATEEC enabled the estimation of soil loss from rill and inter-rill erosion (Mhangara et al., 2012). However, these methods do not enable time-banded scenario assessment based on climate change and land cover alteration. The GIS-based integration of carefully selected factors influenced based on the weighted overlay and multivariate statistical classifiers can offer a more effective spatio-temporal result. Considering the influence of climate change on soil erosion, this study considers the need for the development of a time-banded holistic approach that enables the development of a scenario-based soil erosion model. Due to the significance of land use/land cover change to soil cohesion and its consequence on qualitative and quantitative assemblages of soil, there is a need to assess the temporal dynamics of human impact on catchment modification. The geomorphic and subsurface investigations are considered the fundamental approach for qualitative and quantitative assessment of soil erosion and developmental stages of landforms (Drzewiecki et al., 2014; Batista et al., 2019). Hence, multiple geomorphometry indices that

encapsulate hydrodynamic alterations, terrain roughness, and palaeogeographic layouts are considered essential for the high-precision mapping of areas vulnerable to soil erosion by water.

1.2 Rationale

Considering the rationale that soil erosion is not a once-off event, but a gradual one that may build itself along a long-term temporal scale across climate change and land cover change dynamics, a robust assessment would therefore require the infusion of trends of hydro-climatic oscillation and its contribution to land cover dynamics. Compilation of this historic degeneration can be used to characterize a watershed for soil erosion vulnerability mapping.

Soil erosion develops from episodes of soil cover displacement aided by human-intensive interaction with the land surface for extraction, production, and processing of resources. With the increase in population and urbanization, the interaction with soil cover increases due to the increase in the consumption of resources and waste generation (Montanarella et al., 2016). Globally, the natural integrity of soil resources has been compromised and are in only fair, poor, or very poor condition according to the recent United Nation report (FAO, 2015). This is primarily due to population growth and economic growth.

The most consistent and widespread human interaction with soil cover accounting for soil displacement is agriculture. Agriculture drives soil loss and land degradation through deforestation, tillage system, overgrazing, and poorly coordinated agricultural practices (Montanarella, 2015). In support of this, The Global Soil Partnership reported that arable

farming accounts for the erosion of 75 billion tonnes of soil cover every year globally (Montanarella et al., 2016).

Similarly, Mhangara et al. (2012) provided information on the historical trend of agricultural practices and other land use patterns that degenerated into the present environmental concern in the Tyume basins, Eastern Cape, South Africa. Chungag et al. (2015) explained that the communal land was degraded by stocking densities of cattle that exceed the space allotted and the uncontrolled number of grazing routines. A similar report of historical land use/ land cover effects as the primary driver of soil erosion was made about the Tsitsa (Parwada and Van Tol, 2016) and Umzintlava (Phinzi and Ngetar, 2019) catchments in proximal distance to the study area. Vanwalleghem et al. (2017) discussed extensively the impact of land use/ land cover and poor soil management in South Africa and suggest the integration of the historical variables, such as land use and climate, with and landscape information to quantify the trend of soil erosion. In the South West of Burkina Faso, de Hipt et al. (2019) based the assessment of soil erosion on the trends of land use/ land cover and climate change in the SHETRAN (Systeme Hydrologique Europeen, with sediment and solute TRANsport component) model. El Jazouli et al. (2019) conceptualized the hybridization of Sentinel 2A, Landsat OLI-8, and the Cellular Automata Markoc to forecast the Land use/ land cover trend of Middle Atlas, Morocco. Gessesse et al. (2014) modelled the trend of soil erosion and the changes in the surface runoff in Ethiopia using the Land use/land cover dynamics in the GIS interface of Soil and Water Assessment Tool (SWAT). These were combined with the Revised Universal Soil Loss equation to quantify soil loss due to water erosion from 2003 to 2030. In semi-arid Brazil, Santos et al. (2017) investigated the historical trend of slash and burn of vegetation, grazing, and rainfall-runoff events to measure the rate of soil loss. Ozsahin et al. (2018) examined the

soil erosion intensities of the Maritsa Basin in Greece using the dynamics of land use/ land cover change. Panagos et al. (2015) proposed the use of cover management factors together with some morphometric parameters, and land use historical information. In China, Wang et al. (2015) computed a National Soil Erosion Database of China using the historical information of land use/land cover, vegetation cover, and physiographic information. The uniqueness of the approach adopted here lies in selected themes and the configuration of the geomorphic layers used.

1.3 Research questions

The following questions have been considered to investigate the research problem in a bid to contribute to the existing body of knowledge on the dynamics of soil erosion:

- a) Is there any relationship between the trends of rainfall and the natural land cover change driving soil erosion?
- b) Does a correlation exist between the axial geomorphic and fluvial patterns of the Tyume landscape and the land use/ land cover change dynamics?
- c) How can the thematic layers be classified and integrated to precision to assess the trend of soil erosion by water?

1.4 Specific Aim

The research aims to present an integrated framework model of soil erosion assessment based on the analysis of land use/cover, geological factors, geomorphometric parameters, and hydro-statistical trends in the Tyume River valley.

1.5 Objectives

The work would target the following objectives;

- i. To assess the historic trend of hydro-climatic oscillation on a watershed scale and the land use/ land cover system response to this.
- ii. To assess the fluvial pattern and geomorphometry status for soil erodibility potential.
- iii. To generate a soil erosion vulnerability map based on the information drawn from geomorphometry and land use/ land cover alteration trend.

1.6 Research Justification and Significance

Several kinds of research have revealed the predominance of climate change due to ENSO in South Africa (Engelbrecht and Landman, 2016; Meehl et al., 2016; Hoell et al., 2017; Pomposi et al., 2018; Lakhraj-Govender and Grab, 2019). Hence, in an area where climate change drives frequent downpours and flash flooding, scientific information on the spatial dimension and its contribution to soil erosion by water and land degradation are required for quality decision-making. Flooding can be hazardous and can result in a major transformation in the land use/ land cover system. River flooding can induce soil erosion and result in loss of biodiversity, lives, and properties (Berendse et al., 2015). Meanwhile, studies on soil erosion through a clustered approach of climate change and geomorphological transformation of landform morphometry are few (Kumar et al., 2000; Mhangara et al., 2012; Altaf et al., 2014; Bhatt and Ahmed, 2014; Gajbhiye et al., 2014; Lei et al., 2016; Oroza et al., 2018; Radula et al., 2018; Jadidoleslam et al., 2019; Ouri et al., 2020). Hence, this research would be an important contribution to the body of knowledge.

Studies on climate change, risk, and vulnerability are limited in the Eastern Cape Province (Mhangara et al., 2012; Owolabi et al., 2021) and especially in the selected river catchment area. The area falls under regions of rural livelihood whose economic activities are water-driven (Owolabi et al., 2021). Therefore, it would make a valuable contribution to the host community by providing resourceful information for well-informed decision-making on the sensitivity of the area to flash floods which may generate riverbank erosion and vulnerability of the area to degradation.

1.7 Dissertation structure

The entire work spreads across six chapters.

Chapter 1 presents the introduction to the research scope, rationale, objectives, and justification of the dissertation.



University of Fort Hare

Chapter 2 presents the literature about soil erosion by water and the synthesis of the keywords making up the factors that link with the research idea which are soil erosion, hydro-climate, and land degradation. The topics addressed include the principles and types of erosion by water, the models used, and the conceptual framework developed in this study.

Chapter 3 provides an account of the methodology and materials used in this study. The chapter is segmented into five sections that synthesize the steps of each method. The two major applications used, hydro-statistics and geoinformatics were described in explicit detail to the aim of the study.

Chapter 4 reports the results of analyses in five distinct sections; temporal analysis of streamflow trends, semi-decadal analysis of land use/ land cover system, geomorphometric

dissection and analysis of drainage network, and total wetness index analysis and vulnerability mapping of soil erosion zones and erodibility potentials. With this, the situation report on soil erosion extent and potentials is captured for the Tyume River catchment as a case study.

Chapter 5 set out to establish a discussion on the performance of the hybrid approach of hydro-statistics and geoinformatics. The situation diagnosis, important highlights, performance of the model compared with literature, and implication of the reports to the catchment are elucidated.

Chapter 6 presents the conclusion and important highlights flagged by the study as well as the recommendation for future researches.



University of Fort Hare
Together in Excellence

Chapter 2: A literature review

2.1 Introduction

Soil erosion is a natural denudation process involving the dislodging of soil particles and their transportation from their original site and to a deposition site (Shi et al., 2012; Liu et al., 2016). The natural process is exacerbated by climate change, land use/land cover changes, and poor land management (Issaka and Ashraf, 2017). Land use/land cover changes such as urbanization, deforestation, shifting cultivation, and overgrazing have been reported for their contribution to accelerated erosion (Phinzi and Ngetar, 2019). Soil erosion takes place when hydro-climatic action (such as wind, glaciation, and runoff) on the soil surface abrades the soil. The report of the Global Assessment of Human-Induced Soil Degradation (GLASOD) on soil erosion indicated that about 2 billion ha of the total land area is affected by soil erosion. Of this 15% of erosion is driven by glacier action, 28% is caused by wind erosion while 56% of soil erosion is caused by water action (Issaka and Ashraf, 2017).

Soil erosion by water can render an environment vulnerable to environmental hazards, such as mass wasting, land subsidence, and landslides if it is not given timely attention. Soil erosion complicates natural resource management and causes ecological imbalance. It degrades the land quality for agricultural productivity and also degrades water quality for human consumption and socio-economic suitability. It can alter the land morphology to an extent whereby it becomes too weak or steep for the support and stability of terraces (Lentsoane, 2006). Soil erosion especially accelerated erosion, is a major environmental issue as it poses a threat to the socio-economic value of the land and sustainable development of natural resources. Eroded soil reduces the soil water holding capacity, renders the soil unsuitable for

arable farming (Mehri et al., 2018). Loose sediments transported from eroded soil result in the alluviation of streams, lakes, dams, and reservoirs, thereby increasing the turbidity of the water bodies, disrupting the aquatic biodiversity, and rendering the domestic water supply sterile (Van Oost et al., 2009). Human interaction not only induces soil erosion but also triggers a qualitative alteration in a land cover system such as soil acidification, nutrient leaching, and organic matter depletion (Sharma et al., 2011). Hence, soil erosion can degenerate into the loss of fertile topsoil and diminution of soil productivity (Vanwalleghem et al., 2017).

Watson and Evans (1991) classified the nature of soil erosion into geological and accelerated erosion. Geological erosion is the type due to the natural removal of soil without human influence while accelerated erosion is the type quickened by anthropogenic influence (Watson and Evans, 1991).



2.2 Stages of soil erosion

University of Fort Hare
Together in Excellence

There are four major stages of soil erosion triggered by rain-splash and rain-wash; these are the sheet, rill, gully, and bank erosion stages, although rills to gullies could be continuous and not necessarily progression. The sheet erosion stage is the stage of removal of the thin layer of the topsoil cover by the hydraulic force of raindrops and overland flow. It is a gentle form of erosion peculiar to a large area with an even slope, occurring slowly over the timescale of a rainfall event. Sheet erosion typically leads to the removal of productive topsoil. It can be recognized by the exposure of undulating light-colored soil of the subsoil on the soil surface. The eroded sheet of the topsoil is often deposited at the bottom of the slope (Balasubramanian, 2017).

The rill erosion stage is the stage of removal of soil by overland and overbank flow. Rill erosion can promote soil detachment when the energy of the hydrodynamic flow exceeds the resistance of the soil to detachment. Detachment during rill erosion continues until the overland flow energy drops below the soil's resistance (Magliulo, 2012). This stage of erosion often leads to the development of a stabilized flow channel or streamlet which may also act as a source of sediment.

The gully erosion stage indicates the mature stage of land degradation whereby the landscape becomes unstable soil due to the development of slope and sediment transport (Poesen et al., 2003). It is mainly caused by anthropogenic factors that accelerate land use/ land cover changes such as deforestation, poorly coordinated tillage system (Frankl et al., 2012), and overgrazing (Boardman et al., 2003). Poor soil erosion management such as mutilation of rainfall-runoff system in areas covered by sensitive soils, urbanisation of slope areas (Poesen et al., 2003), poor irrigation design, and overcrowding of vulnerable areas (Hassen and Bantider, 2020) have been highlighted in literature. Gully erosion leads to the formation of a distinctly carved streamflow channel with hillslope-embankment support and valley bottom by ephemeral and intermittent runoff within the channel. This stage of erosion promotes the stripping, abrasion, and removal of significant amounts of the soil layer and the creation of an unstable landform, vulnerable to environmental hazards (Mararakanye and Sumner, 2017). This was noted to have adversely affected both commercial and subsistence farmland (Mararakanye and Le Roux, 2011).

Riverbank erosion is the progressive undercutting, abrasion, exfoliation, and stripping away of a stream or river channel by the hydraulic force of streamflow and stream loads. The three main processes of bank erosion are scouring, mass failure, and slumping. Bank scour involves

the direct removal of bank materials by the shear stress of streamflow. Mass failure is the collapse of large chunks and layers of bank material as a result of the soil erosion or chemical dissolution of its cementing material (Bernatek-Jakiel and Poesen, 2018). Slumping occurs when an exfoliated layer or sheet of soil loses its firm grip on the stream wall. Bank scouring is often particular to the upper reaches of the stream where heavy stream loads abrade the stream embankment, thus, enabling shearing of the bank materials by hydraulic force. Mass wasting and slumping are particular to the lower reaches of the large streams and rivers (Xia et al., 2014).

2.3 Effects of soil erosion



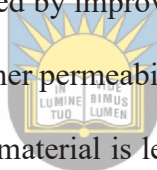
The effects of soil erosion can be grouped into two in the literature; on-site and off-site effects (Mullan, 2013). Onsite effects of soil erosion entail the disruption of the natural soil quantitative and qualitative structure, leading to loss of soil textural assemblages, fertility, cementing materials, and capacity for water retention. The disassembling of the soil aggregates and washing away of soil organic and cementing materials renders the soil vulnerable to mass wasting and slumping, thus, disrupting the soil sorting (Shi et al., 2012). Other net results of the onsite effect of soil erosion are soil acidification and salinization that results from crop damage and leaching of its nitrogen and organic content when the soil nutrients and supporting topsoil have been removed and its root exposed to dehydration (Balasubramanian, 2017). This is often common in steep slopes, areas of intense rainfall, and flash flood sites (Shi et al., 2012). On-site effects impact agricultural productivity and engineering properties of the soil. The onsite effect of soil erosion impacts agricultural productivity by eroding the soil organic

materials and disaggregation of soil structure which affects germination, growth, and yield of crops adversely (Morgan, 2009). The onsite effect of soil induces a negative impact on soil engineering properties through the removal of cementing materials, and water retention capacity which adversely affects the soil triaxial strength and causes soil to become incapable of supporting infrastructures and overlying structures (Shi et al., 2012). This constitutes an engineering problem and reduces the longevity of the overlying structures except where enough reinforcement is provided to increase the soil shear strength. The onsite effect of soil erosion is measured by taking the estimate of the average quantity of soil washed away from an area within a defined period.

Off-site problems of soil erosion occur when eroded soil particles are transported down-slope and deposited where energy is insufficient for further movement. Transportation of sediments, urban and farm chemical and organic products, and waste results in sedimentation of the streams and rivers, promotion of flooding, siltation, and pollution of water bodies (Gao and Puckett, 2012; Al-wadaey and Ziadat, 2014). Sedimentation of particles lowers the flow capacity of streams, widens flow area, and can bring pollutants that alter water quality. Transported loads of sediment can promote bank erosion, increase channel divergence, accelerate flooding risk, clogs pipes, and reduces the life span of reservoirs, and water infrastructure (Sutherland and Ziegler, 2007; Zhai et al., 2010). Off-site soil erosion problem is investigated by modelling or direct assessment of the average quantity of sediment yield and concentration of heavy chemicals in the downstream compared with that of the source (Mullan, 2013).

2.4 Quantification of soil erodibility

Quantification of soil erodibility potential and dynamics are important elements of proper land management plans. Soil erodibility is the rate of soil erosion that depends on the following factors: watershed topography, soil particle size, soil attributes, local climatic situation, land use, and environmental management practices (Zare et al., 2017). Quantification of soil erodibility is the measure of soil susceptibility to detachment. Soil erodibility depends on the mechanical attributes of the soil. While soil structure, permeability, organic and interstitial materials contribute significantly to the geometric aggregate and cohesive assemblages of soil, soil texture is the main characteristic that determines the erodibility of soil (Balasubramanian, 2017). In general, soils characterized by improved soil structure as a result of higher organic and or interstitial materials and higher permeability are highly resistant to soil erosion. Hence, soil rich in loamy or sandy loamy material is less likely to be eroded, compared to soil with higher silty, clayey, or mud-rich materials.



University of Fort Hare
Together in Excellence

Tillage in agricultural practice tends to lower soil organic matter levels and as a result, promotes soil compaction and contributes to an increase in soil erodibility. Formation of soil crusts and an increase in the total impermeable area of the soil, often promoted by chemical cement and urbanization, tend to lower infiltration and reduce soil loss from raindrop impact and splash. However, this also generates an increase in the extent of runoff which potentially poses a more serious erosion menace. Thinning, harrowing, and stumping in agricultural practices also increase the soil's potential for erodibility (Nath and Rattan, 2017). This happens when the subsurface soils which are lower in nutrient level are exposed to erosion.

2.5 Elements of soil erosion modeling

Soil erodibility potential increases when the land has no protective cover against raindrop or wind energy, hence, land conversion and poor management may expose the land to the denudation agents. Among the elements that are of significance to soil erosion in the literature are the following; rainfall and runoff, vegetation, agricultural activities, and slope gradient and length.

2.5.1 Rainfall and runoff

The intensity of soil loss depends on the size and velocity of the raindrop as well as the speed and extent of runoff over the bare soil surface. Importantly, rainfall must meet the threshold of erosivity, which is cited as the intensity equal to or more than 25mm/h within the maximum 5-min intensity and a total of at least 12.5 mm (Stocking and Elwell, 1976; Nel et al., 2010). The susceptibility of soil particles to impacts of a raindrop and faster-moving runoff depends on how fine the soil texture is (Poesen and de Vente, 2005; Magliulo, 2012). Greater impact and flow energy is required to move coarse sand and gravel particles, as well as the clays. Soil erodibility and movement are greater with high-intensity thunderstorms and short duration downpours compared to a long-duration slow-and-steady raindrop, although the amount of soil loss over time by the latter can be of a significant amount (Shen et al., 2016). Short-duration high-intensity downpours are associated with quick ponding and lower infiltration potential compared to a long-duration, steady rainfall. Intensity and potential for rainfall erosivity also vary with altitude (Nel et al., 2016). Tyume River basin is characterized by high intensity and erosive rainfall at a higher altitude and low intensity and less erosive rainfall at a lower altitude (Owolabi et al., 2021). Similarly, the streamflow of the basin is rain-

dependent, hence, the upper stage of the Tyume River basin is characterized by the energetic flow (Owolabi et al., 2021). This is capable of dislodging erodible soil cover during the high-flow session of the river at the hillslope (Pimentel and Burgess, 2013).

2.5.2 Vegetation cover

Numerous studies have established that vegetation cover serves as a major resistance to soil erosion (Mohammad and Adam, 2010; Anh et al., 2014; Sun et al., 2014, 2016; Wang et al., 2018). Vegetation reduces rainfall erosivity by decreasing the impact-energy of raindrops through the protective covering of its canopy and litter, as well as its root network which holds the soil in place and slows down runoff (Gyssels et al., 2005). The effectiveness of vegetation covering also varies with the type of vegetation both in spatial and temporal terms. The soil covering provided by the deciduous tree cannot be compared to that of shrubs, grass, and cropland due to the variation in canopy coverage which reduces the energy of rain-splash and the root system which increases water infiltration and reduces sediment run-off (Zuazo and Pleguezuelo, 2009). Vegetation degradation through irrational land use, especially in semi-arid environments, has simultaneously raised the incidence of land degradation (Kakembo, 2001; Mohammad and Adam, 2010). This, therefore, implies that changes in vegetation density can serve as useful metrics for the assessment of soil erodibility potential.

2.5.3 Agricultural practices

The susceptibility of cropland to soil erosion varies with tillage operation type, depth of tillage, direction, timing, and frequency of tillage operation. Niu et al. (2004) indicate that agricultural practices that reduce or eliminate the tillage system are not inimical to environmental sustainability. Similarly, Zhang et al. (2006) noted that tractor traffic in agricultural sites

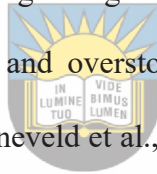
results in the formation of hardpans and a decline in water infiltration, thus, inducing tillage erosion.

Conversely, the development of a tillage system on inclined terrain has successfully mitigated soil erosion. Liu et al. (2011) provide a detailed review of various types of tillage systems and their effectiveness against soil erosion. Contour tillage was described as the simplest tillage system, suitable for less than 10° terrain slope (Liu et al., 2011). It accounts for about 65% to 75% reduction of soil erosion by water while crop yield increase by 25% (Liu et al. 2008). Basin tillage has successfully helped in on sloping terrain inclined at 20° to 30°. It accounts for a 45% to 80% reduction of soil erosion by water while crop yield was increased by more than 50% (Liu et al., 2011). Rat tunnel tillage was noted to be effective for slopes less than 5° inclination and reduces runoff, loss of topsoil, and bulk soil density significantly while crop yield was increased by 15.5%. The emergence of the no-tillage practices has been lauded for many of its potential benefits which include replenishment of soil organic matter (Abdalla et al., 2019), attenuation of climate change impacts (Müller-Nedbock et al., 2015), and decline in runoff rate (Moyo, 2017). Mchunu et al. (2011) noted that the no-tillage approach reduced soil erosion potential by 62% - 68%.

Adoption of traverse ploughing and terracing on hillslope, cross-slope cultivation, terrace farming, strip-cropping, and contour farming techniques reduces surface water ponding and limits runoff and soil movement (Liu et al., 2011). Compared to un-terraced soil, terracing minimizes the effect of soil erosion, although, not as effective as tillage methods. With an increase in slope, it is important to increase the width of terracing for effective soil erosion reduction (Mchunu et al., 2011). The application of fertilizers and manure as an agricultural

practice is also encouraged to treat topsoil removal. The practice stabilizes the soil aggregates and replenishes the soil nutrients in an excellent manner (Liu et al., 2011).

Of all the agricultural practices, overgrazing has been commonly considered as the major cause of devastating soil erosion by water (Thornes, 2007; Li et al., 2019; Sato et al., 2019). Several experimental and field investigations showed that overgrazing contributes significantly to the loss of vegetation cover, whereby loss below 30% aggravates the substantial loss of topsoil cover (Thornes, 2007). Overgrazing accelerates the compaction of soil through animal trampling and this leads to the disruption of the soil surfaces and internal profiles significant to plant nutrients, reduction of soil aeration, and the dispatch of important micro-organisms significant to vegetal growth (Osman, 2018). Inadequate livestock management, free-range practice, and overstocking in rangeland have accounted for the development of gully erosion (Sonneveld et al., 2005; Thornes, 2007; Mhangara et al., 2012; Chungag et al., 2017; Soufi et al., 2020).



University of Fort Hare
Together in Excellence

2.5.4 Slope gradient and Length

Steepness and length of slope increase the saturation and speed of runoff, and consequently, the soil erodibility potential of fine texture soils and the interstitial matrices within the drainage channels (Issaka and Ashraf, 2017). An increase in runoff speed as a function of the steepness of the slope is due to the downslope component of the force of gravity. This increases runoff accumulation, shear stress, and the energy of sediment movement in its channel. The confluence of small drainages increases streamflow strength and erodibility potential, which also increases the degree of scouring and sediment bearing potential. Areas

of complex topography are often associated with hillslope factors that accelerate runoff and lower soil moisture accumulation.

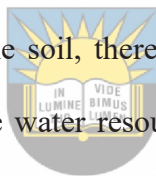
2.5.5 *Rock-type*

The intrinsic property of soil, such as the soil structure, texture, and mineral content, depends solely on the parent material, that is, the bedrock. Kakembo (2001) noted in former Ciskei in the Eastern Cape, that soils underlain by shale and mudstone in the Beaufort Group were more badly eroded than areas underlain by dolerite. Findings by Johnston (1981) reveal that soils emanating from the Ecca Group are highly dispersive and susceptible to compaction and erosion. This is mainly because the Ecca Group has higher shale content than the Beaufort Group which is partly sandy. Liggit and Fincham (1989) reported that the diamicite-dominated Dwyka Tillite revealed the highest incidence of soil erodibility. All these indicate that the potential for soil erosion varies with rock types. The variation is principally dependent on the rock fragment texture and size (Khetdan et al., 2017). For example, soil underlain by highly porous rock fragments such as coarse sandstone has higher soil moisture-holding capacity than rock fragments with very low porosity such as mudstone (Khetdan et al., 2017). The existence and extent of rock fragments or outcrops also has a negative influence on soil water infiltration and soil moisture accumulation. Several studies posited that a large mass of rock fragments has a negative consequence on soil water retention, thus, promoting soil erosion by water (Fiès et al., 2002; Baetens et al., 2009; Beckers et al., 2016). However, rock fragment cover plays an effective role as an artificial slope protection material (Jomaa et al., 2013). It functions as a surface sealing against the impact of raindrops and improves the infiltration coefficient of the soil depending on its percentage of cover and its position on the top layer (Shengqiang and Dongli, 2018). In contrast, Liu and She (2017) suggested that rock

fragment effectiveness for infiltration and runoff control and soil erosion management can be improved by applying polyacrylamide to the topsoil layer.

2.6 Soil erosion in South Africa

Over 70% of South Africa's land has been affected by various forms of soil erosion to an alarming degree (Le Roux et al., 2007). The degradation of the land is mainly due to the geology of the country which is dominated by mud-clast sedimentary terrain (Robb et al., 2006) and poor land management practices (Le Roux, 2011). The dominant fine-textured clastic sedimentary rock accounted for the development of the four problematic soil covers characterized with high soil erodibility; expansive, collapsible, soft, and dispersive soils (Diop et al., 2011). The erodibility of the soil, therefore, poses a threat to land resources where nutrient loss is initiated and to the water resource where sediment yield is aggravated and water quality integrity is compromised (Msadala et al., 2010).



University of Fort Hare
Together in Excellence

Expansive soils are the swelling soils associated with variable cubic expansivity in response to moisture temporal variation (Diop et al., 2011; Liu et al., 2020). Embankment and the exposed site and bare terrain covered by expansive soil may therefore require stabilization to prevent water-related soil erosion induced by rainwater infiltration, suction-graduation, stress-transmission, and slope failure (Farooq et al., 2020; Liu et al., 2020). Diop et al. (2011) indicated that highly expansive soils are spread across the northwest and west of the country, covering the northwestern part of the Eastern Cape, and more than half of the following provinces: Kwazulu-Natal, Free State, Gauteng, Mpumalanga, and Northwest Province. Medium expansive soil covered more than three-quarters of the Eastern Cape, the entire two-fifth of Free State, the south and southeastern half of Northern Cape, and the entire northeast

of Western Cape (Diop et al., 2011). Diop et al.'s (2011) findings indicate that expansive soils were products of weathering of the argillaceous rock units of the Karoo Supergroup, such as the shale and mudstone of Beaufort, Dwyka, and Eccca Group.

Collapsible soils are problematic soils whose aggregate structural strength is disturbed by changes in volume as a response to low in-situ moisture content (Vandanapu et al., 2019). They are often found in association with granite, hence, in South Africa, they are localized in the extreme northeast covering less than the one-quarter landmass of Limpopo and Mpumalanga provinces.

Soft clays are texturally fine soils characterized by low shear strength and high compatibility (Lema et al., 2019). Susceptibility of soft clays to soil erosion is triggered by their differential response to dissolution on account of the heterogeneous distribution of sand and gravel lenses within their matrices and their sensitivity to moisture. Their erosion is accelerated when the exposed soft and non-resistive parts get washed off leaving the hanging walls unstable and vulnerable to failure once the external weight is added (Sachs and Sarah, 2017). Soft clays are abundantly localized at the eastern and southern coastal areas along river channels especially in numerous depositional environments, while inland occurrence is quite scanty in South Africa (Diop et al., 2011).

Dispersive soils are soils with a high proportion of clay containing low Soil Organic Carbon and high Exchangeable Sodium Percentage with their platelet aggregate assembled in a parallel arrangement (Parwada and Van Tol, 2016; Bernatek-Jakiel and Poesen, 2018). These properties are exhibited by Montmorillonite and Illite. Dispersive soils are eroded by water as a result of the transcendence of clay particles repulsive-force above their Van der Waal force

that influences its adhesion (Bennett et al., 2016; Wilson et al., 2016). The underlying factor for the repulsion between the clay layer is the percentage index of absorbed Sodium-ion on the clay surface (Wilson et al., 2016). In South Africa, dispersive soils are components of weathered argillaceous rocks of the Cape Supergroup, granite residual soil, Uitenhage group, and Karoo Supergroup. Elges (1985) indicated that the dispersive soil is concentrated at the coastal plateau of the Cape and Karoo Supergroup. The dispersive soils were mapped to be concentrated in the Beaufort Group of Bloemfontein, while few occurrences were noted in the KwaZulu-Natal Province (Diop et al., 2011). Overall, Diop et al. (2011) showed that the problematic soils not only resulted in acceleration of soil erosion by water and land degradation but that they constitute detrimental impacts on environmental stability and structures erected on them.



On this basis, a regional soil erosion distribution analysis undertaken using Spot 5 satellite imagery revealed that the Eastern Cape, Kwa-Zulu Natal, and the Limpopo Provinces are the most degraded areas in South Africa (Le Roux and Sumner, 2012). Mararakanye and Le Roux (2012) adopted the digitization approach on SPOT 5 imagery to map areas of gully features (Figure 2.1 and Figure 2.2). The result reveals that Eastern Cape ranks highest (161,517 ha) as the Province with the most erosion on account of land areas covered with gullies. The assessment further revealed that 4.3% of the areas suitable for cultivation have been morphogenetically altered by the development of gullies. The major setback in the assessment is the inability to discern between gullies and diminutive stream channels. Due to the untimeliness associated with the manual digitization of SPOT 5, Mararakanye and Nethengwe (2012) harnessed the aptness associated with the use of Geographic Object-Based Image Analysis

(GEOBIA) for easy extraction of gullies. The approach resulted in an overall classification accuracy of 76.33%.

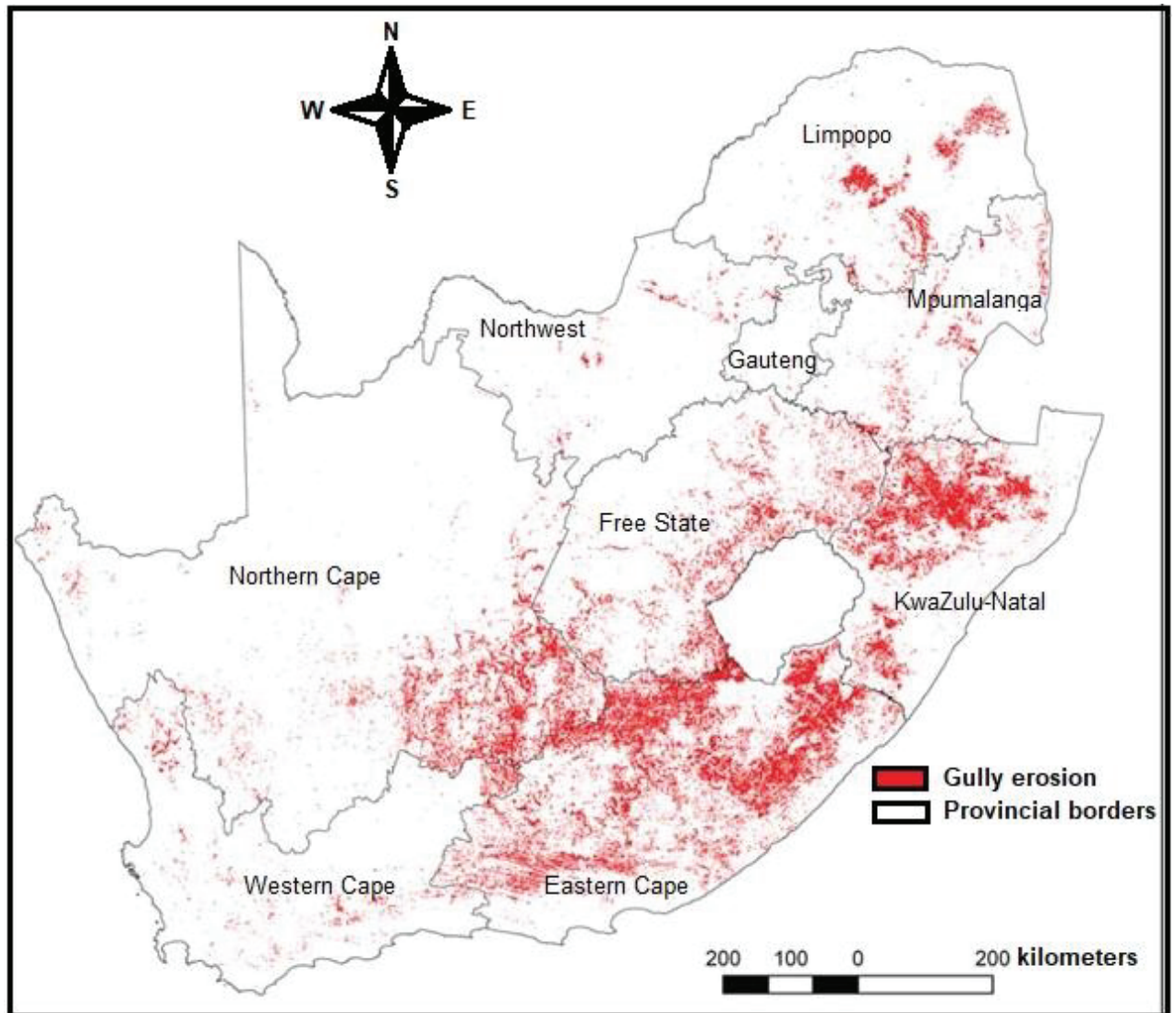


Figure 2.1 The distribution of gully erosion across South Africa (Source; Mararakanye and Le Roux, 2012).

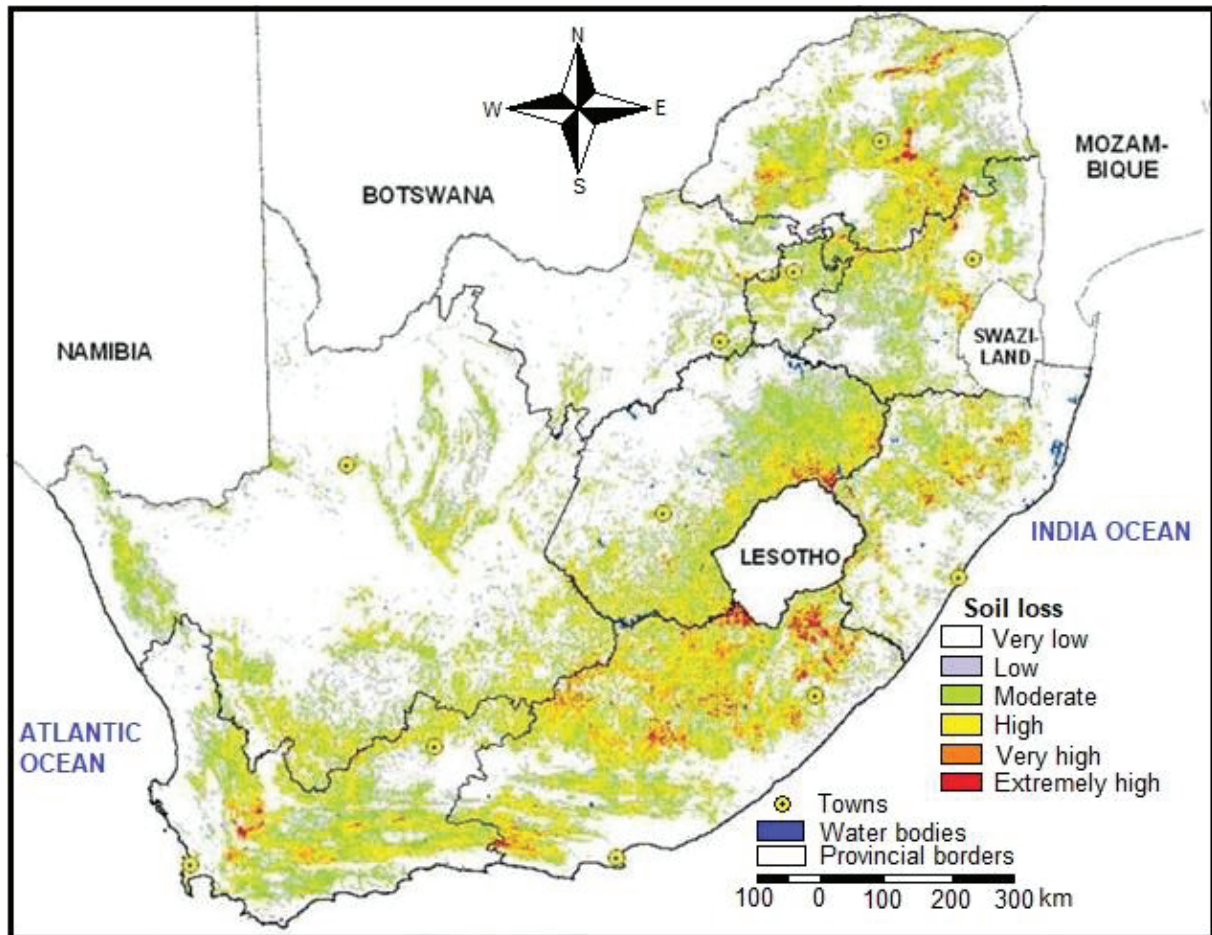
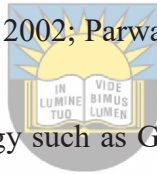


Figure 2.2 The distribution of sheet and rill erosion across South Africa (Source; Mararakanye and Le Roux, 2012).

Parwada and Van Tol (2016) examined the nature of soil erosion on a reduced scale, considering the insensitivity of large spatial scale investigation to site-specific properties that may influence soil erosion. In their findings, Parwada and Van Tol (2016) noted that deforestation and a decline in vegetation cover rank high among the factors accounting for a high rate of soil loss. South African soils have very low soil organic carbon, such that less than 5% of soil cover meets the threshold of 2% organic carbon, thus, making the soil prone to structural destabilization where there is overgrazing (Janzen et al., 1997; Du Preez and Brown, 2011). Further, an important discovery is the sensitivity of duplex soil to soil erosion

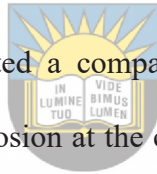
(Parwada and Van Tol, 2016). Duplex soil is an advanced dispersive soil, defined by textural contrast between two horizons, whereby the soils of horizon B are more compacted or sealed with clay underneath the soil of horizon A (Cox and Pitman, 2002). This was noted to be distributed in a non-distinct manner, covering more than 80% of the South Africa soils, and 90% of the Eastern Cape (Fey and Gilkes, 2010). The proneness of duplex soils to soil erosion by water is mainly because of the horizon B, which is clay-rich is characterized by very low hydraulic properties and a high concentration of exchangeable sodium (Fey and Gilkes, 2010). These attributes, therefore, result in reduced suction-head and ponding of water from when the infiltration rate exceeds the suction rate at the surface. Hence, duplex soils are prone to desiccation, waterlogging, crusting, and salinity, thus raising the soil vulnerability to soil erosion by water (Cox and Pitman, 2002; Parwada and Van Tol, 2016).



The advent of geospatial technology such as GIS and remotely sensed imagery has enabled efficient mapping of soil erosion and quantification of land degradation. Following the regional mapping of the gully, rill, and sheet erosion shown in Figures 2.1 and 2.2, Le Roux and Sumner (2012) developed a GIS-based integrated approach for mapping continuous and discontinuous gullies. These were based on the following outlined factors: slope, upslope contributing area, topographic wetness index, sediment transport capacity index, terrain unit, geology type, land type, soil erodibility factor, soil depth, land use, and vegetation cover (Le Roux and Sumner, 2012).

Pandey et al. (2016) developed a monitoring protocol for predicting the evolution and vulnerability of landmass to soil erosion. The investigation engaged a time series analysis of high-resolution aerial photography captured between 1937 and 2009. Singh et al. (2014) reported that the manifestation of erosional features was consistent in the timeline in areas

where there is no vegetation cover. Areas devoid of lateral erosional features growth are linked with high vegetation density, predominated by canopy trees, while areas covered by shrubs are associated with peripheral erosion. Mararakanye and Sumner (2017) integrate a statistical approach that quantifies the temporal influence of biophysical actors in gully development with GIS and remote sensing approach for delineation of spatial scale of the contributing factors. The hybrid approach of information value statistical assessment and digital processing of aerial photographs reveals the development of gully features on soils underlain by colluvium and alluvial deposits. The confluence for drainage, associated with high soil moisture was also reported to be associated with widespread gullies. Areas of weathered granite, gneiss and ultramafic rocks were also associated with gully features.



Phinzi and Ngetar (2019) presented a comparative assessment of vegetation indices for mapping the distribution of soil erosion at the central Umzimvubu Local Municipality. This was achieved using Landsat 8 Operation Land Imager (OLI) as the main data, and SPOT6/7 and Google Earth as ancillary. The vegetation indices employed include the Normalised Difference Vegetation Index (NDVI), Soil Adjusted Vegetation Index (SAVI), and Soil-and-Atmospherically Resistance Vegetation Index (SARVI). The assessment indicated that the SAVI approach proved to be a better estimator based on the result of the error matrix, and confusion matrix, although kappa statistics yielded a moderate agreement (64%). Owing to the resolution of Landsat 8 OLI and the reflectance similitude of soil erosion and non-erosion features, an exception is taken concerning the detection of minor erosion. Phinzi and Ngetar (2019) therefore recommend the conjunctive analysis of spectral and textural information with the aid of object-based image classification.

2.7 Approaches for monitoring/evaluating soil erosion

Several approaches have been employed for monitoring/ evaluating the soil vulnerability to soil erosion by water. These can be grouped into two, namely, field-based methods and computer-based methods.

2.7.1 *Field-based methods:*

It is a traditional approach involving the physical visitation of the site for measurement of the severity of erosion. The method is laborious and spatiotemporally limited in extent (Gillan et al., 2016). The method is divided into three approaches; plot-based methods, point-based methods, and radiometric dating techniques.



The plot-based method is a traditional method of soil erosion assessment based on runoff plots. Runoff plots are defined for hydrologic drainage sizes from unit hydrologic basin to a primary catchment and water management size, depending on the landscape geomorphology and erosional process (Boix-Fayos et al., 2006). It is based on the assessment of erosional impact through redirection of flow from rill and gully channels through weirs in the field. The assessment is based on two assumptions; a) the effect of raindrops is considered negligible; and b) rill and gully are considered the only erosional channels (Evans, 2002). The plot-based method is associated with three main limitations: a) the installation of the weirs results in the alteration of flow gradient, recreation of natural boundaries, and human disturbance that tend to alter the true field result and as a consequence, raises the data uncertainty; b) the laborious process associated with the removal and transportation of weirs and other experimental

gadgets makes long-term studies impossible; and c) it provides limited information on catchment heterogeneity (Boix-Fayos et al., 2006).

The pin-based method is based on the assessment of the rate of soil loss at a defined length using objects installed in the erosion path. Objects often used include pins in the form of a “T” shape, paint collars that are usually longstanding features such as boulders or trees, and pedestals with bottle caps (Stroosnijder, 2005). Assessment of soil loss is carried out by measuring the difference in marked spot height of the pin to the new ground height where erosion reduced the soil level to. The method is simple, inexpensive, and enables the coverage of a large number of points (Hudson, 1993). However, it is time-consuming while the measuring pins are subject to disturbance by animals or human interference (Hudson, 1993).

The radiometric dating technique is based on the assessment of the variation in the amount of Caesium-137 isotope present in the soil. The use of Caesium-137 isotope is a sediment fingerprinting approach used to differentiate between surface and sub-surface sediments. It has proven reliable both in spatial and temporal terms (Soto and Navas, 2008). The application of Caesium-137 is based on the assumption that the isotope has a consistent relationship with the soil and as a result, a measure of its depletion can provide information on soil loss (Walling and Quine, 1992).

2.7.2 Computer-based method

This is based on the modelling of catchment processes and field erosional events with the aid of a computer program. This includes the use of a geographic information system, soil and water assessment tool, and the soil loss equation.

The geographic information system has enabled the mapping and modelling of complex and heterogeneous soil erosion and catchment processes with ease at temporal and spatial scales. Methods such as the Universal Soil Loss Equation (USLE), Revised Universal Soil Loss equation (RUSLE), and Modified Universal Soil Loss equation (MUSLE) have been developed. The method has evolved and has enabled the modelling of both surface and subsurface erosion processes. Inputs such as climate data, land use/ land cover data, and digital elevation models are the major requirement of the simulator (Jain et al., 2005). The main limitations associated with this method include over-simplification of processes, lack of user-friendliness, large data requirement, and underestimation of soil losses in gullies (Van Zyl, 2007; Devia et al., 2015).



The Soil and Water Assessment Tool (SWAT) is a river basin continuous-time model used for assessing the land management contribution to soil loss, sediment, and chemical yield in soil erosion modelling (Gassman et al., 2007). The model enables the simulation of multiple scenarios within a watershed. It makes use of water balance, soil water, and sediment yield equations in its estimations. The main requirements for SWAT models are the digital elevation model, land use/ land cover data, soil characteristics, daily rainfall, and daily temperature. The program also integrates eco-hydrological processes such as water and land use management, water flow, nutrient transport, and vegetation growth processes using a regression equation (Ullrich and Volk, 2009).

Other types of the computer-based model include the Water Erosion Prediction Project (WEPP), Areal Non-point Source Watershed Environment Response Simulation (ANSWERS), Soil Loss Estimation Model for South Africa (SLEMSA), Erosion Potential Method (EPM), Modified Pacific Southwest Inter-Agency Committee (MPsiac), and

Chemicals Runoff and Erosion from Agricultural Management Systems (CREAMS). From the perspective of land degradation, integrated approaches involving the use of mathematical models, statistical models, cellular models, agent-based models, system models, and evolutionary models have been used to weigh the chances of change in land use/ land cover. From the flood potential assessment perspective, statistical analysis of rainfall frequency, hydrologic unit flood routing, and morphometric analysis have been engaged.

Sediment Assessment Tool for Effective Erosion Control (SATEEC), a modified version of RUSLE, based on the incorporation of sediment delivery ratios estimator was employed in the map and estimate soil loss in the study area (Mhangara et al., 2012). Mhangara et al. (2012) noted that the approach achieved an overall accuracy of 79.1%, a Khat measure of 54.8%, a Z score of 4.129, and a p-value less than 0.001, which were concluded to be inaccurate. However, the analysis noted that the negative impact of land use/land cover change, agricultural site abandonment, uncoordinated farming, and activities on highly erodible soils are responsible for soil loss in the area. Meanwhile, the essence of stringent conservation practices for the reduction of soil loss to water erosion recognized was lauded to be effective for soil management (Mhangara et al., 2012).

Breetzke et al. (2013) presented a comparative assessment of USLE and SLEMSA for estimation of soil loss rate as a function of a specific land use type in a quaternary catchment in KwaZulu-Natal, South Africa. The study indicated that SLEMSA is a better estimator in a poorly managed ecological site while USLE performed better in a cultivated land use type. Through overlay analysis, USLE highlighted that high soil loss rates were due to crop management factors while SLEMSA highlighted the influence of topography (Breetzke et al.,

2013). Moreover, high sensitivity to variation in slope steepness was shown by SLEMSA show while USLE showed sensitivity to canopy cover and crop effects.

2.7.3 Emerging computer-based approach for soil erosion vulnerability assessment

Vulnerability mapping involving the integration of temporal trends of land use/ land cover map with morphometric analysis and topographic wetness index map appears as an emerging GIS approach for identifying areas of potential erosional features (Singh et al., 2014). Supervised classification of a land cover system based on pixel tone regrouping has enabled the classification of imagery through the selection of a suitable algorithm. The most common classifier for land use/ land cover mapping is maximum likelihood whose algorithm is based on the Gaussian estimate of its probability density function for a selected class of feature (Lambin, 1997; Leh et al., 2013). The success rate of temporal analysis of land use/ land cover mapping using the maximum likelihood classifier for modeling of soil erosion has been proven in the literature (Zelege and Hurni, 2001; Leh et al., 2013).

2.7.3.1 Morphometric parameters

An increase in awareness of the watershed management against hazardous geomorphic processes, such as floods, water resource contamination, and mass waste, has advanced the study of morphometric characteristics such that it is presently adapted to soil erosion analysis (Bhatt and Ahmed, 2014). Morphometrics involves the calculation of morphometric parameters associated with various drainage characteristics to inform on the influence of lithology, climate, and sustainable development procedure on the status of the hydrologic unit (Kumar et al., 2000). The application of morphometric analysis has been combined with land use/ land cover mapping for multi-criterial analysis of soil erosion by Altaf et al. (2014).

Gajbhiye et al. (2014) employed the eight parameters of morphometric analyses to prioritize areas prone to soil erosion in 14 sub-watersheds. Their investigation provided results that agree with the lithological variation. Also, Hlaing et al. (2008) indicated that the variability across the morphometric parameters (MP) is influenced by soil surface condition, and the soil thickness relative to the bedrock. The runoff production and fluid/ moisture transfer function are specifically controlled by terrain information (Jadidoleslam et al., 2019). This is because soil loss has shown a significant relationship with the areas of active runoff production, contribution at the outlet, and the interconnectedness of the runoff influencing areas. Terrain information derived from MPs such as drainage density, topographic wetness index, terrain ruggedness index, topographic position index, and vector ruggedness measure has significantly provided soil surface condition changes due to runoff and soil erosion by water. MP information has been proven to indicate soil infiltration proneness, aspect relationship with flow velocity, terrain ruggedness to the energy of raindrop, and the potential for soil detachment (Jadidoleslam et al., 2019; Ouri et al., 2020). MPs are deduced through digital processing and empirical computation of remote sensing data.

The topographic wetness index (TWI) has served as a useful metric for describing the influence of hillslope factors on soil water transport and soil moisture accumulation (Cassidy et al., 2017). TWI relationship with soil cover and soil moisture indices have also been noted in the literature (Lei et al., 2016; Oroza et al., 2018; Radula et al., 2018). Enrichment of the soil with organic matter has been identified as one of the main soil stabilizers against soil erosion. Similarly, Pei et al. (2010) revealed that multiple-flow direction on based TWI is a strong quantitative indicator of soil moisture as the study reports a very strong correlation with

soil organic matter. This information accounted for the adaptation of TWI in TOPMODEL developed in the early 1990s for simulation of areas of potential soil erosion.

The terrain ruggedness index (TRI) serves as a derivative for the two-dimensional variation in relief across a given area (Riley et al., 1999). It has provided soil surface roughness information that shows a significant correlation with the acceleration potential of overland flow, surface depression storage, and infiltration potential (Yang and Chu, 2015). TRI plot enables the delineation of the unique landforms such as heaps, ridges, head scarps, col, pass, and valleys relative to topographic subsidence induced by extreme geologic activities such as orogeny, volcanicity, rifting, and tectonic activities (Amatulli et al., 2020). Areas with high TRI are characterized by a high potential for overland flow which can trigger soil loss while the areas with low TRI are associated with high infiltration potential.



Topographic position index (TPI) has been proven to indicate the impact of relative displacement of runoff-contributing areas within a watershed through calibration of terrain hyperspectral aggregation or dispersion through the computation of the backscattering coefficient of DEM (Schmidt and Hewitt, 2004; Neteler and Mitasova, 2013). TPI is based on the variability in slope in a specific flow line. Areas of aggregated terrain curvature are indicated by high concavity (high TPI) and could therefore induce high runoff while the areas with dispersed terrain hyperspectral response produce high terrain convexity and could therefore exhibit flow/ moisture transfer function (Jennes, 2006; Amatulli et al., 2020). These metrics are thus important for the measurement of erodibility and soil deposition tendency.

Vector ruggedness measure (VRM) has provided three-dimensional geospatial information on slope curvature and gradient. VRM provides a conjunctive summation of slope and aspect

heterogeneity through the creation of holographic dispersion of vector normal to the planar aspect on a landscape (Sappington et al., 2007). VRM deduction enables the identification of relative positions of geomorphic incision produced by gravity, soil surface condition, and hydrographic network (Smith, 2014). VRM metrics have enabled the calibration of geomorphic pathways controlling hydrologic flow, flow velocity, and flow accumulation which are relative to the flow/ moisture transfer function between the terrain surface and the vadose zones (Bogaart and Troch, 2006; Amatulli et al., 2020). VRM is therefore significant for the analysis of hydrologic variation between overland flow and through-flow. Areas of high VRM area are therefore associated with the potential for runoff production and acceleration of soil loss while areas of low VRM are associated with the potential for through-flow and baseflow.



Many researchers have engaged with the integration of morphometric parameters and other important environmental variables such as land use/land cover assessment to model the landscape ruggedness and the environment for its vulnerability to soil erosion by water (Sappington et al., 2007; Gruber et al., 2019; Amatulli et al., 2020; Arabameri et al., 2020; Bosino et al., 2020; Sadhasivam et al., 2020). In doing so, Bosino et al. (2020) used 13 morphometric parameters together with the normalized difference vegetation index to assess the terrain proneness and the environmental predictors of soil erosion by water. Also, Sadhasivam et al. (2020) adopted 13 morphometric parameters to investigate areas sensitive to soil erosion by water. The approach engages the same MPs as Bosino et al. (2020) and these include drainage density, mean bifurcation ratio, stream frequency, texture ratio, length of overland flow, infiltration number, form factor, circularity ratio, elongation ratio, relief ratio, ruggedness number, relative relief, and watershed mean slope. These were computed from the

Terra Synthetic Aperture Radar X-band add-on for digital elevation models while their standardized weightage was determined using an analytical hierarchical process. The outcome ranked the most significant MPs in the following order of priority as thus; watershed mean slope, stream frequency, ruggedness number, and the relative relief. Arabameri et al. (2020) convolved the morphometric parameters for their linear dimension, relief, and shape using Advanced Land-Observing Satellite, Phased-array L-type synthetic-aperture radar, and DEM generated from Interferometric synthetic aperture radar for analysis of soil erosion susceptibility. Their results ranked relief characteristics, terrain geometry, morpho-tectonic parameters, and hydrographic network textures high as the dominant factors driving soil erosion by water. Gruber et al. (2019) employed the Random forest classification to determine the order of morphometric parameters that exhibit terrain stability similar to their parent rocks and to train classifiers for modelling of parent rock dispersivity. The analysis indicated that the combination of VRM and TRI can provide reliable results on areas of high resistance and proneness to soil erosion by water. Generally, most morphometric parameter approaches in the previous analysis were based on a mathematical model. The few cases where GIS-based morphometric parameters were adopted were in landslide and groundwater potential zone analyses. To the knowledge of the researchers, no work has developed an integrated approach involving the themes of TPI, TRI, VRM, TWI, LU/C, drainage density, and geology.

The novelty in this study lies in the holistic combination of themes of hydrologic, geomorphic, and environmental themes to assess the vulnerability of watershed to soil erosion by water. The mapping of watershed vulnerability to soil erosion by water based on the clustered analysis of TPI, TRI, VRM, TWI, drainage density, LU/C, and geology using a weighted overlay geostatistical classifier is new regionally. The conceptual approach presented here is

budget-friendly, time-effective, effortless, and valuable where there is a paucity of data. More so, the analysis of the semi-decadal trend of LU/C and its relationship with the streamflow time series set out to provide profound information on environmental practices contributing to soil erosion by water. The conventional approach of LU/C usually involves the assessment of the decadal change rate. In this study, a comparative analysis of LU/LC trends with streamflow dynamics, the axial assessment of LU/LC dynamics, and the spatial assessments of soil erosion susceptibility trends in the Tyume basin were unique gaps covered.



University of Fort Hare
Together in Excellence

Chapter 3: Study Area and Methods

3.1 Introduction

This chapter outlines the materials and analytic procedures engaged in deciphering the trends of storm-flow that may aggravate soil erosion by water. The analytic parameters are largely focused on the assessment of long-term streamflow amplitudes, changes in vegetal grades, and morphogenetic alteration. The chapter presents the hydro-statistical estimation for flood analysis, geoinformatics approach for land cover change assessment, wetness index assessment, and morphometric analysis. This enables a thorough comparative analysis of sub-basins vulnerable to soil erosion by water and also sets the track for emerging research paths for land degradation and soil erosion by water.



3.2 Study area

The study area is the Tyume River catchment, spanning an estimated area of 642.37 km² and an altitudinal range of 308 - 1826 m.a.s.l. (Figure 3.1). It is geographically situated within latitude 32° 32' S and 32° 54' S and longitude 26° 45' E and 27° 00' E. The climatic situation has a mean annual temperature and precipitation value of 11° to 18°C and 450 – 600 mm (Owolabi et al., 2021).

The catchment is drained by the Tyume River, 75 km long, which runs in a southward direction from the Hogsback State Forest, through the town of Alice and several rural settlements to Manqulweni community where it confluences with Keiskamma River. The Tyume drainage is impounded by the Binfield Dam, for surface water supply to neighbouring communities.

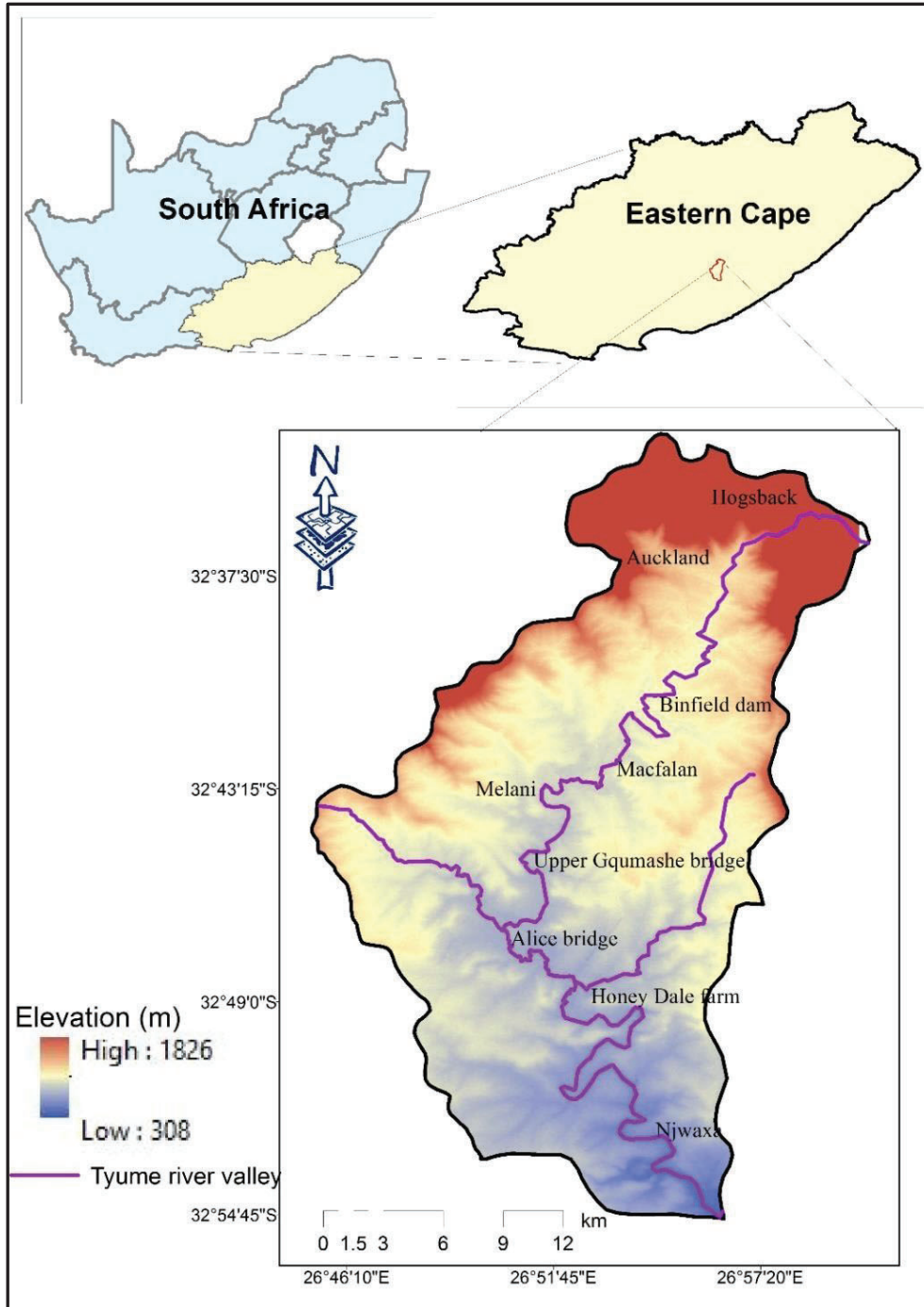


Figure 3.1 Map of the Tyume River basin showing the main river valley and elevation.

Landforms in the Tyume basin can be classified into two; the sub-range hilly terrain at the extreme north which connects to the major escarpment that runs across Auckland and

Hogsback and flanking the west-northwest-north-northeast-east, and the pediplain that graduates to the foot hill in the south (Dijkshoorn et al., 2008). The catchment covers three main geological formations; Katberg, Balfour, and Middleton Formations, of the great Karoo Supergroup (Owolabi et al., 2020). Each of the formations comprises varying sections of sandstone and mudstone lithosomes (Oghenekome, 2012).

The dominant soil fractions are the Calcic Vertsols at the north, the Calcaric Regosols at the centre, and coarse deposits at the south (Dijkshoorn et al., 2008). The natural vegetation of the area is classified into three major biomes; the dense forest (north extreme at Hogsback), savanna (centre to the west), and the tropical thicket (centre to the east and south).

Historical information about the settlement within the Tyume basin emerged after the Frontier wars between the indigenous Xhosa and their colonial dictators in 1835 - 1878 (Hebinck et al., 2018). The war began when the indigenous dwellers were forcefully driven away from their land and homestead to make space for white farmers by the colonial dictators (Mills and Wilson, 1952). In 1899, the land across the basins was delimited between various tribal zones, residential areas, rangeland, and farmlands by the colonial administrators (Hebinck and Smith, 2007). In 1981, the land tenancy was restored to the indigenous tribal authorities when the basin was constituted as part of the Ciskei homeland (Hebinck et al., 2018). Following the land allocation and reform, the townships within the basin emerged from the nucleated communal settlements and clustering of the villages.


The land use and land cover features within the basin during the early settlement periods were dominated by forest plantation in the Amatola mountain range, grazing, grain, and vegetable farming (Hebinck and Smith, 2007). The hilltops and valley-floors of the basin at the north

notably served as communal rangeland for pastures while arable farming which commonly comprises of maize and sorghum cultivation was done at proximal layouts to the rivers (Mostert, 1992). At present, there has been economic diversification from ruralized “agrarian” income to an urbanized “deagrarian” income (Masterson, 2016) while agriculture is the mainstay of the economy despite the decades of overgrazing, deforestation, and the inadequate land management (Mhangara et al., 2012). These factors rank high among the main drivers of soil erosion by water and environmental concerns requiring immediate attention.

3.3 Materials

For this purpose, the materials used in the study are highlighted below:

- Long-term daily streamflow data ranging from 1 January 1979 to 31 December 2018.
- Multispectral Scanner (MSS) Collection 1, and 4 – 5 for winter months from 1984 to 2009.
- Landsat 8 Operation Land Imager (OLI) for the winter months from 2013 to 2019.
- Shuttle Radar Topographic Mission (SRTM) Digital Elevation Model (DEM) with 30 m by 30 m resolution.


University of Fort Hare
Together in Excellence

The software used for data processing includes MS-Excel version 2013, Envi 5.4, ArcGIS 10.3.1, and plugins such as XLStat, Arcmap 10.3.1, ArcHydro 10.3.1, and Hec-GeoHMS 10.3.1.

3.4 Methods and Techniques adopted

The study adopts the following methods;

- a. Statistical analysis of long-term streamflow trends;

- b. Analysis of land use/ land cover change;
- c. Morphometric analysis;
- d. Topographic wetness index analysis for basins, and;
- e. Vulnerability analysis.

3.4.1 Streamflow variability assessment

Following the collation of daily streamflow data, 1 January 1979 to 31 December 2018, from the Department of Water Affairs and Sanitation, the annual data set was queried for missing records to assess its conformity of less than 3% missing records per annum for hydrological analysis (Mishra and Singh, 2010). Previous work has also demonstrated that about 30 to 40 years of long-term data is required for trends and variability analysis for climate change study (Henson et al., 2016). The collated data agrees with the requirement, however, the missing streamflow records were corrected by extrapolating relative mean values of relative date in other annual records with similar trends. The missing records across the streamflow data, in general, are less than 0.001%. The refined daily streamflow data were computed into a monthly streamflow data series, for each annual record.

The streamflow time-series was plotted on a line graph to deduce its inter-annual linear regression. The baseline assessment of storm-flow and flood history was achieved through a non-parametric assessment of the trend of the response of streamflow using the Mann-Kendall (MK) test and Theil-Sen's slope (TS) assessment. Twain tests of MK and TS were carried out using XLSTAT plug-in for Microsoft excel package. The results from the assessment were plotted such the length of the bar indicates the rate of change of streamflow trend (Sen's slope)

while the direction of the bar indicates the either on the increasing or decreasing side (Mann-Kendall test), meanwhile the year of significant response is indicated with a deeper colour.

3.4.1.1 Man-Kendall test computation

MK computation is defined using equation (1.1), based on Mann (1945), Kendall (1975), and Yue et al. (2002):

$$S = \sum_{k=1}^{n-1} \sum_{j=k+1}^n \text{sgn}(X_j - X_k) \quad (1.1)$$

Where X_k is the Tyume streamflow data series for the annual record based on the length k ;

X_k which is defined by the rank $k = 1, 2, 3, \dots, n-1$;

X_j , which is also defined by the rank $j = k + 1, 2, 3, 4, \dots, n$.

n is the 12 month of the year.

Each data point of X_k is compared with the rest of the data point X_j using the conditional statement in equation (1.2):

$$\text{sgn}(X_j - X_k) = \begin{cases} 1 & \text{if } X_j - X_k > 0 \\ 0 & \text{if } X_j - X_k = 0, \\ -1 & \text{if } X_j - X_k < 0 \end{cases} \quad (1.2)$$

Where the difference between X_j and X_k represents the monthly values in months k and j ($j > k$) respectively. MK assumes that the measurement over time is independent and identically distributed when a trend is absent, that is, the observation obtained represents the true conditions at the sampling time (Kisi and Ay, 2014; Pohlert, 2016). For such a condition, where statistic ‘S’ is normally distributed with the mean and $E(S)$ becoming zero, the number of observations must exceed 10 (Kendall, 1975; Asfaw et al., 2018). The variance statistics are derived using equation (1.3):

$$\text{Var}(S) = \frac{\{n(n-1)(2n+5) - \sum_{q=1}^p q_k(q_k-1)(2q_k+5)\}}{18} \quad (1.3)$$

Where n is the number of observations, p is the number of the tied groups in the data set and q_k is the number of data points in the k th tied group. The significance of the trend is tested by comparing the Z -transformation in equation (1.4) with the standard normal variate at a designated significant level α where the computation of unity in Z -transformation is a continuity correction (Kendall, 1975; Hamed, 2008):

$$Z = \begin{cases} \frac{S-1}{\sigma} & \text{if } S > 0 \\ 0 & \text{if } S = 0 \\ \frac{S+1}{\sigma} & \text{if } S < 0 \end{cases} \quad (1.4)$$

Consistent variability in the trend of time series is assessed using equation (1.5) where Z lies in the critical region of the significance level of α for a two-sided test:

$$-Z_{1-\frac{\alpha}{2}} \leq Z \leq Z_{1-\frac{\alpha}{2}} \quad (1.5)$$

Where $Z_{1-\alpha/2}$ = the critical value of Z from the standard normal table. In this work, the critical value is estimated using a 5% significant level. The null hypothesis is accepted when $Z \leq Z_{1-\alpha/2}$, and rejected when $Z \geq Z_{1-\alpha/2}$. Positive values of Z indicate increasing trends while negative Z values indicate decreasing trends in the time series.

3.4.1.2 Theil-Sen rate of change computation

Theil-Sen (TS) estimation (also referred to as Sen slope) was used to quantify the rate of change in the trend of series (Sen, 1968). It enables the estimation of the rate of change of median of an annual series with time. The median of slope from the trendline, $y = \beta t + C_t$, was deduced through pairs of points, where β = Slope and C_t = Constant of timeline t . Constant C_t was computed for each time-step t , by estimating the median of n values (annual values) using the difference of $x_i - \beta t_i$ (Pohlert, 2016).

Theil-Sen's slope was estimated using the equation (1.6):

$$\beta = \text{median}\left(\frac{x_j - x_l}{j - l}\right) \text{ for } 1 \leq l \leq j \leq n \quad (1.6)$$

Where x represents the variable, i and j are indices and n is the number of data. Both MK and Theil-Sen Slope are insensitive to outliers (Dinpashoh et al., 2011).

3.4.2 Assessment of Land use land cover change dynamics

The available Landsat satellite images for the study area run from 1984 to 2019. However, winter images, with a specific interest in August month, were selected. This is because rainfall intensity, wind speed, and cloud cover are very low with high cloud clarity in this period, hence, enhancing the spectral reflectance of the raster (Gehring et al., 2021). Satellite images of Landsat Thematic Mappers and Landsat Operational Land Imager were acquired for the representation of semi-decadal spectral radiation assessment using the series of 1984, 1989, 1994, 1999, 2004, 2009, 2014, and 2019. The images were pre-processed by calibrating their radiometric values and ensuring their atmospheric correction. The bands 1, 2, 3, 4, 5, and 6 of MSS 1, 4 – 5 and bands 1, 2, 3, 4, 5, 6, and 7 of Landsat 8 OLI were exported into ArcMap 10.3.1 and stacked accordingly using composite band processor of image analyst.

The resulting semi-decadal composite rasters were clipped into the area of focus using the Tyume River basin shapefile. The computation of land use /land cover change adopted the supervised mapping approach. For the development of a training manager sample for the computation exercise, the false-colour composite bands for vegetation, water bodies, and built-up areas were computed using the information presented in Table 3.1.

Table 3.1. Band selection and arrangement for land use/land cover characterization (Butler, 2013).

Composite feature	Band combination used					
	MSS 1, 4 – 5 band combo			Landsat 8 OLI band combo		
Natural color	3	2	1	4	3	2
Built-up areas	6	5	3	7	6	4
Woodland	4	5	1	5	6	2
Scrubs and velds	5	4	1	6	5	2
Water bodies/bare	4	5	3	5	6	4

At least, 20 return on investments training samples were selected per three cells for every tonal variation randomly in areas with a concentration of spectral reflectance. However, selected points for the training manager samples were matched with historical images of the study area acquired from the Google Earth map and mean aerial photographs of the environment in relation to the respective Landsat TM/OLI used. The land use land cover (LU/C) computation was based on the five major features with high sensitivity to processes of soil erosion by water as presented in Table 3.2. Following the characterization of false-colour composite band reflectance, a signature file was generated. The supervised raster characterization was mapped using a maximum likelihood approach at an equal priority probability weighting (Owolabi et al., 2020). The image classification accuracy for respective years of the LULC was performed with 72 samples using the confusion matrix. The matrix was computed by sampling 72 training cells randomly as the user's value on the LULC. The sample is compared with Google Earth pro image of the same time slide and recorded as the producer's value.

Table 3.2. Thematic categories for land use/land cover mapping.

LU/C Features	Description
Built-up areas	Areas predominated with artificial imperviousness cover, such as tarred or plastered roads, plastered parks, residential, institutional, and commercial buildings.
Waterbody	Areas with evidence of natural ponds or flow. This includes lakes, dams, open streams, rivers, natural pools, etc.
Woodland	Areas predominated with an advanced stage of tree growth with a possible high vegetation density greater than 50%. This includes areas dominated by thickets, canopy trees, and deciduous trees.
Scrubs and Veld	Areas with sparse shrubs, veld, possible cropping or grazing activities with vegetation density within 20% - 50% and vegetation height, not more than 1.80 m.
Bare-ground	Areas exhibiting signs of severe degradation, clear-cuts, with scanty grass cover and shrubs, and with low vegetation density, less than 20%.



The overall accuracy and the Kappa coefficient is calculated as shown in equation 1.7 and 1.8:

$$\text{Overall Accuracy} = \frac{\text{Sum of Correctly classified pixels}}{\text{Total number of reference pixels}} \times 100 \quad (1.7)$$

$$K = \frac{N(\sum_{i=1}^r x_{ii}) - (\sum_{i=1}^r (x_{i+} \times x_{+i}))}{N^2 - (\sum_{i=1}^r (x_{i+} \times x_{+i}))} \quad (1.8)$$

where r is number of rows in the error matrix, x_{ii} is the classified pixels in row i and column i, x_{i+} and x_{+i} are the pixels in row i and column i, while N is the total number of the sampling points used.

The overall classification accuracy and the Kappa coefficient value for the resultant error matrix for year 1984 to year 2014, presented in Table 3.3, showed substantial agreement for all the years (60% - 80%) while the year 2019 is near perfection. The user's value is computed along the rows while the producer's value is computed along the column.

Table 3.3. Land use/ land cover classification accuracies as provided by confusion matrix

	<i>LULC variable</i>	Built-up area	Bare ground	Forest	Veld	Water body	Interrater reliability
1984	<i>Built-up area</i>	11	1	0	1	0	O.A (%) = 70.83 K.C. (%) = 63.08
	<i>Bare ground</i>	3	12	1	2	1	
	<i>Forest</i>	1	1	8	2	0	
	<i>Veld</i>	0	2	4	12	0	
	<i>Water body</i>	0	2	0	0	8	
1989	<i>Built-up area</i>	10	0	0	2	0	O.A (%) = 80.56 K.C. (%) = 75.24
	<i>Bare ground</i>	0	11	1	2	0	
	<i>Forest</i>	0	3	8	0	0	
	<i>Veld</i>	0	1	2	18	0	
	<i>Water body</i>	0	1	1	1	11	
1994	<i>Built-up area</i>	9	4	0	1	1	O.A (%) = 72.22 K.C. (%) = 65.00
	<i>Bare ground</i>	3	11	0	0	0	
	<i>Forest</i>	0	3	8	0	0	
	<i>Veld</i>	1	1	3	15	0	
	<i>Water body</i>	0	2	0	1	9	
1999	<i>Built-up area</i>	11	3	1	3	0	O.A (%) = 73.61 K.C. (%) = 66.78
	<i>Bare ground</i>	1	9	0	2	2	
	<i>Forest</i>	0	3	9	0	0	
	<i>Veld</i>	1	2	1	14	0	
	<i>Water body</i>	0	0	0	0	10	
2004	<i>Built-up area</i>	11	3	0	3	1	O.A (%) = 75.00 K.C. (%) = 68.59
	<i>Bare ground</i>	0	9	0	1	3	
	<i>Forest</i>	0	4	10	1	0	
	<i>Veld</i>	0	1	1	16	0	
	<i>Water body</i>	0	0	0	0	8	
2009	<i>Built-up area</i>	4	3	0	1	0	O.A (%) = 70.83 K.C. (%) = 62.65
	<i>Bare ground</i>	0	10	0	1	3	
	<i>Forest</i>	1	1	13	4	1	
	<i>Veld</i>	4	2	0	16	0	
	<i>Water body</i>	0	0	0	0	8	
2014	<i>Built-up area</i>	5	2	0	1	0	O.A (%) = 73.61 K.C. (%) = 65.52
	<i>Bare ground</i>	0	9	0	2	1	
	<i>Forest</i>	0	1	11	4	0	
	<i>Veld</i>	2	4	2	18	0	
	<i>Water body</i>	0	0	0	0	10	
2019	<i>Built-up area</i>	11	1	0	3	0	O.A (%) = 86.11 K.C. (%) = 82.49
	<i>Bare ground</i>	0	15	0	3	0	
	<i>Forest</i>	0	0	10	1	0	
	<i>Veld</i>	0	1	1	14	0	
	<i>Water body</i>	0	0	0	0	12	

The reflectance distribution was classified as values while the characteristic cells were enumerated as counts in the attribute table which was extracted for each raster for further statistical estimation. The percentage, area, and descriptive statistics of tracked changes across the eight distinct semi-decadal LU/C elements were assessed. Comparative analysis of the long-term streamflow variability to the long-term LU/C dynamics was obtained for assessment of the period with the highest soil erosion risk by water.

3.4.3 Vulnerability mapping of soil erosion zones

The conceptual approach that guides the production of soil erosion by water vulnerability map is presented in Figure 3.1.

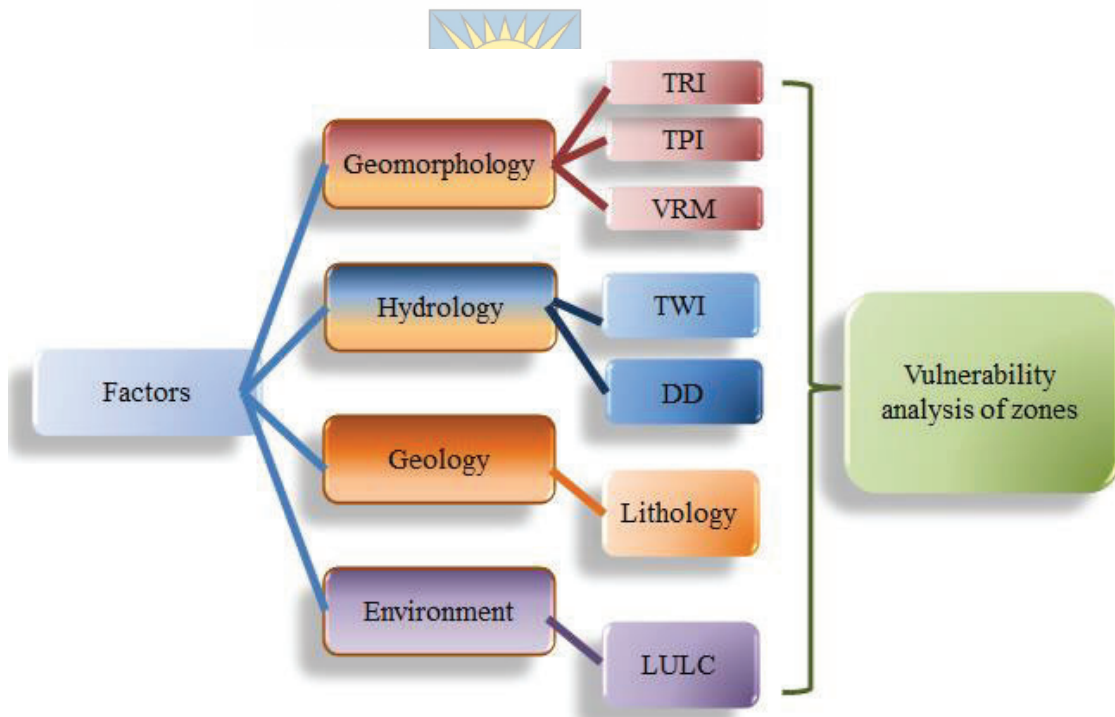


Figure 3.1 Conceptual approach for vulnerability analysis of areas of soil erosion by water (Source = Author). As shown, TRI = Terrain Roughness Index, TPI = Topographic Position Index, VRM = Vector Ruggedness Measure, TWI = Topographic Wetness Index, DD = Drainage density, and LULC = Land use/ land cover.

The vulnerability map of regions with potential for soil erosion by water was computed through overlay analysis of the essential thematic layers that determine soil susceptibility to mass waste. These involve the factors of the environment, geology, geomorphology, and hydrology. Layers of land use/land cover change, lithology, drainage density, topographic wetness index, and ruggedness indices were assembled based on the susceptibility of some of their attributes to soil erosion by water.

3.4.3.1 Geology and LU/C maps

The geology map of the Eastern Cape was acquired from the Council for Geologic Survey. The area of focus was clipped out of the polygon shapefile. The clipped data was converted into a raster file and reclassified based on the mudstone-sandstone ratio and while dolerite was recognized as the most resistant rock type in the classification of the lithology. Rozycka et al. (2017) noted that mudstone-dominated materials are highly susceptible to landslide and mass waste. Hence, this basis serves as a yardstick for litho-material reclassification for vulnerability mapping. Details of mudstone content in the Eastern Cape Karoo Supergroup are documented in Baiyegunhi and Gwavava (2017). Hence, the rock types of the Tyume River basin are in the following order: Balfour Formation, Middleton Formation, Katberg Formation, Quaternary sands, and Jurassic Dolerite. The 2019 LU/C map computed according to section 3.3.2 was used for the overlay analysis.

3.4.3.2 Geomorpho-metric analysis

Geomorpho-metric analysis has provided valuable information on the potential of a hydrologic basin for flash floods and the existence of geospatial evolution (Mahajan and Sivakumar, 2018). The analysis provides information relative to drainage system development, landform

geometry, and altered morphogenesis specifically influenced by erosion, geology, and geomorphological processes (Rai et al., 2017). Morphometric parameters of roughness indices characterize the terrain attributes to terrain curvature and flat area. The measure of concavity and convexity of topography has served as an important regressor for the analysis of landslide development, gully development, and soil erosion development (Smith, 2014; Rózycka et al., 2017). These roughness indices include terrain roughness index, topographic position index, and vector roughness measure, while the morphogenetic path estimator includes drainage density and the topographic wetness index.

The downloaded Advanced Spaceborne Thermal Emission and Reflection Radiometer (ASTER) Digital Elevation Model (DEM), with a 30 m by 30 m resolution, was processed for watershed delineation by converting the raw DEM raster into fil (a geodatabase file) data. Flow direction was generated from the fil raster. The resulting stream flow direction raster was processed for the drainage accumulation track. The resulting accumulation raster was refined for drainage tracks not less than 100 units per path inflection (DEM ridgeline). The sink, snap pour point, and stream links were computed for stream order computation. Computation of the stream order was carried using the Strahler approach. The resulting stream order was converted from raster into polylines for the configuration of the drainage map.

3.4.3.2.1 Drainage density

Drainage density was computed from the generated polyline features and its radius in the line density engine of ArcMap 10.5.1. The value column of the attribute table is selected as the population field; the area unit is set at square kilometres for estimation accuracy, while the default cell size of 138.58 was used based on effective annulus cells. Tyume watershed

polygon was the input for the mask in the raster analysis environment. The resulting featured class raster is classified into five according to Table 3.4.

Table 3.4. Classification scheme for Tyume drainage density map (Owolabi et al., 2020).

Class name and rate	Range of Drainage density
Very low	0 – 150
Low	151 – 240
Moderate	241 – 360
High	361 – 600

3.4.3.2.2 Topographic wetness index

The topographic wetness index (TWI) indicates tracks of hydrological response to climate-catchment-related alteration such as the areas of high hydraulic variations pressure, water accumulation, and effective runoff scarps. Information provided by TWI is considered relevant to the analysis of soil erosion by water. TWI analysis was generated from the elevation map extracted from ASTER DEM in ArcMap 10.5.1. The study area DEM raster was processed to generate the slope map in ArcMap. In so doing, the output measurement was carried out in degree format at the Z factor of 1 (at default) to reduce the influence of variogram overestimation. Calculation of the TWI was carried out in the raster calculator, using equation (1.9) (Kirkby, 1975; Hojati and Mokarram, 2016);

$$TWI = \ln \left[\frac{\alpha}{\tan(\beta)} \right] \quad (1.9)$$

where α , specific catchment area = catchment area, A, per unit contour length, L, (A/L), and $\tan(\beta)$ = slope. However, the TWI was converted into an integer format to classify the zones of TWI within the upper and lower quartile to enable the projection of the zones of high and

low TWI. The resulting projection of TWI spots was classified into four according to Table 3.5.

Table 3.5. Classification scheme for the projected Topographic Wetness Index (Owolabi et al., 2020).

Class name	Range of values of TWI
Ponding area	6.3 – -12.7
Slight ponding	-12.8 – -14.4
Gentle hillslope	-14.5 – -16.6
Steep hillslope	-16.7 – -20.5

3.4.3.2.3 Terrain ruggedness index

Terrain ruggedness index (TRI) computes the mean of the absolute spatial variation in focal cell elevation relative to its neighbourhood according to the Riley et al. (1999) algorithm. The analysis was carried out by computing the square of the summation of grid cell difference, relative to its neighbouring cell at the scale of 75 m where a slight elevation change can be significant. TRI is based on the equation of Riley et al. (1999) as presented in equation 1.10:

$$TRI = (\Sigma(Z_c - Z_i)^2)^2 \quad (1.10)$$

Where;

Z_c = elevation of a central cell

Z_i = elevation of each cells in the neighbourhood at the scale of 75 m

$i = 1, 2, \dots, 8.$

3.4.3.2.4 Topographic position index

The topographic position index buffers the displacement of a grid cell relative to its neighbourhood based on the difference between the grid cell and its neighbourhood mean

elevation (Jenness, 2006). The plot is based on equation 1.11, formulated by Weiss (2001) and modified by Jenness (2006):

$$TPI = Z_0 - \Sigma_{n-1}(Z_0/n) \quad (1.11)$$

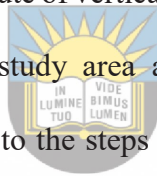
Where; Z_c = elevation of a focal cell

Z_n = elevation of integrated neighbourhood cells within the scale of 75m

n = The total number of the neighbouring cells around the focal cell.

3.4.3.2.5 Vector ruggedness measure

The vector roughness measure estimates the degree of dispersion of vectors at the edge of a grid cell relative to its specific neighbourhood. It is based on the computation of slope variability as a 3-dimensional attribute of vertical and horizontal components of aspect. Hence, the slope and the aspect of the study area are computed first. It is based on standard trigonometric operation according to the steps as presented in equation 1.12 (Sappington et al., 2007):



University of Fort Hare
Together in Excellence

$$VRM = 1 - \left(\sqrt{X_{sum}^2 + Y_{sum}^2 + Z_{sum}^2} \right) / 75^2 \quad (1.12)$$

Where; $X_{sum} = Focal(\sin \Lambda, \oint = sum)$

$Y_{sum} = Focal(\cos \Lambda, \oint = sum)$

$Z_{sum} = Focal(\cos \int, \oint = sum)$

Λ = Aspect, \int = slope, and \oint = interface function, while 75 m represent the scale of computation.

3.5 Overlay analysis

The maps prepared earlier were reclassified and assigned a weight based on their degree of susceptibility. An area of high significance to soil erosion is given bias weightage. Table 3.6 presents the weight assigned to each class of subsets of the layers.

Table 3.6 Weightage of thematic layer for overlay analysis of vulnerability map production (Owolabi et al., 2020).

Thematic layer (Weight)	Classes	Field score	Field Weight
Drainage density (15)	Very low	1	1.88
	Ineffective	2	3.75
	Effective	7	13.13
	Ponding	8	15.00
Topographic wetness index (15)	Accumulation zone	1	2.5
	Gentle drain zone	2	5.0
	Fairly steep hillslope	5	12.5
	Steep hillslope	6	15.0
Terrain ruggedness index (15)	Very low	1	3
	Low	2	6
	High	4	12
	Very high	5	15
	Very low	1	3.75
Topographic position index (12)	Low	2	7.50
	Moderate	4	26.25
	High	5	26.25
	Very high	6	30.00
	Vector roughness measure (12)	Very low	1
Low		2	4.8
High		4	9.6
Very high		5	12
Geology (15)	Jurassic Dolerite	1	2.5
	Quaternary sand	2	5
	Middleton Formation	3	7.5
	Katberg Formation	4	10
	Balfour Formation	6	15
Land use/ land cover (16)	Woodland	1	2
	Scrub and Veld	2	4
	Build-up	5	10
	Water bodies	6	12
	Bare	8	16

Based on previous literature, drainage density and the topographic wetness index indicate the area with the propensity for soil erosion by water, hence, they were both assigned similar and higher weights. Geology has a higher weight based on its information concerning the susceptibility of soil to erosion, hence it is assigned higher weight compared to LU/C which were also ranked to exposure and vulnerability tendency. The weight sum method of overlay analysis was employed to compute the vulnerability analysis and the resulting analysis was presented in Table 3.6.

3.6 Validation of soil erosion vulnerability map

Validation of assessment was carried using a Google Earth map survey. Unlike the field mapping which may be limited by inaccessibility and coverage, the Google Earth map offers a 3-dimensional view without a restriction to length. Sixty-three spots within the moderate to high soil erosion zones were georeferenced randomly from the soil erosion vulnerability map for visual inspection and analysis under the Google Earth map. The Google Earth time was set to the default for the latest satellite images (with variation between December 2019 and April 2020) deployed by CNES/Airbus. There are occasional multiple sampling in a point to prevent monotonous attribute sampling. The sampling points were mostly selected around the tributaries to prevent monotony of attributes at the river valley, hence, the non-existence of sampling points in the centre of the catchment. Information filtered from the use of Google Earth includes the following:

1. Discrimination of erosion channel from a drainage channel.
2. Identification of erosion type.
3. Linear measurement of the erosional path.

4. Extraction of camera height for the resolution of magnification.
5. Classification of slope and bareness of the affected area.
6. Estimation of soil erosion proneness.

The estimation of Soil erosion proneness using the Google Earth map survey was informed by Shit et al. (2015) indicated in equation 1.13:

$$E_p = \frac{f_b \times f_s \times M_c (\sum N_g + \sum N_r + \sum N_s)}{100} \quad (1.13)$$

where E_p is the erosion proneness, f_b is the bareness factor, f_s is the slope factor, M_c is the camera magnification in km, N_g is the normalized length of a gully in km, N_r is the normalized length of a rill in km, and N_s is the length of the sheet in km. The length of the rill and gully are normalized by the multiples of 2 and 3 respectively, due to the variation in depth of impact.

The designation of rating factors based on bareness and the extent of the slope was based on Table 3.7.



University of Fort Hare
Together in Excellence

Table 3.7. The rating factor is used for calculating erosion proneness (Shit et al. 2015).

Attributes	Rating factors
Bareness	1
Densely riparian	2
Lightly vegetated	3
Veld	4
Bared	5
Penplain	1
Pediplain	2
Fair hillslope	3
Abrupt hillslope	4

The calculated soil erosion proneness was tabulated together with its georeference and the corresponding grid-codes for soil vulnerability drawn from georeference identity. The

extracted grid-codes are plotted against the E_p for its coefficient of determination. Based on the coefficient of determination (R^2), $R^2 < 0.5$ indicates that the model is unreliable does not replicate the field observation. $R^2 = 0.5$ indicates that the model is reliable as 50% of the field observation correlates with the simulation provided by the model while $R^2 \geq 0.75$, suggests that the model is excellent in replicating the field observation (Dougherty et al., 2000).

Receiver operating characteristics curves (ROC) were computed to enable the agglomeration, visualization, and corroboration of model performance as elaborated by Streiner and Cairner (2007) and Verbakel et al. (2020). ROC is the plot of the sensitivity of the model against “1 – Sphericity” of the model (Fawcett, 2006; Verbakel et al., 2020). In this work, the class threshold was obtained by extracting the frequencies of the grid codes. This enables the computation of the sensitivity variables, $(1 - G(c))$, and the sphericity variables $(1 - F(c))$, where G and F are the continuous distribution function (c) of the grid-codes and the actual erodibility potential respectively provided that $-\infty \leq c \leq \infty$ (Streiner and Cairner, 2007). The positive likelihood ratio was derived by obtaining the slope of sensitivity/(1-sphericity), while the Area Under Curve (AUC) was obtained by integrating the sensitivity variables over sphericity variables. The optimum threshold was obtained from the outcome resulting in the largest sensitivity and sphericity from the grid codes.

In summary, the approach set out in this work is basically due to the significance of pluviometric patterns and anthropic factors to the vulnerability of terrain to soil erosion by water. Hence, the temporal assessment of the watershed vulnerability encapsulates the comparative analysis of streamflow processes as the natural agent with the LULC variables as the anthropogenic agents. Similarly, the geospatial assessment entails the development and integration of thematic layers of anthropic factors and the natural geomorphometry modifiers

to assess the active hotspot of soil erosion by water. The results of the desktop analysis are presented in the same order in the subsequent chapter.



University of Fort Hare
Together in Excellence

Chapter 4: Results

4.1 Introduction

This chapter presents the reports of the analysis carried out towards the vulnerability mapping of the Tyume River catchment. This covers streamflow variability trend assessment, land use land cover change dynamics, geomorphometric analysis, topographic wetness index, soil erosion vulnerability mapping, and the validation exercise for the soil erosion vulnerability map. Also covered in this chapter are the interpretation of the indices, and their implication to land management.

4.2 Streamflow variability trend assessment



The result of the time series plot of the streamflow data series and its variability trend analysis is represented in Table 4.1 and as a plot in Figure 4.1 (A and B). From the plot, the bars with positive projection represent the positive Mann-Kendall trend of the streamflow and vice versa. The height of the bars indicates Sen's slope estimation. The bar lengths with positive projection imply the acceleration of the high-flow of Tyume River while those with negative projection imply the acceleration of low-flow of the River. Peak high-flow acceleration with the flood propensity and soil erosion by water, occurred in 1979 and 1982 while the acceleration of low-flow with draught propensity occurs in 2016. There was no significant year of high-flow acceleration while there are five significant years of low-flow acceleration. The proportion of years of low-flow acceleration (23) to years of high-flow accelerations (12) is approximately 2:1. These situations, accounting for the strong significance of low-flow

acceleration and the predominance of low-flow in Tyume River further confirms the status of the region as a semi-arid environment.

Table 4.1: Mann-Kendall trend test and Sen's slope results for Tyume streamflow station data of 1979-2018.

Year	Sen's	MK	<i>p-value</i>	Year	Sen's	MK	<i>p-value</i>
1979	28	0.424	0.063	1999	-8	-0.121	0.638
1980	10	0.152	0.545	2000	-12	-0.182	0.459
1981	-11	-0.168	0.45	2001	-4	-0.061	0.841
1982	28	0.424	0.063	2002	-2	-0.030	0.947
1983	0	0	0.947	2003	-34	-0.515	0.021
1984	-14	-0.212	0.381	2004	-4	-0.061	0.841
1985	4	0.061	0.841	2005	-14	-0.212	0.381
1986	12	0.182	0.459	2006	0	0	0.947
1987	-20	-0.303	0.197	2007	-8	-0.121	0.638
1988	6	0.091	0.737	2008	-42	-0.636	0.003
1989	0	0	0.947	2009	-8	-0.121	0.638
1990	-14	-0.212	0.381	2010	4	0.061	0.841
1991	-4	-0.061	0.841	2011	4	0.061	0.841
1992	-32	-0.485	0.031	2012	10	0.152	0.545
1993	12	0.182	0.459	2013	-6	-0.091	0.737
1994	-22	-0.333	0.153	2014	-26	-0.394	0.086
1995	-8	-0.121	0.638	2015	0	0	0.947
1996	-26	-0.394	0.086	2016	-44	-0.667	0.002
1997	-30	-0.455	0.045	2017	-2	-0.030	0.947
1998	2	0.030	0.947	2018	14	0.212	0.381

There is a major increase in the recurrence of heavy discharge across the time series (Figure 4.1A) and, in contrast, the trend analysis depicts a negative inter-annual variability (Figure 4.1B). Hence, the years 1985, 1988, 1996, 1999, and 2010 are years of wetness while the period of effective storm-flow acceleration succeeding the extremely dry period were portrayed in 1986, 1993, 2012, and 2018. The streamflow long-term projections indicate a periodic rarefaction of discharge pattern across the hydrological regime accounting for the increase in discharge at the catchment mouth.

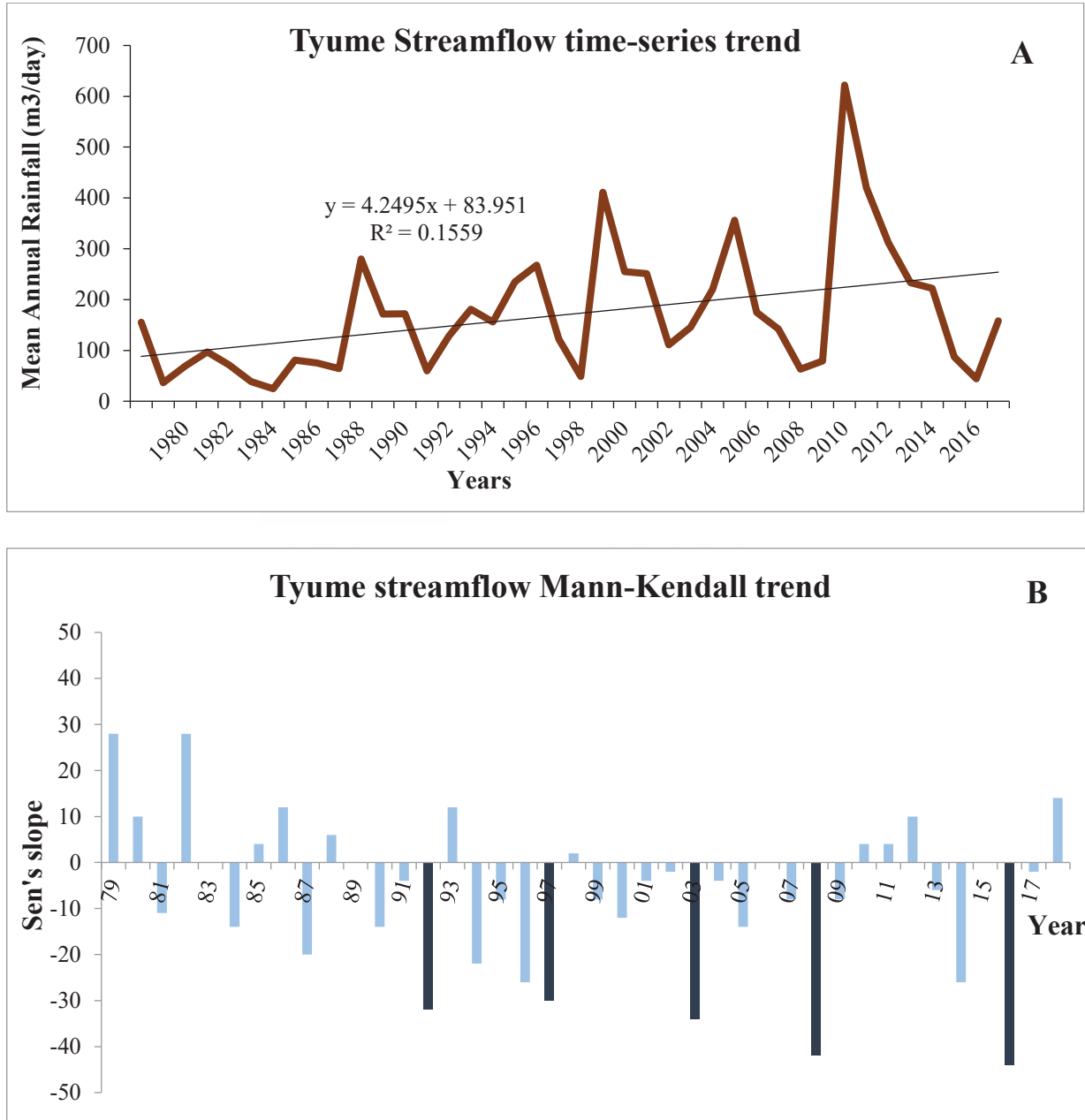


Figure 4.1 The plot showing; A. the time-series trend and, B. Time series Mann-Kendall trend (bar direction) and Sen's slope assessments (bar length) result for Tyume long-term streamflow (1979 – 2018). The years of significant changes in the trend are shown in a deep blue tone.

The trend analysis suggests the existence of hydrological alteration and a hundred percent shift in rainfall regime. The four-time increase in high-flow amplitude has a huge implication on

the runoff intensity, erosivity, and hydraulic pressure of the drainage path, inter-rills, and river channel. As a consequence, the trend of streamflow intensity may have a severe consequence on the drainage path and render Tyume Basin vulnerable to soil erosion by water depending on the land use/land change dynamics. The streamflow trend also suggests that the future trend of climate change may progress into a more severely intense flow period. Sen's slope also indicates that the strength and transition of streamflow acceleration are in a recurrent semi-decadal pattern.

4.3 Land use/land cover change dynamics

4.3.1 The axial changes in land use/land cover spatial density

The plots of the land use/land cover change analysis are combined in Figure 4.2. The plot indicates that the scrubs and veld (39%) have the highest mean percentage coverage, followed by built-up areas (27%), bare (16%), woodland (16%), and waterbodies (2%). The built-up areas are concentrated along the longitudinal section and west of Tyume River, thus revealing the socio-economic significance of the river to the development of the environment. The woodland is concentrated in the extreme north and northwest of the area, which suggests that the area is associated with high soil moisture content that can support forest management. The high forest spatial density in the north also suggests the richness of interflow and baseflow, forcible enough to generate soil erosion by water. The bare intersperse the built-up area in all the LU/C maps, hence, in inclined terrain with light/loose soil cover with poor drainage, the potential for soil erodibility is expected to be high due to the impact of gravity. In most of the LU/C maps, the scrubs and veld appear as the divisor or transitional zone between the built-up area and the woodlands.

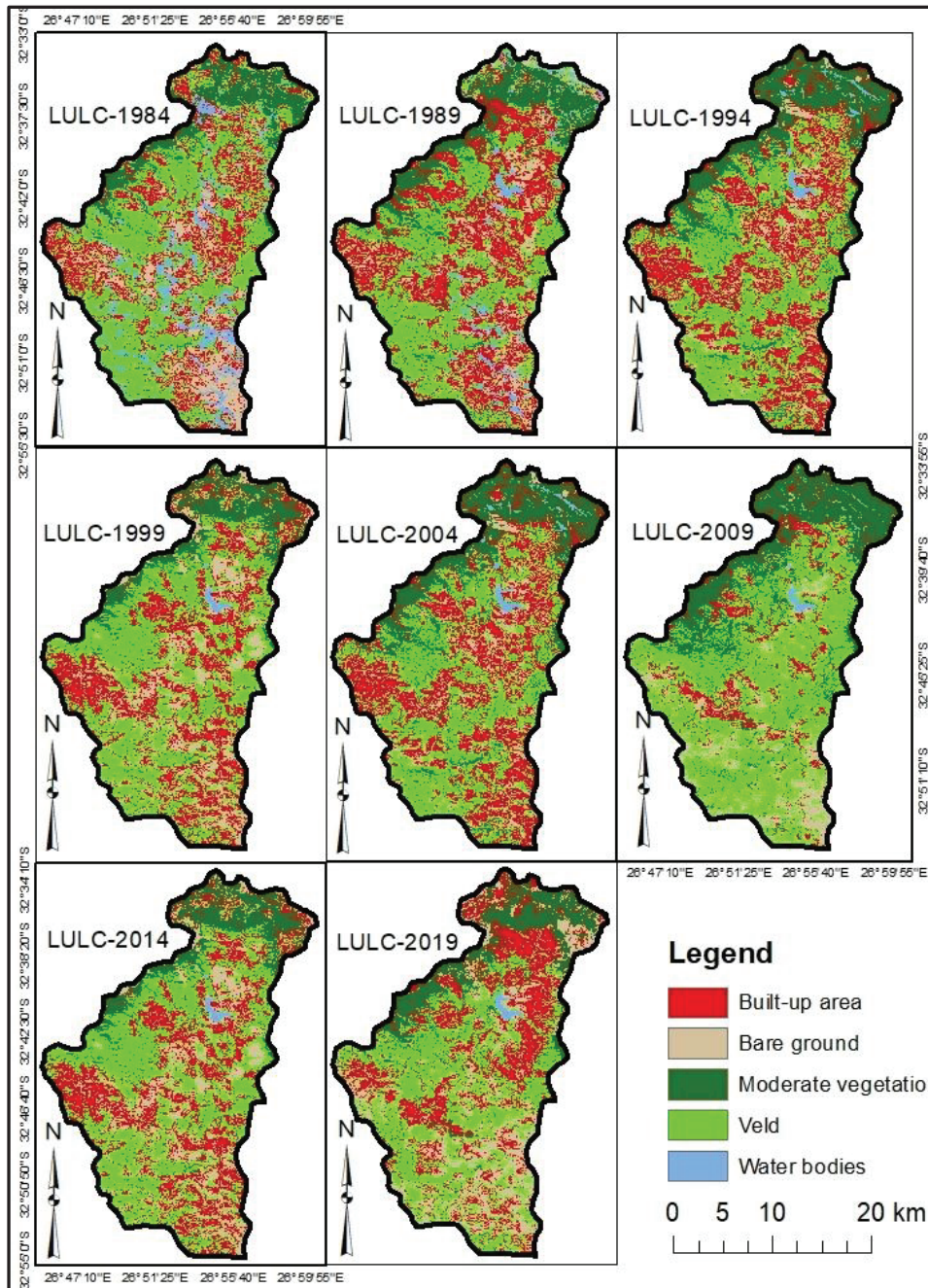


Figure 4.2 Plot showing the land use/land cover change dynamics from 1984 to 2019.

According to Table 3.2, the croplands, plantation fields, and grazing fields were classified under the scrubs and veld, this, therefore, implies that the widening or narrowing of the transition zone can be influenced by agricultural activities. The most revealing coverage of

the waterbodies lies in the north-central area, in the area within a two kilometre radius of where the Binfield Dam is located. Other maps as indicated by LU/C-1984 (Figure 4.2) runs across the entire length of the river.

Axially, the LU/C analysis, therefore, indicates that there is a transition from a high soil moisture environment in the far north, through the moderate in the centre to the low soil moisture content environment in the extreme south. The socio-economic sensitivity of the Tyume River is therefore depicted due to the concentration of settlements along the river valley. There is minimal flow or shift in the concentration of features. There is a conspicuous shift in the concentration of forest to the north in the middle and tail-end of the time-series analysis. Also, the built-up areas experienced a notable shrinkage in 2009 and concentration contraction from the south in the tail-end of the time-series. The contraction in the area covered by built-up is connected with the vivid appearance of bare areas, thus, indicating the contribution of urbanization to the bareness spatial density. The spatial distribution of waterbodies is associated with the most serious contraction from the beginning of the time-series. This portends the basin as being highly vulnerable to soil erosion by a flash flood as suggested in section 4.2.

4.3.2 Rate of change across the land use/land cover spatial features

The statistical changes across the LU/C plots are presented in Table 4.2 and Figures 4.3 and 4.4. The significance of land use/land cover change to the study of the magnitude of soil erosion in Tyume is highlighted by the abrupt increment rate in the bareness of the Tyume River basin (Figure 4.4).

Table 4.2 Estimates of land use/land cover changes from 1984 to 2019.

Features	Parameters	1984	1989	1994	1999	2004	2009	2014	2019
Built-up	<i>Counts</i>	34196	183344	172483	155289	172483	59746	123675	149134
	<i>Percentage</i>	25.51	34.19	32.17	28.96	32.17	11.14	23.06	27.81
	<i>Area</i>	174.24	233.54	219.71	197.80	219.71	76.10	157.53	189.96
Bare	<i>Counts</i>	20599	67297	68493	106522	68493	88406	80147	129316
	<i>Percentage</i>	15.37	12.55	12.77	19.87	12.77	16.49	14.95	24.12
	<i>Area</i>	104.96	85.72	87.25	135.69	87.25	112.61	102.09	164.72
Woodland	<i>Counts</i>	14310	69774	100839	58542	100839	123290	80488	75027
	<i>Percentage</i>	10.68	13.01	18.81	10.92	18.81	22.99	15.01	13.99
	<i>Area</i>	72.91	88.88	128.45	74.57	128.45	157.04	102.52	95.57
Scrubs and Veld	<i>Counts</i>	47880	180172	186211	213291	186211	259901	248908	179675
	<i>Percentage</i>	35.72	33.60	34.73	39.78	34.73	48.47	46.42	33.51
	<i>Area</i>	243.96	229.50	237.19	271.69	237.19	331.06	317.05	228.87
Water	<i>Counts</i>	17061	35616	8177	2559	8177	4860	2985	3051
	<i>Percentage</i>	12.73	6.64	1.52	0.48	1.52	0.91	0.56	0.57
	<i>Area</i>	86.93	45.37	10.42	3.26	10.42	6.19	3.80	3.89


University of Fort Hare
Together in Excellence

Across the thirty-five years' timeline, the bareness has the highest change range of 8.75%. After the first 4 years, there is an increase in built-up area which may have resulted in the negative changes in bareness and scrub and veld, as well as the aggravating slump in water bodies rate on account of human's developmental need for water. By 1994 and 1999, there was a progressive decline in the built-up rate which may have resulted in the precipitous increase in bareness.

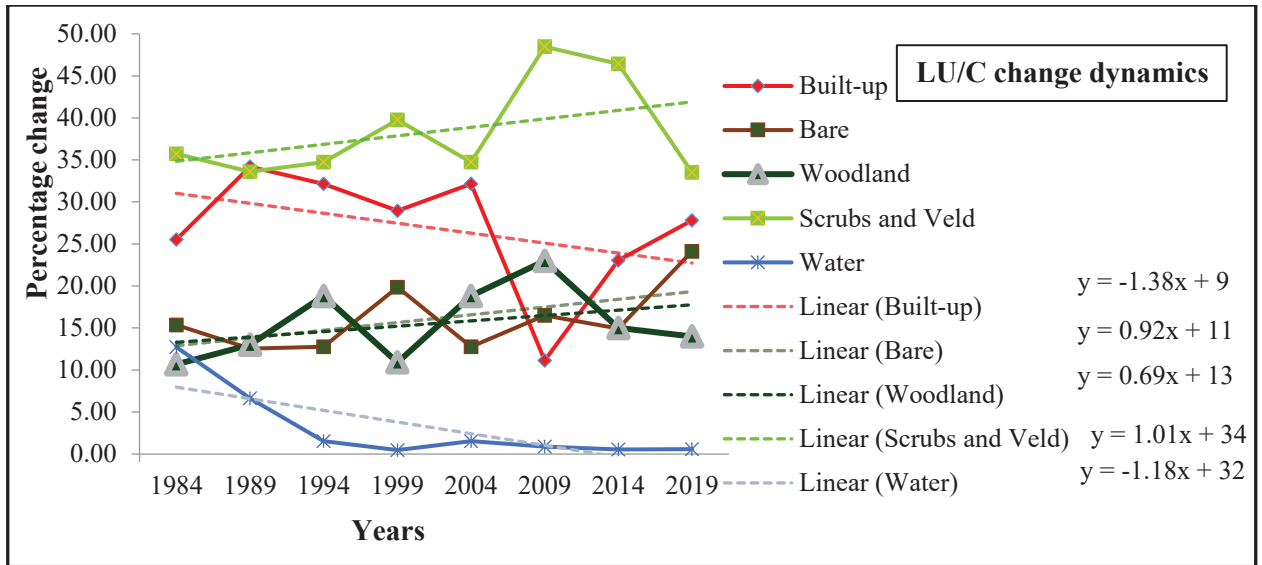


Figure 4.3 Plot showing the LU/C change dynamics in the Tyume River basin from 1984 to 2019.

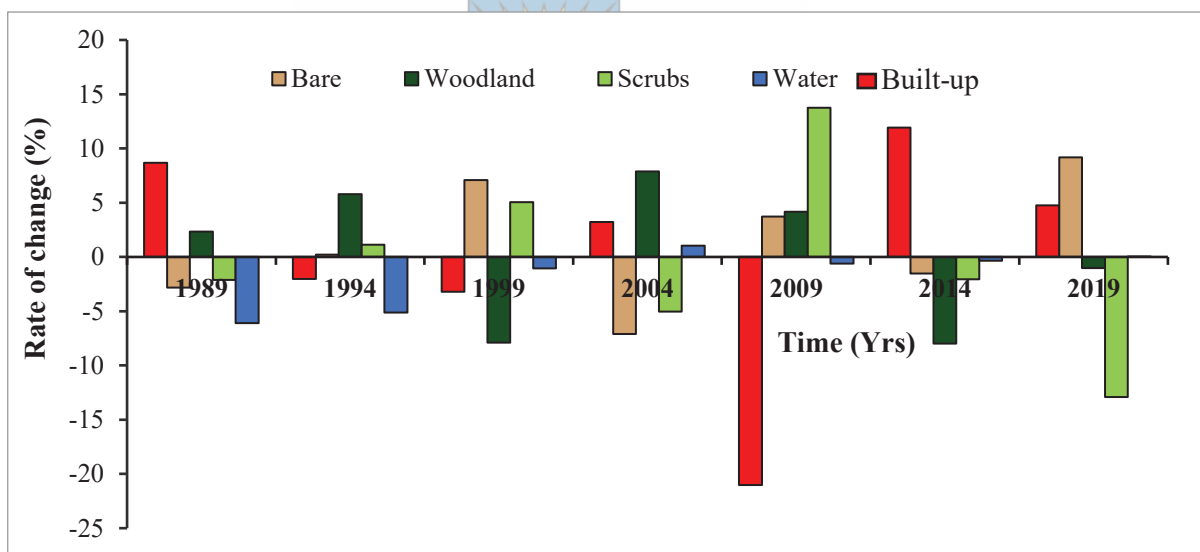


Figure 4.4 Plot showing the rate of changes across the LU/C mapping across 1984 – 2019.

The changes in the third cycle (1999) had a positive impact on scrubs and veld and this can be perceived to have been due to the fallowness of the basin, which allowed the increase in the spatial density of grassland/cropland. The significant change rate in the scrubs and veld is

considered to be a positive mitigator to soil erosion proneness. The increase in the rate of change in the scrub and veld signifies an increase in the surface area of impact of climate change which may possibly contribute to siltation of dams and waterways and consequentially, the water-bodies shrinkage.

In the fourth LU/C analysis cycle, a remarkable increase in the built-up rate has resulted in a significant decline in the bare and scrubs. The water-bodies witness an increase which may have accounted for the significant response in the spatial density of the indigenous forest. The following cycle showed a huge slump in built-up. This may have brought about a positive change in the rate of bareness and a significant increase in the areal coverage of scrubs and veld. In 2014 and 2019, built-up rate is marked by an accelerated increase which may have resulted in the decline in scrubs and forests. Although the bare area showed a decrease in 2014, it was marked by a significant increase in 2019. The expansion and contraction in the spatial extent of bare, water-bodies, and the built-up areas can be detrimental to the stability of the softcover soil especially in the areas of constant disturbance. Hence, 1999, 2004, and 2019 are cycles of time that may be associated with accelerated changes in water-bodies and may induce soil erosion by water.

4.3.3 Land use/land cover feature trend analysis

The trend analysis of the features shows that the features are sinusoidal across the thirty-five years except for the trend of water-bodies (Figures 4.3 and 4.4). It indicates that scrubs and veld (1.01), bare (0.92), and woodland (0.64) show positive trends while Built (-1.18) and water bodies (-1.39) show negative trends. Based on the visual perception, the changes in the built-up triggers corresponding inverse changes in the scrubs-and-veld and the bare. The sharp decline in the trend of waterbodies shows a strong visual correlation with the streamflow trend

plot (Figure 4.1). Hence, the decline can be linked with anthropogenic factors as initiated by the encroachment of settlement which accelerate the rate of siltation and reduced the natural drainage path into halves between 1984 to 1988, and by the end of the thirty-year time-series, the riparian lands were reduced to one-twentieth of their size.

Based on the aim of the study, the changes across the bare-ground and vegetation features are important parameters for assessing the spatio-temporal propensity for soil erosion by water. In the LU/CC plot (Figures 4.3), the positive long-term trend of woodland, scrubs, and veld dynamics indicates that there is a possible tendency for a reduction in soil erosion by water. However, the short-term declination from 2009 to 2019 in the vegetation parameters and the inclination of bare are major factors LULCC that may raise the risk of soil erosion by water. An important highlight of the decline is the changes in built-up areas to bare ground in LULCC in 1994 and 1998 and the southern half of the area of LULCC catchment from 2014 to 2018. The extreme north-north-east also indicates the degradation of woodland into the bare ground from 2009 to 2019. Hence, there are possible chances of soil erosion by water at the north-north-east, west, centre, and the south of the catchment depending on the geologic rock type in the areas, wetness index, and drainage density of the area.

4.4 Vulnerability analysis of zones of soil erosion by water

The aspect map which describes the terrain configuration is presented in Figure 4.5a. The aspect and the stream network analysis indicate that the Tyume River composes of six stream orders, whose stream valley is terraced along the longitudinal cross-section of the watershed. Most of the contributing distributaries are characterized by a trellis pattern, thus indicating the poor geomorphic configuration of the sub-watershed as a result of geological configuration.

4.4.1 Hydrological characterization of Tyume River Basin

4.4.1.1 Drainage density

The classification of the drainage map as presented in Figure 4.5b, shows that the high section covers 28 km² (4%), the moderate section covers 270 km² (40%), the low section covers 245 km² (36%), while the very low drainage density section spread across 139 km² (4%) (Table 4.3).

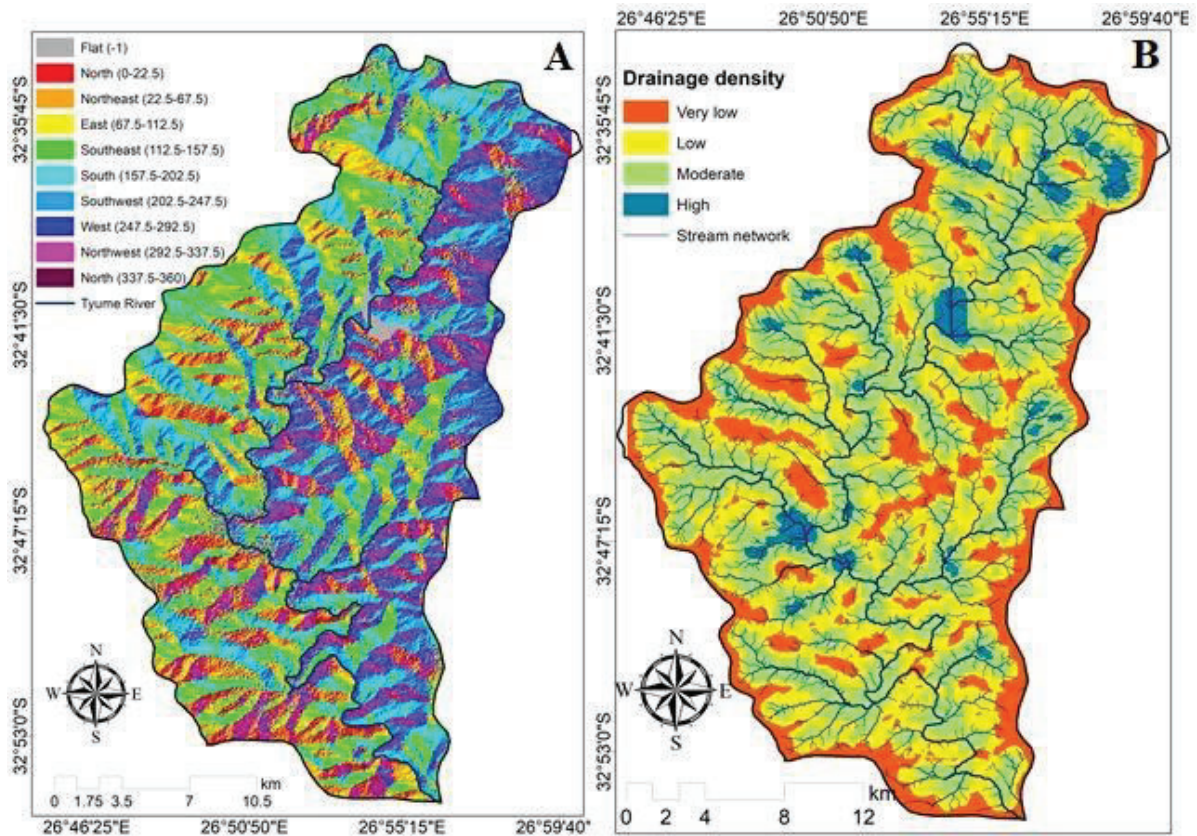


Figure 4.5 Map showing; a) the aspect and main river channel (left) and; b) drainage density together with the stream network (right) of Tyume basin.

The watershed delineation shows that the Tyume River flow is southward and mainly controlled by the terrain physiography which also influences the linearity of the stream orders. The fluvial network exhibit a dendritic pattern with a high possibility of derangement under a flash flood as exhibited by the drainage density (Figure 4.5b). The high sections are possibly associated with surface water accumulation. This may be due to the presence of a potential spring, the existence of an impermeable divide, or a depression. The moderate sections are areas of active hydraulic actions with the tendency for soil moisture movement and soil transportation. The low sections are areas of infrequent drainage actives while the very low sections are possibly ridges. Hence, the high drainage sections are given the highest weightage due to their significance to soil erosion by water while the very low sections are given the least weightage.



Table 4.3 Estimates for the drainage density and topographic wetness index map analyses.

Drainage density	Counts	Area	Percentage
Very low	122036	139	20
Low	215431	245	36
Moderate	237450	270	40
High	25356	29	4

4.4.1.2 Topographic wetness index

Topographic wetness index maps have been noted to provide information on the areas of soil moisture accumulation, soil depth, soil thickness, and zones of possible offsite soil erosion by water (Figure 4.5). The classification of the TWI revealed that the high TWI (4%) has the least coverage, followed by the moderate TWI (8%), the low (36%), and the none TWI section (52%) having the largest coverage (Table 4.4).

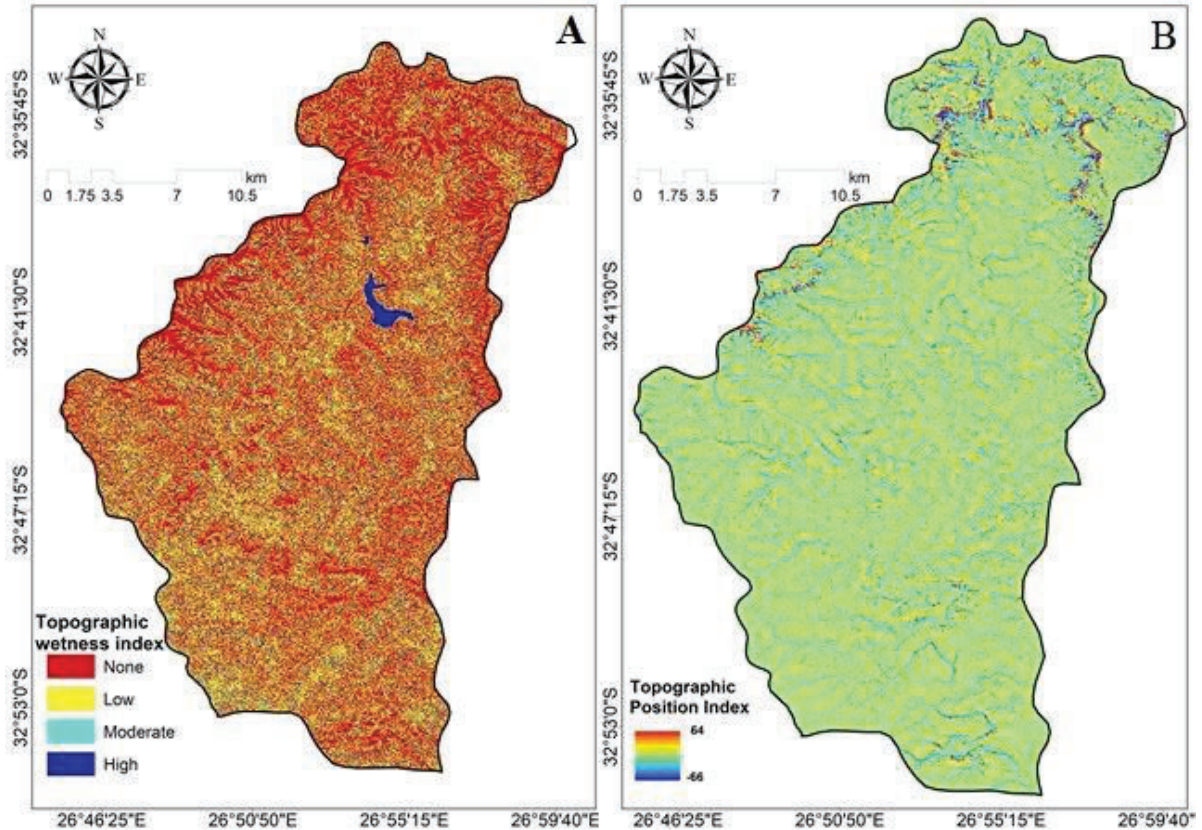


Figure 4.6 Maps showing; A) the topographic wetness index (left) and; B) topographic position index.

Table 4.4 Estimates for the drainage density and topographic wetness index map analyses.

TWI	Counts	Area	Percentage
High TWI	310523	352	52
Steep hillslope	215055	244	36
Gentle zone	51078	58	8
Low TWI	25041	28	4

The high and moderate TWI zones are characterized by heterogeneous spatial patterns that vary discontinuously. The none TWI zones dominate the north, extreme northeast, and extreme northwest in a fashion that indicates twain control of physiography and drainage,

rather than by geology. Perfect alignment was shown by the Binfield Dam area which suggests that the accumulation point (high TWI) is possibly a syncline structure. The track of the low and moderate TWI section, which indicates the steep and gentle hillslope varies continuously in correlated alignment with the directions of drainage lateral scarps.

The imprints of the low and moderate TWI (steep and gentle slopes) at the southern half of the catchment, replicate braided and dendritic drainage patterns. They suggest that the non-periodic streamflow shows the potential for flash flood especially at the gentle slope path that degenerates into an accumulation zone (high TWI). The high TWI suggests the possible preferential path of active soil erosion arcs, perpendicular to the contour line (Figure 4.6). Hence, the ranking of TWI for their proneness to soil erosion was from high TWI to low (None) TWI.



4.4.2 Terrain characterization

University of Fort Hare

4.4.2.1 Topographic position index *Together in Excellence*

The TPI map reveals the areas of high convexity and concavity such that the areas of abrupt steepness and gentleness are associated with myriads of TPI signatures as indicated in the north and the south (Figures 4.6 and 4.7). The plot shows a strong visual correlation with elevation and slope information of the area (Figure 4.7). The existence of depressions was shown along the track where Tyume River runs (Figure 4.7). The variation in terrain configuration of the north where high hillslope factor may influence runoff acceleration compares to that of the south where Tyume River is braided and widens out was buffered by TPI plots. The low TPI sections are therefore considered more significant to soil erosion by water based on runoff residence time and longer duration of hydraulic action compared to the hillslope factor-influenced area.

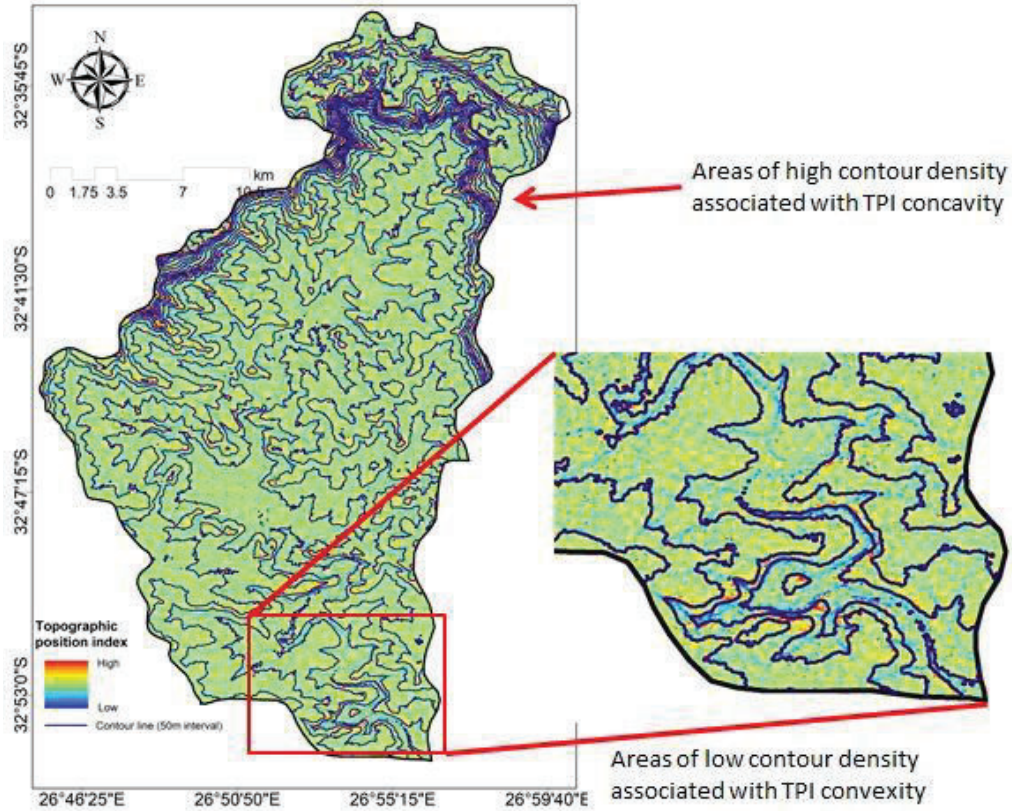


Figure 4.7. The TPI plots indicate a high visual correlation with elevation.

4.4.2.2 Terrain roughness index

The maps of terrain roughness index (TRI) and vector ruggedness measure are presented in Figure 4.8a. TRI reveals landforms corresponding to terrain features such as the hilly terrains, ridges, heaps, cols, pass, and valley. More than half of the high TRI zones show a strong visual correlation with the geologic outcrop of dolerites spanning across the northern half of the study area. This further indicates that the high TRI sections are possibly associated with zones of high resistance to erosion. Meanwhile, the flat TRI which corresponds to the plain reveals more detailed information compared to the aspect map (Figure 4.5a). The flat and low areas are therefore considered more susceptible to soil erosion by water than the moderate and high, hence they are assigned higher weightage.

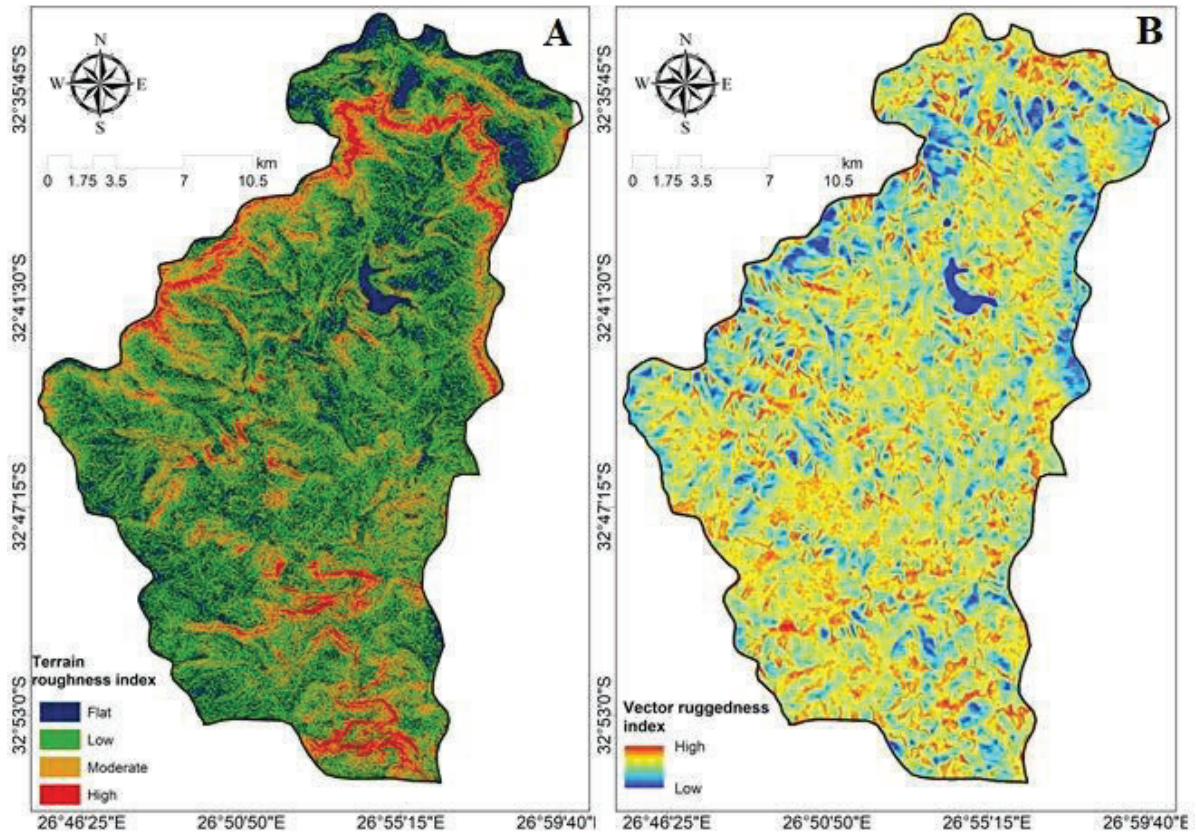


Figure 4.8 Map showing; a) the terrain roughness index (left) and; b) vector ruggedness index (right).

University of Fort Hare
Together in Excellence

4.4.2.3 Vector ruggedness measure

Vector ruggedness measure (VRM) has been acknowledged to provide more detailed information on terrain erodibility tendency based on its high-resolution estimation of the slope to a defined local scale. Hence, areas of low VRM indicate the areas where soil erodibility is possibly insignificant due to the terrain relative slope while areas of high VRM are the areas with significant potential for soil erodibility due to the combined influence of the force of gravity and hydraulic pressure. For example, the Binfield Dam area which was included under TRI as the area with a high tendency for erodibility is secluded under the VRM. Interestingly also, the regions of high TRI which are also associated with Dolerite Outcrops at the northern half of the study area were mapped as low VRM. The VRM map shows a fair and refined

visual correlation with TRI (Figure 4.8b). The north-central, map centre, and southwest tend to show high VRM. Based on the soil erodibility potential as an influence of relative slope, the force of gravity, the hydraulic pressure, areas of high VRM is prioritized with high weightage while areas of low VRM are prioritized with low weightage.

4.4.3 Geology characteristics

The lithological information of the Tyume basin is presented in Figure 4.9, comprising of a single basement (hard rock) amidst four different sedimentary rocks.

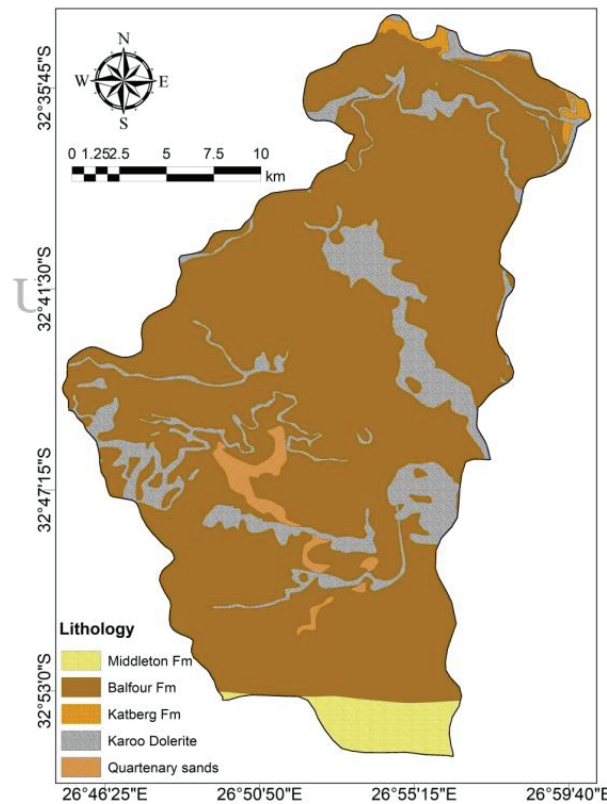


Figure 4.9 Lithology map of Tyume basin, where Fm means Formation. Middleton and Katberg Formation are arenaceous, that is, sandstone dominant, Balfour Formation is argillaceous, that is, rich in mudstone and clay materials while dolerite is a basement and clay materials while dolerite is a basement (An clipped portion from the regional geological map sheet of the Council of Geological Survey of South Africa (Robb et al., 2006)).

The dominant rock type is Balfour Formation, covering about 553 km² (81%) while the basement covers 90 km² (13%) of the whole area. The Quarternary sediments (2%) indicate the existence of periodic flash-floods. This is because the Quaternary Sediments are products of fluvial outwash from bedform assemblages through the complex interplay of climate and geo-allogenic processes such as tectonic subsidence, rifting, and hinterland erosion (Wilson et al., 2014). The high mudstone content of the Balfour Formation typifies its high tendency for soil erodibility, hence, it is scored higher weightage than the Katberg and Middleton Formations, Quarternary sands, and Dolerite which is highly resistant to hydraulic fracturing.

The spatial spread of the basement (Dolerite outcrops) has been compared to the TRI and VRM, however, the sedimentary rocks have no distinct spatial trend. The dolerite outcrops relationship with TRI indicates that the outcrops at the extreme north, west, and south are uplifted outcrops, and this is capable of intercepting and lowering runoff acceleration, and as a result, serving an offsite soil erosion zone. Meanwhile, the outcrop running from the dam area to the east is possibly emplaced as a flat-topped outcrop whereby the seal is eroded as a result of high hydraulic pressure and turbulent flow of the upper stage of Tyume River.

4.5 Soil erosion by water vulnerability zoning

The result obtained from the overlay analysis of areas vulnerable to soil erosion by water is presented in Figure 4.10. According to Table 3.6, the following thematic layers in their order of weight (in bracket) were used; LULC (16), geology (15), drainage density (15), TWI (15), TRI (15), TPI (12), and VRM (12). The vulnerability indexes mapped out are classified into five; the critically high section which covers approximately 40 km² (6%), the high zone, 135

km² (20%), the moderate, 209 km² (31%), the low, 186 km² (27%), and none vulnerable section, 113 km² (17%).

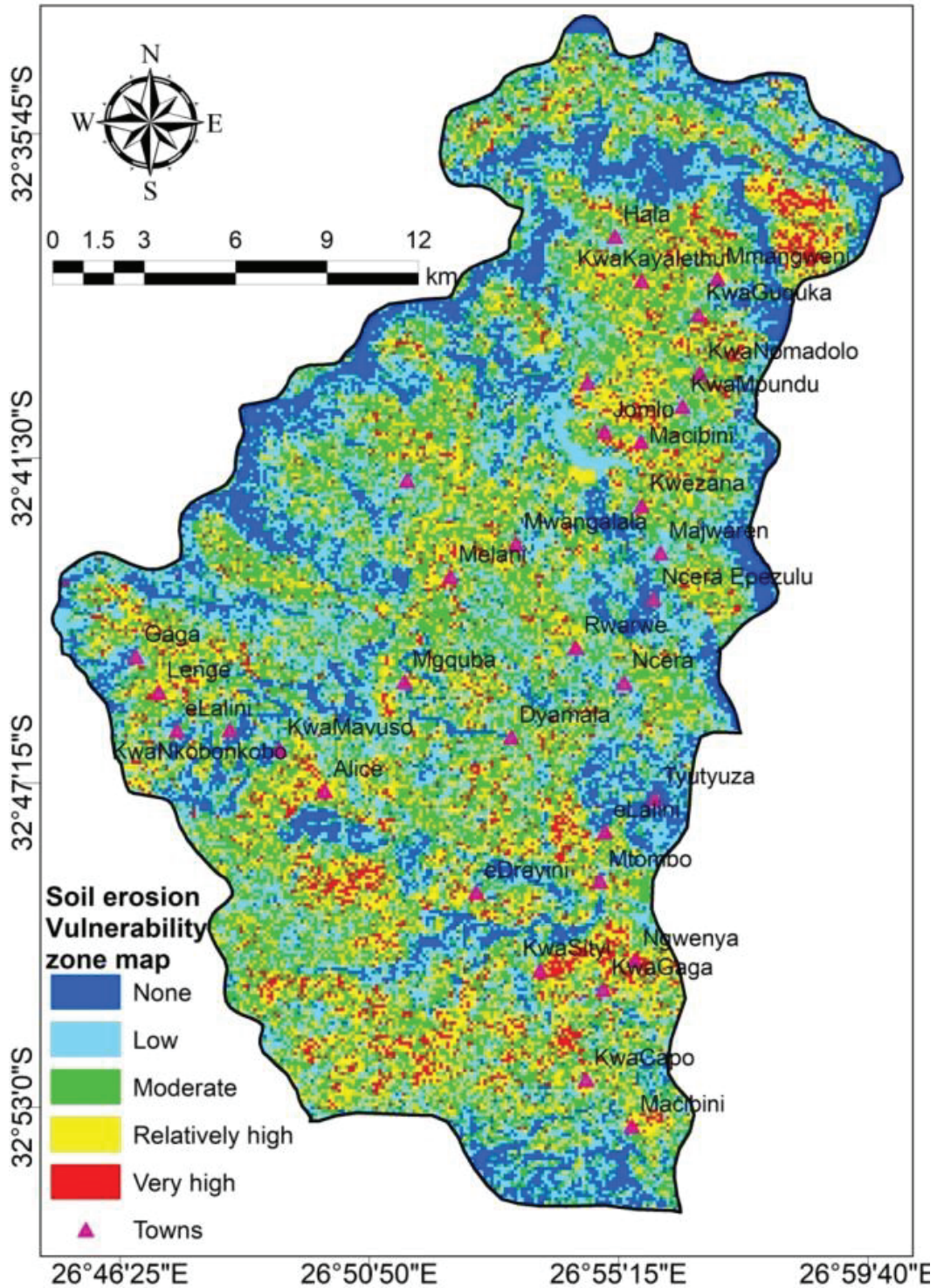


Figure 4.10 Tyume River basin vulnerability map of soil erosion by water.

The zone of high soil erosion vulnerability is more concentrated on the northwest (around Mmangweni and Macibini), centre (Jomlo), and the south (especially around KwaGaga, Ngwenya, and KwaSityi). The areas with moderate vulnerability cover 145 km² (21%), spreading around the highly vulnerable area. Fundamentally, drainage paths often follow alterable morphogenetic paths with high permeability or high susceptibility to hydraulic abrasion. Exposure and disaggregation of the soil profile of such a drainage path to accelerating runoff through human activities such as deforestation, increase in rural settlement, and certain agricultural activities render such an area vulnerable to soil erosion by water. This may have accounted for the majority of the vulnerable areas linked with the zones of human settlement. This further confirms that the increase in human settlement is the major driver of soil erosion by water.



4.6 Validation of soil erosion vulnerability map

The points of assessments were picked at random within the moderate to the highly vulnerable zones as shown in Figure 4.11. Of the sixty-three points, seven points have no soil erosion indication or erosional drainage, while twenty-one of the points show mild soil erosional tracks as shown in Figure 4.12A. 55% of the sampled field points show distinct erosional features of a gully, rill, and sheet erosions, and areas where mass wastes resulted from aggregation of the soil erosions (Figure 4.12B and Figure 4.12C). Related grid-code of sampled points were extracted in the ArcMap to provide a platform for assessment of model accuracy, validation, and corroboration (Table 4.5).

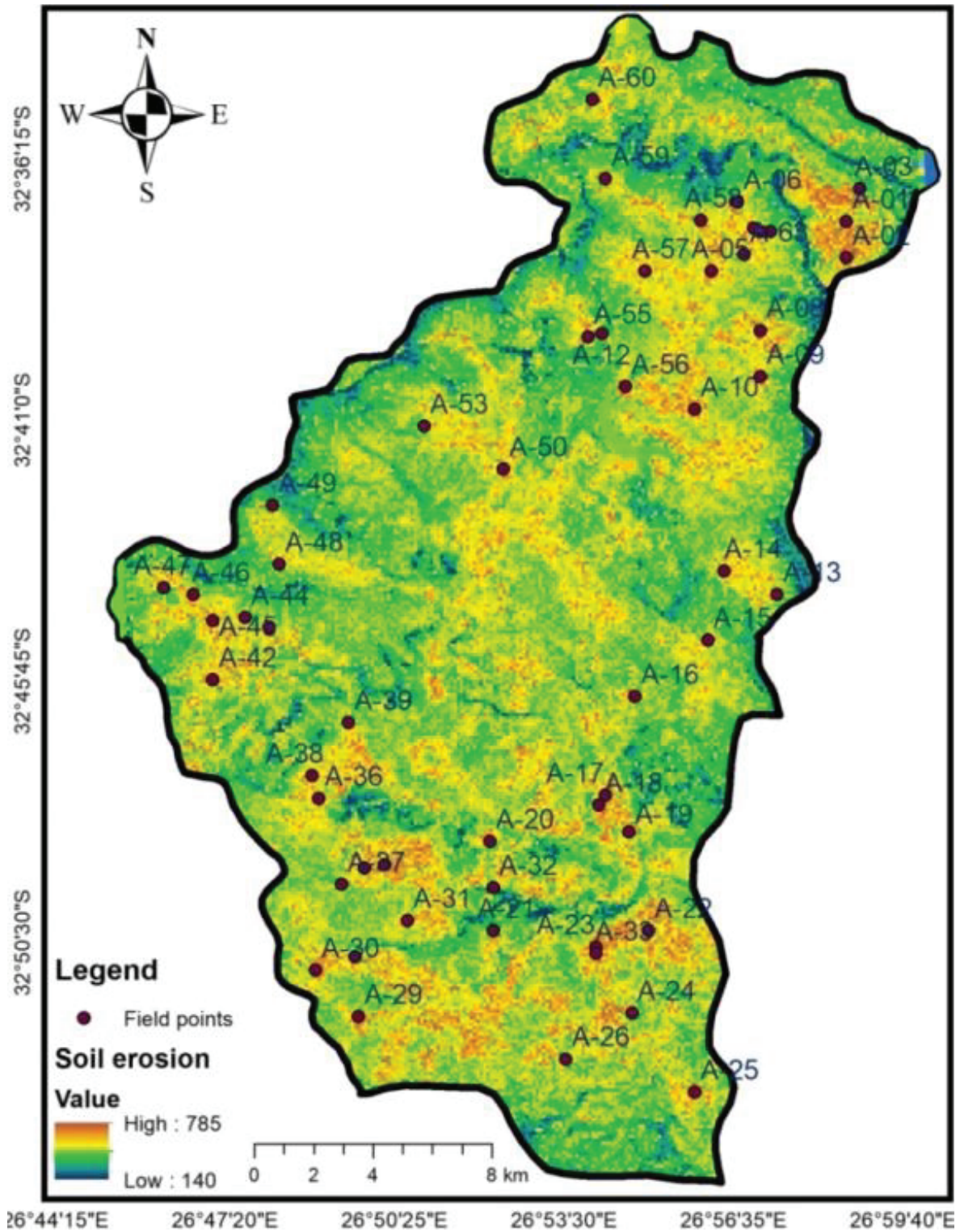


Figure 4.11 Soil erosion vulnerability maps showing the sampling points for field assessment.



Figure 4. 12A Pictorial view of areas of mild soil erosion by water (shown with blue arrows).

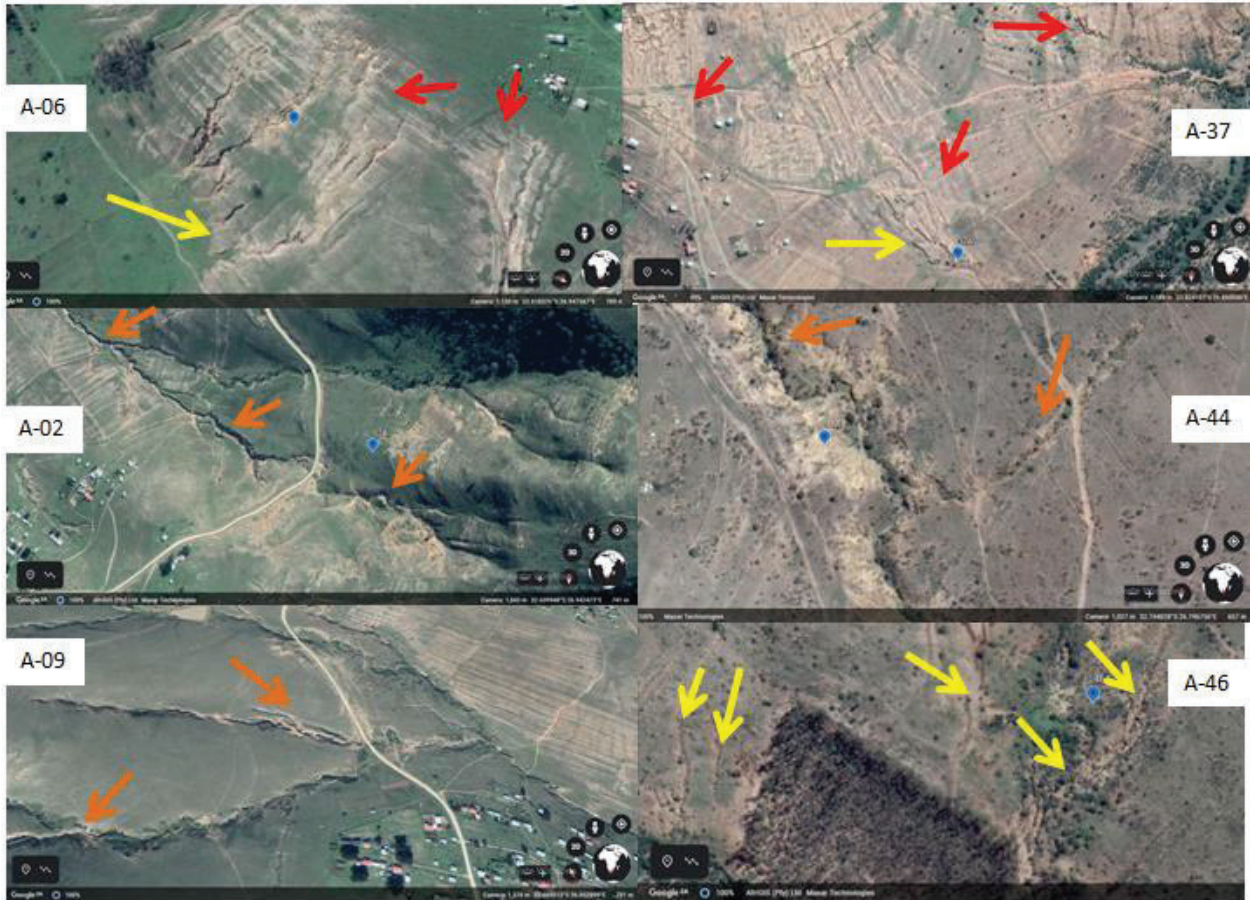


Figure 4. 12B. Pictorial view of tracks of soil erosion by water (Areas of mass waste resulting from rill erosion are shown with red arrows, rill erosion tracks are shown with yellow arrows while gully erosion is shown with orange arrows).

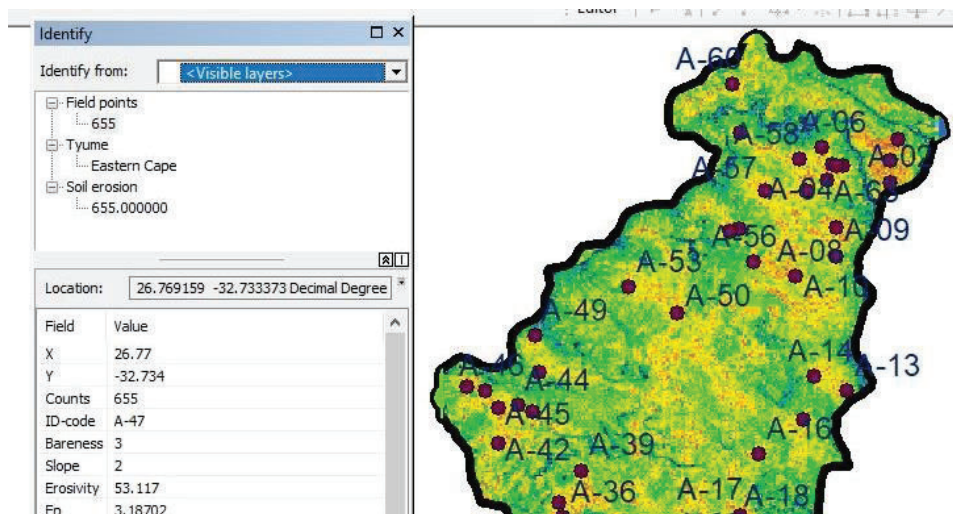


Figure 4.12 C. Extraction of soil erosion grid-codes

Table 4.5 Data of estimated erosion proneness with Tyume River basin

Longitude	Latitude	Counts	ID-code	Bareness	Slope	Erodibility	Camera
26.977	-32.623	730	A-01	4	4	120.676	753
26.977	-32.634	725	A-02	3	4	261.048	759
26.981	-32.613	690	A-03	3	4	37.5937	1035
26.951	-32.626	745	A-04	4	2	78.823	1179
26.936	-32.638	750	A-05	3	2	68.236	1027
26.944	-32.617	745	A-06	4	3	162.453	784
26.951	-32.656	655	A-08	2	3	48.745	1189
26.951	-32.67	750	A-09	3	3	274.65	789
26.931	-32.68	540	A-10	3	1	6.841	1060
26.903	-32.657	495	A-12	1	1	0.231	2160
26.956	-32.736	735	A-13	2	2	74.792	1304
26.94	-32.729	565	A-14	2	1	6.562	1217
26.935	-32.75	425	A-15	1	1	0.113	1843
26.913	-32.767	535	A-16	2	2	11.286	922
26.904	-32.797	740	A-17	3	2	69.474	1130
26.902	-32.8	735	A-18	3	3	73.392	1668
26.911	-32.808	745	A-19	3	2	67.138	1047
26.869	-32.811	730	A-20	4	2	59.261	811
26.87	-32.838	435	A-21	3	1	0.626	1520
26.917	-32.838	635	A-22	2	1	35.927	943
26.901	-32.843	550	A-23	2	2	16.588	2326
26.912	-32.863	740	A-24	3	3	98.763	668
26.931	-32.887	635	A-25	3	2	32.558	864
26.892	-32.877	550	A-26	3	3	12.256	1202
26.853	-32.877	455	A-27	2	1	0.102	2139
26.828	-32.846	490	A-28	1	1	0.145	1048
26.829	-32.864	495	A-29	1	1	0.156	1150
26.816	-32.85	470	A-30	1	1	0.245	1342
26.844	-32.835	475	A-31	3	3	0.287	1334
26.87	-32.825	490	A-32	4	3	0.234	1374
26.901	-32.844	640	A-33	2	2	23.316	867
26.837	-32.818	535	A-34	3	2	10.556	1460
26.831	-32.819	575	A-35	3	2	2.723	1162
26.817	-32.798	455	A-36	2	1	0.532	940
26.823	-32.824	710	A-37	4	3	135.939	865
26.815	-32.791	410	A-38	2	1	0.362	1609
26.826	-32.775	570	A-39	3	1	2.31	1334
26.785	-32.762	750	A-42	4	2	72.661	1204
26.802	-32.746	625	A-43	4	2	23.153	3379

The result of the scattered diagram is presented in Figure 4.13.

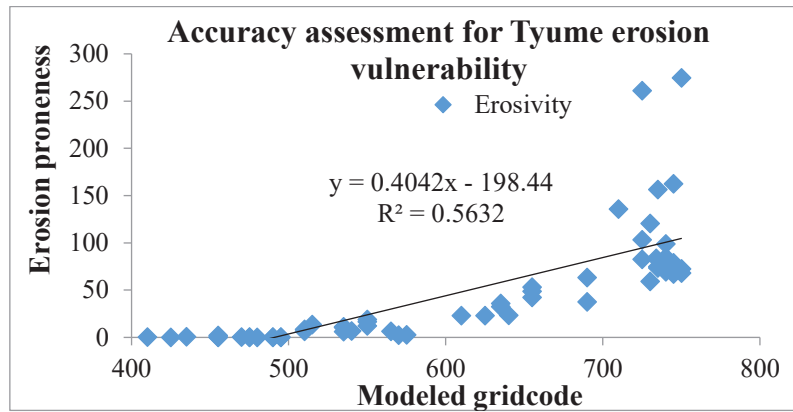


Figure 4.13 Plot of accuracy assessment of Tyume soil erosion by water modeling.

The assessment shows that there is a reliable level of confidence in the model as the actual field condition is represented as an average condition. This suggests that about 55% percent degree of evaluation is satisfied by the assessment and also indicated that the themes employed can be adopted for soil erosion modeling if the statistical classifier can be improved upon. The model was further diagnosed using the Receiver Operating Characteristics curve (ROC) due to its robustness and the in-depth information it provides (Figure 4.14).

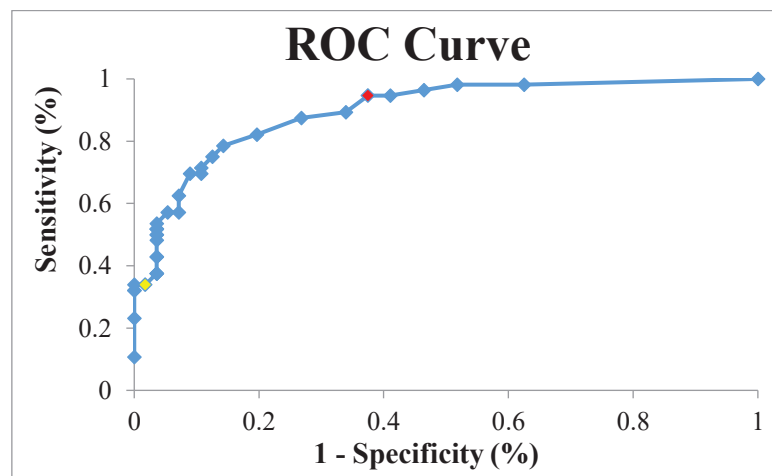


Figure 4.14 ROC curve of soil erodibility validation

The plot indicated that the model is reliable and will provide a good performance due to the concavity of the ROC curve, that is, the proximity of threshold 1 (optimum tangential path of the parabola) which drifts away from the diagonal to the standard angle. The area under the ROC is 0.899 and this implies that the degree of separability of the model between the positive and the negative outcome to the actual soil erodibility potential is excellent, reliable, and highly predictive. The optimum sensitivity and sphericity lie on 510 grid-code hence grid-codes value greater than this indicate the possible existence of soil erosion features.

The validation exercise shows that there is no discrimination between the gully and rill erosion features captured by the high zones of the vulnerability assessment. This is probably due to the resolution of the digital elevation model used which was 30 m by 30 m. Meanwhile, most of the gully features were continuous from the rill features, whereas the latter is the dominant feature in the basin. The erosion features are peculiar to the areas of bareness which is often in the proximity of settlements or townships. The majority of the eroded areas within the bare zones were characterized by rill erosion. Hillslope in the areas of high relief also contributes significantly to the soil erosion features where most features taper from sheet to gully erosional features. Most of the erosional features were connected to the natural drainage.

According to the validation, exercise shows that many of the vulnerable spots are associated with either gullies or a collection of long inter-rills. In the north, most of them lie in the bare or grassland area while in the centre and south of the basin, the vulnerable area occupies the cultivated and bare grounds surrounding the riparian lands (Figure 4.12A; A-10, A-14). The google photo showed that the bare area and grassland are deforested plots possibly for cultivation or expansion purposes. There are clear differences between the gullies and interrill created on the bare gentle land at the foothill and those created on the hillslopes as those on

the foothills are a maze of inter-rills or badlands (Figure 4.12B; A-06, A-37) while those on the hillslopes are strands of deeper inter-rills or gullies (Figure 4. 12B; A-02, A-09). The south which is the widest vulnerable area is characterized by an overgrazed expanse of rangeland whose drainage channel is badly mutilated possibly by overstocking or uncontrolled cattle patronage.

In summary, the disruption in the hydro-climatic regime and the increase of runoff intensity suggest the possible increase in rainfall erosivity and shear strength of hydraulic abrasion of the Tyume drainage path. Concurrently, the increase in temporal trend of bareness, scrubs, and veld are pointers to the cumulative susceptibility of the basin through exposure to the process of soil detachment. The non-axial trend of highly vulnerable areas flagged the impact of poor land management and inadequate spatial planning. Ground-truthing showed that poor tillage systems such as fallowing and abandonment of farm area add to the basin exposure and vulnerability of Tyume basin to soil erosion. The discussions, synthesis and critical evaluation of the findings are presented in the subsequent chapter.

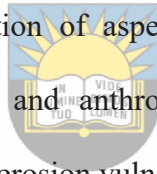


University of Fort Hare
Together in Excellence

Chapter 5: Discussion

5.1 Introduction

The study of soil erosion by water through an integrated framework model of physiographic and land use/cover characteristics has enabled the delineation of the Tyume River basin into zones of soil erosion vulnerability. The hydro-statistical trends also enabled the investigation of environmental flow which may induce soil erosion over the long term. The mapping of land use/cover dynamics provides adequate information on the land surface changes that may have enhanced environmental degradation as a result of the exposure of the soil surface and how the land cover dynamics respond to hydrological variability. The clustering of morphometric parameters enabled the visualization of aspect, physiographic roughness, and landform alteration caused by the natural and anthropic events. This chapter provides general discussions on the findings on soil erosion vulnerability assessment and its implications.



University of Fort Hare
Together in Excellence

5.2 Temporal variability that impacts soil erosion

The hydro-statistical approach in this study shows that there is a decline in the trend of streamflow, which suggests the possibility of a decline in the amount of rainfall annually, in conformity to Owolabi et al. (2021). The possible decline in the amount of annual rainfall suggests that there is possibly a decline in the amount of soil loss and sediment yield. No adequate information on the rate of soil erosion to streamflow intensity could be provided due to the scarcity of data on sediment loads and turbidity. However, soil erosion by water is expected to be high during the period of high-flow acceleration due to the potential for high rain frequency and its association with rainfall erosivity in the Tyume Basin (Owolabi et al., 2021). Nciizah and Wakindiki (2014) discovered that the erosivity of rainfall pattern has a

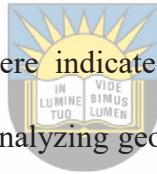
significant influence on steady-state infiltration rate and erosion processes driving the generation of streamflow within Tyume Basin and other proximal areas in the Amathole region. In this study, the streamflow rate of change serves to replicate the measure of the kinetic energy of storm-flow and rainfall intensity that influences sediment transport (Nel and Sumner, 2007), indicated to be recurrent every three years (Figure 4.1).

A visual correlation is established between the temporal trend of streamflow and the drainage size possibly induced by both the hydro-climatic contraction and the turbidity caused by human encroachment and interaction with the water body in agreement with Van Oost et al. (2009) and Wang et al. (2018). Van Oost et al. (2009) noted that the turbidity concentration and rate of human encroachment rate are strongly correlated due to construction, farming activities, and human activities that promote turbidity in streamflow. Also, Mukundan et al. (2013) indicated that the turbidity concentration, agricultural activities, and urbanization rate are the more significant metrics for soil erosion than precipitation intensity. In conformity with Mukundan et al. (2013) and Wang et al. (2018), the period of a concurrent increase in streamflow and settlement possibly indicates the period of induced soil erosion. The concurrent increase in streamflow and rural settlement occurs in 1989, 1995, 2004, 2012, and 2018, while a significant increase in bare value is associated with 1995, 2005, and 2018 in a decadal trend. The finding suggests that significant information on sediment loading and turbidity concentration in the Tyume basin is likely to exhibit a 10-year recurrent trend.

5.3 Spatial variability of soil erosion

Due to the biophysical and the socio-hydrological significance of land use/cover features, hydrological elements, and geological information, the suitability of morphometric parameters

(MPs) for modelling landscape morpho-genetical changes has not been popularly recognized. Comparison of the aspect and the drainage density suggest that Tyume drainage is characterized by the young dendritic fluvial network with low stream frequency, that is, the stream length per unit area. Aher et al. (2014) noted that the growth stage of stream geomorphology provides important information about its flood history and developmental stage. The low level of dissection exhibited by Tyume drainage suggests that the historical trend of the Tyume River is characterized by low energy fluvial style. Although, the rainforest at the north of the catchment may have played an active role in controlling the energy of stormflow at the upper stage of the Tyume River. This deduction on the gentleness of streamflow aligns with the trend of the streamflow exhibited by the time series.



The validation results obtained here indicate that morphometric parameters are reliable estimators to GIS studies and for analyzing geo-environmental changes. Their suitability for soil erosion analysis is consequential to their remote sensing resolution for altered soil conditioning factors and the watershed physiognomical configuration. The drainage density presents the visual assessment of the soil vulnerability map and the MPs showed the TPI has the most effectual contribution. This further indicates the significance of relief characteristics in the assessment of soil erosion vulnerability. This finding agrees with Hembram et al. (2019), who noted that soil erosion characteristics showed the highest sensitivity to relief characteristics among other contributing morphometric factors.

The spatial trend exhibited by the soil erosion vulnerability map indicated that the major factors contributing to soil erosion and land degradation are the land conversion from vegetated expanse to bare surface (Figure 4.10). The LU/C plot showed that the extremity of soil erosion vulnerability in the northeast Tyume is possibly due to a high degree of land cover

alternation between agricultural activities and rural settlement. This was shown to have deepened the extent of bareness in 2019. The soil erosion degree in the northeastern Tyume may have been aggravated by the hillslope and the abrupt concavity in the region. The Tyume south is characterized by a high rate of rural settlement and alternation between scrub-and-veld and bare, possibly as a result of overgrazing, and this most distorts the natural drainage channel of the Tyume basin.

The discovery of the alarming rate of soil erosion in the highlands with a high LU/C conversion rate in this study is consistent with the findings of Phinzi and Ngetar (2019) in the Umzintlava catchment, Eastern Cape, South Africa, which also shares a similar pattern of the hydrology between 1989 and 2016. Rahman (2009) also noted that vegetation loss, poorly-managed agricultural practices, poor soil quality, and climatic conditions are critical drivers of high soil erosion impacts. Hence, the outcome here aligns with Rahman's (2009) findings. Similarly, visual assessment of spatial variability in vegetation density of the LU/C plot aligns with Mhangara et al.'s (2012) findings on rainfall erosivity map within the Tyume basin. It also aligns with Phinzi and Ngetar's (2019) report on the spatial variability of hydrological intensity across the eco-topographical zones of southern Karoo. The incidence of rain-splash which triggers soil erosion as a result of high precipitation intensity in the north is expected to induce a high degree of degradation in the exposed portion of the northeast.

Meanwhile, in the south of Tyume where the downstream flow is gentle, the riparian land is covered by grasses, and this serves as the source of pasture for grazing (Mhangara et al., 2012). Chungag et al. (2017) noted that the southern terrain in this catchment is characterized by free-range animal husbandry. Disturbance of the drainage channel and physical disaggregation of soil clods and the topsoil profile, which may raise river turbidity and soil erosion among other

environmental consequences, are a consequence of river boundary grazing and overgrazing. In addition, the uncontrolled episodic overgrazing and construction activities around the riparian cause soil compaction, porosity reduction, blockage, diversion, and siltation of the drainage channel, which possibly aggravate the hydrologic alteration and the increase in streamflow discharge.

In contrast, Boardman et al. (2017) asserted that the current land degradation which culminates into badlands and gullies develops from the 200 years history of overgrazing. In support of Boardman et al. (2017), Hebinck et al. (2018) noted that the evolution of the Tyume landscape into the present state is due to the combination of historical land-use, culture, and its socio-political system. Hebinck et al. (2018) noted that the Tyume basin has been subject to unguarded continuous communal grazing, which was politically strengthened by the cattle herders committee from 1847 to 2005. The valley-bottom at the east of KwaGuquka was noted to be the most grazed area. Similarly, Smith and Hebinck (2007) noted that the overgrazed areas were converted to residential areas in the 1980s to accommodate the people who were driven out of their lands in the 1960s. Hence, the finding in the current study conforms to Chungag et al.'s (2017) assertion on soil degradation due to poor environmental practices in the area and the long-term transformation due to excessive grazing and land-use conversion by Hebinck and Lent (2007) and Hebinck et al. (2018). The study seeks advocacy for the remediation of sites already degraded by unguarded LU/C activities through afforestation policy considering the negative response of degraded land to the natural hydrological process and the potential for soil erosion.

Overall, the findings on the soil erosion vulnerability strongly correspond to Mhangara et al.'s (2012) findings on soil loss within the Tyume section of Keiskamma catchment, which was

based on the Sediment Assessment Tool for Effective Erosion Control approach. This study agrees with Mhangara et al.'s (2012) deduction that vegetation enrichment is highly instrumental in soil erosion mitigation. However, Mhangara et al. (2012) produced a significant error matrix that is consistent with the conservation rating factor used. This study, therefore, shows that geology information and terrain ruggedness index are better hybrids over the conservation rating factor used in Mhangara et al.'s (2012) approach, as the error matrix within the extremely rugged area was significantly reduced.



University of Fort Hare
Together in Excellence

Chapter 6: Conclusion and Recommendations

This study investigated the vulnerability of the Tyume River basin to soil erosion and the temporal dynamics in streamflow timing that may influence soil erosion by water. In doing so, a clustered framework modelling of morphometric parameters, geo-environmental factors, and a hydro-statistic trend was adopted. The monthly streamflow trend of Tyume River and its acceleration across twenty-eight years provided information on the periods of possible extreme hydro-meteorological events that may trigger soil erosion by water and its frequency through time. The information was corroborated with a land-use time series to examine how environmental practices in the basin were adapted to the hydro-climatic variability to induce soil erosion. GIS-based morphometric parameters were mapped, weighted, and overlaid together with land use/cover and geology maps.



The major highlight from the analysis of the historical trend of hydro-climatic oscillation is the hydrologic alteration of the streamflow discharge timing by one-hundred and ten percent. As a consequence, the amplitude (amount) of discharge and the frequency of peak discharge were increased along the timeline by four times. The study showed that the streamflow event in the Tyume basin is recurrent in high flow every three years and this points to the pattern of hydro-climatic oscillation in the environment. The plausible increase in streamflow intensity provides the standpoint for an accelerated increase in the runoff erosivity, hydraulic stress, and vulnerability of Tyume foothill to soil erosion by water. Despite the lack of rainfall information to provide the information on the distribution of rainfall erosivity, the inter-relationship between streamflow dynamics and rainfall trends as elaborated in literature provides the perception of the hydro-climatic process in Tyume Basin. The relief characteristics and the variability in ecological zoning as shown by the LU/C suggest that the

north exhibits a rainfall forest climate type whereby rainfall is likely to be characterized by high intensity and long duration compared to the south which exhibits a low-intensity rainfall, and short duration.

The collocation of the LU/C water bodies assessment with streamflow trend analysis depicted a concomitant action, projecting the effect of poor land management on catchment hydrology. Tyume waterways have been badly impacted on by human encroachment and overgrazing that results in the shrinkage of the riparian lands by one-twentieth of their size after thirty years. Moreover, the mutilation of the catchment soil structure aggravates the drainage's response to the altered hydrologic regime and consequently resulted in the increase in streamflow discharge. The formation of badlands in Tyume develop from deforestation and its conversion into farmland and rangeland, land occupancies and abandonment, and the increase in bareness caused by overgrazing around the riparian land.



University of Fort Hare

The assessment shows that the bareness of the Tyume basin contributes significantly to the susceptibility of the terrain to soil erosion by water. The east of KwaGuquka which is historically renowned as communal rangeland and the south of Tyume, renowned for unguarded continuous grazing was zoned as the most vulnerable areas to soil erosion. The bareness develops from the inelastic conversion rate between forested areas and shrubs, farmland and rangeland, and desertification of built-up areas, which is possibly due to rural-urban migration. Poor grazing and environmental practices that encroach forested and vegetated areas were identified as the possible cause of the high state of bareness in the Tyume River Basin.

The selected morphometric parameters proved to be reliable for future mapping of vulnerable areas to soil erosion by water. The drainage density reveals that Tyume is characterized by a young dendritic fluvial network. The apposition of the watershed network and TPI suggest that the fluvial pattern is characterized by a historical low energy braided sinuosity. Comparison of the historical pattern with projection depicted by the time-series further confirms the evidence of hydrologic alteration by human encroachment. Among the five MPs, TPI showed to have the strongest contribution to the mapping, possibly on account of relief influence on soil erosion. The TPI and TRI proved to be strongly significant for the identification of a highly consolidated platform and high topographic gradient based on its strong visual correlation with the outcrops of Karoo dolerite. The geology map showed that the Karoo dolerite contributes significantly to the configuration of the terrain, stability of the highly erodible soils, and settlement distribution in the Basin. Considering that Balfour formation is richly argillaceous, and dominated by expansive soils, the exposure of the non-basement terrain renders some of the area vulnerable to soil erosion by water. Hence, the areas of high potential for soil erodibility were identified based on the high TWI, high VRM, and flat TRI. This include; KwaNomadolo, KwaMbundu, KwaSityi, KwaGaga, Dyamata, and Mgquba.

The validation information showed that the assessment is moderately reliable, although, the validation shows that there are few cases of overestimation (< 5%), where small drainage picked up considerably large soil erosion grid codes. However, the study flagged the sensitive areas with high soil erosion potential. The streamflow analysis indicates that the rate of streamflow discharge may continue to accelerate every three years, hence, adequate preparation is required to forestall damages due to erosive action of the river. Specifically, this

study highlighted the problem of unsustainable land management in the Tyume Basin, which could aggravate the erosive force of hydroclimatic agents and considering the proneness of the soil to erosion. This study, therefore, calls the attention of the Department of Environment, Forestry and Fisheries, and Department of Water and Sanitation, and other concerned stakeholders to work together to review the policy against human encroachment on the riparian lands and the mutilation of river channels. Issues of deforestation, land development, and abandonment need to be addressed to control the rate of the bareness of the land which renders the basin vulnerable to soil erosion by water. Stakeholders are requested to raise awareness on the issues of land degradation as a result of overstocking of livestock and carefree grazing. Proactive steps should be taken at the identified critical spots considering the need to achieve the sustainable development goal focused on desertification combat and the restoration of degraded land and soil.



A major limitation in this study is the inability to embark on a field sampling for soil physicochemical properties to corroborate the findings with a spatial distribution map of soil erodibility factor, due to resource constraint. Ground-truthing of the obtained results and field measurements of gullies were also not possible due to the pandemics. Similarly, the study could not lay hold of the 2.5 m high resolution historical geospatial data from the National Geospatial Information for validation of the findings, due to the pandemics. However, the free available Google Earth Pro proved to be valuable for the computation of soil and channel erodibility.

This study recommends that future studies adopting this approach make use of the study area with rainfall data set from sufficient gauged stations. Soil data and numeric-based morphometric parameters may be incorporated in the future soil erosion assessment. Future

assessment may also improve the model accuracy by employing statistical classifiers such as analytical hierarchical process, frequency ratio, logistic regression, or machine learning techniques such as multivariate adaptive regression splines, artificial neural network, and radial basis function. To build on this study in the future, the researchers would be interested in assessing how the GIS-based morphometric analysis aligns with the numerical model of morphometric analysis. The researcher would be interested in examining the robustness of the geomorphometric estimators based on their correlation analysis with soil erodibility factors and other soil erodibility indices derived from soil physicochemical properties. Overall, the present approach is suitable for soil erosion assessment in any environment and a comparative assessment with the Revised Universal Soil Loss Equation or Sediment Assessment Tool for Effective Erosion Control approach may provide strong ramification.



University of Fort Hare
Together in Excellence

References

- Abdalla, M., Hastings, A., Cheng, K., Yue, Q., Chadwick, D., Espenberg, M., and Smith, P. (2019). A critical review of the impacts of cover crops on nitrogen leaching, net greenhouse gas balance, and crop productivity. *Global Change Biology*, 25(8), 2530-2543.
- Aher, P. D., Adinarayana, J., and Gorantiwar, S. D. (2014). Quantification of morphometric characterization and prioritization for management planning in semi-arid tropics of India: a remote sensing and GIS approach. *Journal of Hydrology*, 511, 850-860.
- Al-Wadaey, A. and Ziadat, F. (2014). A participatory GIS approach to identify critical land degradation areas and prioritize soil conservation for mountainous olive groves (case study). *Journal of Mountain Science*, 11(3), 782-791.
- Altaf, S., Meraj, G., and Romshoo, S. A. (2014). Morphometry and land cover-based multi-criteria analysis for assessing the soil erosion susceptibility of the western Himalayan watershed. *Environmental Monitoring and Assessment*, 186(12), 8391-8412.
- Amatulli, G., McInerney, D., Sethi, T., Strobl, P., and Domisch, S. (2020). Geomorpho90m, empirical evaluation and accuracy assessment of global high-resolution geomorphometric layers. *Scientific Data*, 7(1), 1-18.
- Anh, P. T. Q., Gomi, T., MacDonald, L. H., Mizugaki, S., Van Khoa, P., and Furuichi, T. (2014). Linkages among land use, macronutrient levels, and soil erosion in northern Vietnam: a plot-scale study. *Geoderma*, 232, 352-362.
- Anyamba, A., Tucker, C. J., and Mahoney, R. (2002). From El Niño to La Niña: Vegetation response patterns over east and southern Africa during the 1997–2000 period. *Journal of Climate*, 15(21), 3096-3103.
- Arabameri, A., Chen, W., Loche, M., Zhao, X., Li, Y., Lombardo, L., Cerda, A., Pradhan, B., and Bui, D.T. (2020). Comparison of machine learning models for gully erosion susceptibility mapping. *Geoscience Frontiers*, 11(5), 1609-1620.
- Arnold, J. G., Srinivasan, R., Mutiah, R. S., and Williams, J. R. (1998). Large area hydrologic modeling and assessment part I: model development 1. *JAWRA Journal of the American Water Resources Association*, 34(1), 73-89.

- Asfaw, A., Simane, B., Hassen, A., and Bantider A. (2018). Variability and time series trend analysis of rainfall and temperature in Northcentral Ethiopia: A case study in Woleka sub-basin. *Weather and Climate Extremes*, 19, 29-41.
- Ashok, K., Behera, S. K., Rao, S. A., Weng, H., and Yamagata, T. (2007). An unusual coupled mode in the tropical Pacific during 2004. *Journal of Geophysical Research*, 28, 4499– 4502.
- Balasubramanian, A. (2017). Soil erosion—causes and effects. Centre for Advanced Studies in Earth Science, University of Mysore, Mysore. <https://doi.org/10.13140/RG.2.2.26247.39841>
- Batista, P. V., Davies, J., Silva, M. L., and Quinton, J. N. (2019). On the evaluation of soil erosion models: Are we doing enough? *Earth-Science Reviews*, 197, 10-28.
- Baetens, J. M., Verbist, K., Cornelis, W. M., Gabriels, D., and Soto, G. (2009). On the influence of coarse fragments on soil water retention. *Water Resources Research*, 45(7), W07408.
- Baiyegunhi, C. and Gwavava, O. (2017). Magnetic investigation and 2½ D gravity profile modelling across the Beattie magnetic anomaly in the Southeastern Karoo Basin, South Africa. *Acta Geophysica*, 65(1), 119-138.
- Beckers, E., Pichault, M., Pansak, W., Degré, A., and Garré, S. (2016). Characterization of stony soils' hydraulic conductivity using laboratory and numerical experiments. *Soil*, 2, 421-431.
- Bennett, J. M., Marchuk, A., Marchuk, S., and Raine, S. R. (2019). Towards predicting the soil-specific threshold electrolyte concentration of soil as a reduction in saturated hydraulic conductivity: The role of clay net negative charge. *Geoderma*, 337, 122-131.
- Berendse, F., van Ruijven, J., Jongejans, E., and Keesstra, S. (2015). Loss of plant species diversity reduces soil erosion resistance. *Ecosystems*, 18(5), 881-888.
- Bernatek-Jakiel, A., and Poesen, J. (2018). Subsurface erosion by soil piping: significance and research needs. *Earth-Science Reviews*, 185, 1107-1128.
- Bhatt, S. and Ahmed, S. A. (2014). Morphometric analysis to determine floods in the Upper Krishna basin using Cartosat DEM. *Geocarto International*, 29(8), 878-894.
- Blair, D., Shackleton, C. M., and Mograbi, P. J. (2018). Cropland abandonment in South African smallholder communal lands: Land cover change (1950–2010) and farmer perceptions of contributing factors. *Land*, 7(4), 121.

- Boardman, J., Foster, I. D., Rowntree, K. M., Favis-Mortlock, D. T., Mol, L., Suich, H., and Gaynor, D. (2017). Long-term studies of land degradation in the Sneeuberg uplands, eastern Karoo, South Africa: a synthesis. *Geomorphology*, 285, 106-120.
- Boardman, J., Parsons, A. J., Holland, R., Holmes, P. J. and Washington, R. (2003). Development of badlands and gullies in the Sneeuberg, Great Karoo, South Africa. *Catena*, 50(2-4), pp.165-184.
- Bogaart, P. W. and Troch, P. A. (2006). Curvature distribution within hillslopes and catchments and its effect on the hydrological response. *Hydrology and Earth System Sciences Discussions*, European Geosciences Union, 3 (3), 1071-1104
- Boix-Fayos, C., Martínez-Mena, M., Arnau-Rosalén, E., Calvo-Cases, A., Castillo, V., and Albaladejo, J. (2006). Measuring soil erosion by field plots: Understanding the sources of variation. *Earth-Science Reviews*, 78(3-4), 267-285.
- Bosino, A., Giordani, P., Quénéhervé, G., and Maerker, M. (2020). Assessment of Calanchi and rill-interrill erosion susceptibilities using terrain analysis and geostochastics: A case study in the Oltrepo Pavese, Northern Apennines, Italy. *Earth Surface Processes and Landforms*, 45(12), 3025-3041.
- Breetzke, G. D., Koomen, E., and Critchley, W. R. S. (2013). GIS-assisted modelling of soil erosion in a South African catchment: evaluating the USLE and SLEMSA approach. In: Wurbs R. (Ed), *Water resources planning, development and management*. Rijeka (Croatia): InTech, pp 53–71.
- Capotondi, A., Wittenberg, A. T., Newman, M., Di Lorenzo, E., Yu, J. Y., Braconnot, P., and Jin, F. F. (2015). Understanding ENSO diversity. *Bulletin of the American Meteorological Society*, 96(6), 921-938.
- Cassidy, R., Doody, D. G., and Watson, C. J. (2017). Impact of legacy soil phosphorus on losses in drainage and overland flow from grazed grassland soils. *Science of the Total Environment*, 575, 474-484.
- Chungag, A., Tol, J. J. V., and Magagula, B. (2017). Effect of unguided cattle husbandry on selected soil physical properties in common property regimes in Alice, Eastern Cape Province, South Africa. *Range Management and Agroforestry*, 38(2), 176-180.

- Compton, J. S., Herbert, C. T., Hoffman, M. T., Schneider, R. R., and Stuu, J. B. (2010). A tenfold increase in the Orange River means Holocene mud flux: implications for soil erosion in South Africa. *The Holocene*, 20(1), 115-122.
- Cox, J. and Pitman, A. (2002). Catchment scale water and soil balance modelling in Southern Australia. In 12th ISCO Conference Beijing (pp. 1-8). Sourced from: <https://www.tucson.ars.ag.gov/isco/isco12/VolumeII/CatchmentScaleWaterandSoilBalance.pdf>
- de Hipt, F. O., Diekkrüger, B., Steup, G., Yira, Y., Hoffmann, T., Rode, M., and Näschen, K. (2019). Modeling the effect of land use and climate change on water resources and soil erosion in a tropical West African catchment (Dano, Burkina Faso) using SHETRAN. *Science of the Total Environment*, 653, 431-445.
- DEA (Department Environmental Affairs, RSA) (2015). 2013 - 2014 South African national land-cover dataset. online avail. <https://egis.environment.gov.za/> (last mod.: 2015-07-30) (accessed: 2020-10-10).
- Devia, G. K., Ganasri, B. P., and Dwarakish, G. S. (2015). A review on hydrological models. *Aquatic Procedia*, 4, 1001-1007.
- Dijkshoorn, J. A., van Engelen, V. W. P., and Huting, J. R. M. (2008). Soil and landform properties for LADA partner countries (Argentina, China, Cuba, Senegal and The Gambia, South Africa, and Tunisia). ISRIC report 2008/06 and GLADA report 2008/03, ISRIC – World Soil Information and FAO, Wageningen (23).
- Diop, S., Stapelberg, F., Tegegn, K., Ngubelanga, S., and Heath, L. (2011). A review on problem soils in South Africa. Council for Geoscience Report number: 2011-0062
- Dougherty, E. R., Kim, S., and Chen, Y. (2000). Coefficient of determination in nonlinear signal processing. *Signal Processing*, 80(10), 2219-2235.
- Drzewiecki, W., Wężyk, P., Pierzchalski, M., and Szafrńska, B. (2014). Quantitative and qualitative assessment of soil erosion risk in Małopolska (Poland), supported by an object-based analysis of high-resolution satellite images. *Pure and Applied Geophysics*, 171(6), 867-895.
- Du Preez, P. J. and Brown, L. R. (2011). Impact of domestic animals on ecosystem integrity of Lesotho high altitude peatlands. In Grillo, O. and Venora, G. (Eds.), *Ecosystems Biodiversity*. Intech, Croatia, pp. 249-270.

- DWS (Department of Water and Sanitation) (2017). Hydrological services - surface water: Reservoir sites, online avail. <https://www.dwa.gov.za/Hydrology/Verified/HyCatalogue.aspx>.
- El Jazouli, A., Barakat, A., Khellouk, R., Rais, J., and El Baghdadi, M. (2019). Remote sensing and GIS techniques for prediction of land use land cover change effects on soil erosion in the high basin of the Oum Er Rbia River (Morocco). *Remote Sensing Applications: Society and Environment*, 13, 361-374.
- Elges, H. F. W. K. (1985). Dispersive soils: problem soils in South Africa - state of the art The Civil Engineer in South Africa, 27, 347-353.
- Engelbrecht, C. J. and Landman, W. A. (2016). Interannual variability of seasonal rainfall over the Cape south coast of South Africa and synoptic type association. *Climate Dynamics*, 47(1-2), 295-313.
- Evans, R. (2002). An alternative way to assess water erosion of cultivated land—field-based measurements: and analysis of some results. *Applied Geography*, 22(2), 187-207.
- FAO, I., 2015. Status of the world's soil resources (SWSR)—main report. Food and agriculture organization of the United Nations and intergovernmental technical panel on Soils, Rome, Italy, 650.
- Farooq, M. U., Mujtaba, H., Farooq, K., Sivakugan, N., and Das, B. M. (2020). Evaluation of stability and erosion characteristics of soil embankment slope reinforced with different natural additives. *Iranian Journal of Science and Technology, Transactions of Civil Engineering*, 44 (Suppl. 1), S515–S524.
- Fawcett, T. (2006). An introduction to ROC analysis. *Pattern Recognition Letters*, 27(8), 861-874.
- Fey, M. and Gilkes, R. (2010). A short guide to the soils of South Africa, their distribution and correlation with World Reference Base soil groups. In: Gilkes R.J. and Prakongkep, N. (Eds), *Soil solutions for a changing world: proceedings of the 19th World Congress of Soil Science, Brisbane, Australia, 1–6 August 2010*. Crawley: International Union of Soil Sciences, 32–35
- Fiès, J. C., Louvigny, N. D. E., and Chanzy, A. (2002). The role of stones in soil water retention. *European Journal of Soil Science*, 53(1), 95-104.

- Flanagan, D. C. and Nearing, M. A. (1995). USDA-Water erosion prediction project: Hillslope profile and watershed model documentation. National Soil Erosion Research Laboratory, West Lafayette, Indiana Report No. 10., 123pp.
- Frankl, A., Poesen, J., Deckers, J., Haile, M. and Nyssen, J. (2012). Gully head retreat rates in the semi-arid highlands of Northern Ethiopia. *Geomorphology*, 173, 185-195.
- Gajbhiye, S., Mishra, S. K., and Pandey, A. (2014). Prioritizing erosion-prone area through morphometric analysis: an RS and GIS perspective. *Applied Water Science*, 4(1), 51-61.
- Gao, P. and Puckett, J. (2012). A new approach for linking event-based upland sediment sources to downstream suspended sediment transport. *Earth Surface Processes and Landforms*, 37(2), 169-179.
- Gassman, P. W., Reyes, M. R., Green, C. H., and Arnold, J. G. (2007). The soil and water assessment tool: historical development, applications, and future research directions. *Transactions of the ASABE*, 50(4), 1211-1250.
- Gessesse, B., Bewket, W., and Bräuning, A. (2015). Model-based characterization and monitoring of runoff and soil erosion in response to land use/land cover changes in the Modjo watershed, Ethiopia. *Land degradation & Development*, 26(7), 711-724.
- Gholami, H., Kordestani, M. D., Li, J., Telfer, M. W., and Fathabadi, A. (2019). Diverse sources of aeolian sediment revealed in an arid landscape in southeastern Iran using a modified Bayesian un-mixing model. *Aeolian Research*, 41, 15-47.
- Gillan, J. K., Karl, J. W., Barger, N. N., Elaksher, A., and Duniway, M. C. (2016). Spatially explicit rangeland erosion monitoring using high-resolution digital aerial imagery. *Rangeland Ecology & Management*, 69(2), 95-107.
- Gehring, J., Ferrone, A., Billault-Roux, A. C., Besic, N., Ahn, K. D., Lee, G., and Berne, A. (2021). Radar and ground-level measurements of precipitation collected by the École Polytechnique Fédérale de Lausanne during the International Collaborative Experiments for PyeongChang 2018 Olympic and Paralympic winter games. *Earth System Science Data*, 13(2), 417-433.
- Gruber, F. E., Baruck, J., Mair, V., and Geitner, C. (2019). From geological to soil parent material maps-A random forest-supported analysis of geological map units and topography to support soil survey in South Tyrol. *Geoderma*, 354, 11-38.

- Gyssels, G., Poesen, J., Bochet, E., and Li, Y. (2005). Impact of plant roots on the resistance of soils to erosion by water: a review. *Progress in Physical Geography*, 29(2), 189-217.
- Hamed, K. H. (2008). Trend detection in hydrologic data: the Mann–Kendall trend test under the scaling hypothesis. *Journal of Hydrology*, 349(3-4), 350-363.
- Hassen, G. and Bantider, A. (2020). Assessment of drivers and dynamics of gully erosion in case of Tabota Koromo and Koromo Danshe watersheds, South Central Ethiopia. *Geoenvironmental Disasters*, 7(1), 1-13.
- Hebinck, P. G. M. and Lent, P. C. eds. (2007). *Livelihoods and landscapes: the people of Guquka and Koloni and their resources (Vol. 9)*. Brill: Leiden.
- Hebinck, P., Mtati, N., and Shackleton, C. (2018). More than just fields: Reframing deagrarianisation in landscapes and livelihoods. *Journal of Rural Studies*, 61, 323-334.
- Hemram, T. K., Paul, G. C., and Saha, S. (2019). Comparative analysis between morphometry and geo-environmental factor-based soil erosion risk assessment using the weight of evidence model: a study on Jainti River Basin, Eastern India. *Environmental Processes*, 6(4), 883-913.
- Henson, S. A., Beaulieu, C., and Lampitt, R. (2016). Observing climate change trends in ocean biogeochemistry: when and where. *Global Change Biology*, 22(4), 1561-1571.
- Hladky, J., Kynický, J., Dvořáčková, H., Elbl, J., and Brtnický, M. (2017). Effect of long-term erosion on humus content and quality on chernozem soils. *International Multidisciplinary Scientific GeoConference: SGEM*, 17, 179-184.
- Hlaing, K. T., Haruyama, S., and Aye, M. M. (2008). Using GIS-based distributed soil loss modeling and morphometric analysis to prioritize watershed for soil conservation in Bago river basin of Lower Myanmar. *Frontiers of Earth Science in China*, 2(4), 465-478.
- Hoell, A., Funk, C., Zinke, J., and Harrison, L. (2017). Modulation of the Southern Africa precipitation response to the El Niño Southern Oscillation by the subtropical Indian Ocean dipole. *Climate Dynamics*, 48(7-8), 2529-2540.
- Hoffman, M. T. and Todd, S. (2000). A national review of land degradation in South Africa: the influence of biophysical and socio-economic factors. *Journal of Southern African Studies*, 26(4), 743-758.
- Hojati, M. and Mokarram, M. (2016). Determination of a topographic wetness index using high-resolution digital elevation models. *European Journal of Geography*, 7(4), 41-52.

- Hosseini, S. H. and Khaleghi, M. R. (2020). Application of SWAT model and SWAT-CUP software in simulation and analysis of sediment uncertainty in arid and semi-arid watersheds (case study: the Zoshk–Abardeh watershed). *Modeling Earth Systems and Environment*, 6, 1-11.
- Hudson, N. (1993). Field measurement of soil erosion and runoff (Vol. 68). Food & Agriculture Organisation. *Soils Bulletin*, 68, 139 pp.
- Issaka, S. and Ashraf, M. A. (2017). Impact of soil erosion and degradation on water quality: a review. *Geology, Ecology, and Landscapes*, 1(1), 1-11.
- Jain, M. K., Kothiyari, U. C., and Raju, K. G. (2005). GIS-based distributed model for soil erosion and rate of sediment outflow from catchments. *Journal of Hydraulic Engineering*, 131(9), 755-769.
- Jadidoleslam, N., Mantilla, R., Krajewski, W. F., and Goska, R. (2019). Investigating the role of antecedent SMAP satellite soil moisture, radar rainfall and MODIS vegetation on runoff production in an agricultural region. *Journal of Hydrology*, 579, 124-130.
- Janzen, H. H., Campbell, C. A., Gregorich, E. G., and Ellert, B. H. (1997). Soil carbon dynamics in Canadian agroecosystems. *Soil processes and the carbon cycle*. CRC Press, Boca Raton, FL, 57-80.
- Jenness, J. (2006). Topographic position index (tpi_jen. avx) extension for ArcView 3. x, v. 1.3 a. Jenness Enterprises.
- Johnston, M. A. (1981). Properties of selected soils derived from Middle Ecca and Dwyka sediments with particular reference to their physical sensitivity to sodium. In Paper delivered at the 10th National Congress of the Soil Science Society of South Africa, East London.
- Jomaa, S., Barry, D. A., Heng, B. C. P., Brovelli, A., Sander, G. C., and Parlange, J. Y. (2013). Effect of antecedent conditions and fixed rock fragment coverage on soil erosion dynamics through multiple rainfall events. *Journal of Hydrology*, 484, 115-127.
- Kakembo, V. (2001). Trends in vegetation degradation in relation to land tenure, rainfall, and population changes in Peddie district, Eastern Cape, South Africa. *Environmental Management*, 28(1), 39-46.
- Kendall, M. G. (1975). Rank correlation methods. 2nd impression. Charles Griffin and Company Ltd. London and High Wycombe.

- Khetdan, C., Chittamart, N., Tawornpruek, S., Kongkaew, T., Onsamrarn, W., and Garré, S. (2017). Influence of rock fragments on hydraulic properties of Ultisols in Ratchaburi Province, Thailand. *Geoderma Regional*, 10, 21-28.
- Kisi, O. and Ay, M. (2014). Comparison of Mann–Kendall and innovative trend method for water quality parameters of the Kizilirmak River, Turkey. *Journal of Hydrology*, 513, 362-375.
- Kumar, A., Bilker, W., Jin, Z., and Udupa, J. (2000). Atrophy and high-intensity lesions: complementary neurobiological mechanisms in late-life major depression. *Neuropsychopharmacology*, 22(3), 264-274.
- Lakhraj-Govender, R. and Grab, S. W. (2019). Assessing the impact of El Niño–Southern Oscillation on South African temperatures during austral summer. *International Journal of Climatology*, 39(1), 143-156.
- Lal, R., Hall, G. F., and Miller, F. P. (1989). Soil degradation: I. Basic processes. *Land Degradation & Development*, 1(1), 51-69.
- Lambin, E. F. (1997). Modelling and monitoring land-cover change processes in tropical regions. *Progress in Physical Geography*, 21(3), 375-393.
- Le Roux, J. J. (2011). Monitoring soil erosion in South Africa at a regional scale. Geohazards Project Report for the Council of Geoscience; ARC-ISCW Report No. GW/A/2011/23 Project GW, 59(004).
- Le Roux, J. J. (2015). Sediment yield modelling in the Mzimvubu River Catchment: Report to the Water Research Commission. Water Research Commission: Pretoria.
- Le Roux, J. J. and Sumner, P. D. (2012). Factors controlling gully development: comparing continuous and discontinuous gullies. *Land Degradation & Development*, 23(5), 440-449.
- Le Roux, J. J., Mashimbye, Z. E., Weepener, H. L., Newby, T. S., and Pretorius, D. J. (2008). Erosion status of priority tertiary catchment areas identified by the soil protection strategy of the Department of Agriculture. ISCW Report No. GW/A/2008/17. ARC-Institute for Soil, Climate, and Water: Pretoria.
- Le Roux, J. J., Newby, T. S., and Sumner, P. D. (2007). Monitoring soil erosion in South Africa at a regional scale: review and recommendations. *South African Journal of Science*, 103(7-8), 329-335.

- Leh, M., Bajwa, S., and Chaubey, I. (2013). Impact of land-use change on erosion risk: an integrated remote sensing, geographic information system, and modeling methodology. *Land Degradation & Development*, 24(5), 409-421.
- Lei, S., Chen, H., Bian, Z., and Liu, Z. (2016). Evaluation of integrating topographic wetness index with backscattering coefficient of TerraSAR-X image for soil moisture estimation in a mountainous region. *Ecological Indicators*, 61, 624-633.
- Lema, B., Mesfin, S., Kebede, F., Abraha, Z., Fitiwy, I., and Haileselassie, H. (2019). Evaluation of soil physical properties of long-used cultivated lands as a deriving indicator of soil degradation, north Ethiopia. *Physical Geography*, 40(4), 323-338.
- Lentsoane, P. M. M. (2006). Evaluation of erosion models and field assessment methods as tools for monitoring and evaluation of soil erosion in LandCare (Doctoral dissertation, University of Pretoria).
- Li, Y., Li J., Are, K. S., Huang Z., Yu H., and Zhang Q. (2019). Livestock grazing significantly accelerates soil erosion more than climate change in Qinghai-Tibet Plateau: Evidenced from ^{137}Cs and ^{210}Pb measurements. *Agriculture, Ecosystems and Environment*, 285, 1-8
- Liggit, B. and Fincham, R. J. (1989). Gully erosion: the neglected dimension in soil erosion research, *South Africa Journal Science*, 85 (1989), pp. 18-30.
- Liu, D. and She, D. (2017). Can rock fragment cover maintain soil and water for saline-sodic soil slopes under coastal reclamation? *Catena*, 151, 213-224.
- Liu, K., Hou, X., Ren, Z., Lowe, R., Wang, Y., Li, R., and Wu, H. (2020). Climate factors and the East Asian summer monsoon may drive large outbreaks of dengue in China. *Environmental Research*, 183, 109-119.
- Liu, J., Li, S., Ouyang, Z., Tam, C., and Chen, X. (2008). Ecological and socioeconomic effects of China's policies for ecosystem services. *Proceedings of the National academy of Sciences*, 105(28), 9477-9482.
- Liu, G., Xiao, H., Liu, P., Zhang, Q., and Zhang, J. (2016). An improved method for tracing soil erosion using rare earth elements. *Journal of soils and sediments*, 16(5), 1670-1679.
- Liu, X., Zhang, S., Zhang, X., Ding, G., and Cruse, R. M. (2011). Soil erosion control practices in northeast China: A mini-review. *Soil and Tillage Research*, 117, 44-48.

- Magliulo, P. (2012). Assessing the susceptibility to water-induced soil erosion using a geomorphological, bivariate statistics-based approach. *Environmental Earth Sciences*, 67(6), 1801-1820.
- Mahajan, S. and Sivakumar, R. (2018). Evaluation of physical and morphometric parameters for water resource management in Gad Watershed, Western Ghats, India: an integrated geoinformatics approach. *Environmental Earth Sciences*, 77(15), 556.
- Mann, H. B. (1945). Nonparametric tests against trend. *Econometrica: Journal of the Econometric Society*, pp.245-259.
- Mararakanye, N. and Le Roux, J. J. (2011). Manual digitizing of gully erosion in South Africa using high-resolution SPOT 5 satellite imagery at 1: 10 000 scales. Department of Agriculture, Forestry and Fisheries report: Pretoria.
- Mararakanye, N. and Nethengwe, N. S. (2012). Gully features extraction using remote sensing techniques. *South African Journal of Geomatics*, 1(2), 109-118.
- Mararakanye, N. and Sumner, P. D. (2017). Gully erosion: A comparison of contributing factors in two catchments in South Africa. *Geomorphology*, 288, 99-110.
- Masterson, V. A. (2016). Sense of place and culture in the landscape of home: understanding social-ecological dynamics on the Wild Coast, South Africa. PhD thesis. Stockholm University, Stockholm.
- Mchunu, C. N., Lorentz, S., Jewitt, G., Manson, A., and Chaplot, V. (2011). No-till impact on soil and soil organic carbon erosion under crop residue scarcity in Africa. *Soil Science Society of America Journal*, 75(4), 1503-1512.
- Meehl, G. A., Hu, A., and Teng, H. (2016). Initialized decadal prediction for transition to positive phase of the Interdecadal Pacific Oscillation. *Nature Communications*, 7(1), 1-7.
- Mehri, A., Salmanmahiny, A., Tabrizi, A. R. M., Mirkarimi, S. H. and Sadoddin, A. (2018). Investigation of likely effects of land use planning on reduction of soil erosion rate in river basins: A case study of the Gharesoo River Basin. *Catena*, 167, 116-129.
- Mhangara, P., Kakembo, V., and Lim, K. J. (2012). Soil erosion risk assessment of the Keiskamma catchment, South Africa using GIS and remote sensing. *Environmental Earth Sciences*, 65(7), 2087-2102.
- Mills, M. and Wilson, W., (1952). Land tenure. Keiskammahoek Rural Survey, vol. 4 Shuter & Shooter: Pietermaritzburg.

- Mishra, A. K. and Singh, V. P., 2010. Changes in extreme precipitation in Texas. *Journal of Geophysical Research: Atmospheres*, 115(D14).
- Modi, A., Tare, V., and Chaudhuri, C. (2021). Usage of long-term river discharge data in water balance model for assessment of trends in basin storages. *Modeling Earth Systems and Environment*, 7, 953–966.
- Mohammad, A. G. and Adam, M. A. (2010). The impact of vegetative cover type on runoff and soil erosion under different land uses. *Catena*, 81(2), 97-103.
- Montanarella, L., 2015. Agricultural policy: Govern our soils. *Nature News*, 528(7580), 32.
- Montanarella, L., Pennock, D.J., McKenzie, N., Badraoui, M., Chude, V., Baptista, I., Mamo, T., Yemefack, M., Singh Aulakh, M., Yagi, K., and Young Hong, S. (2016). World's soils are under threat. *Soil*, 2(1), pp.79-82.
- Morgan, R.P.C. (2009). *Soil erosion and conservation*. John Wiley & Sons.
- Morgan, R.P.C., Quinton, J.N., Smith, R.E., Govers, G., Poesen, J.W.A., Auerswald, K., Chisci, G., Torri, D., and Styczen, M. E. (1998). The European soil erosion model (EUROSEM): a dynamic approach for predicting sediment transport from fields and small catchments. *Earth Surface Processes and Landforms*, 23(6), 527-544.
- Mostert, N. (1992). *Frontiers. The epic of South Africa's creation and the tragedy of the Xhosa People*. Pimlico: London. *Together in Excellence*
- Moyo, M. (2017). Impacts of sustainable land management practices on soil physical properties and agricultural drought adaptation in Eastern Cape, South Africa. Master's thesis, Pan African University Institute for Water and Energy Sciences. <http://repository.pauwes-cop.net/handle/1/142>
- Msadala, V., Gibson, L., Le Roux, J., Rooseboom, A., and Basson, G. R. (2010). Sediment yield prediction for South Africa: 2010 edition. University of Stellenbosch & ARC/WRC Project K, 5.
- Msadala, V. C. and Basson, G. R. (2017). Revised regional sediment yield prediction methodology for ungauged catchments in South Africa. *Journal of the South African Institution of Civil Engineering*, 59(2), 28-36.
- Mukundan, R., Pradhanang, S. M., Schneiderman, E. M., Pierson, D. C., Anandhi, A., Zion, M. S., Matonse, A. H., Lounsbury, D. G., and Steenhuis, T. S. (2013). Suspended sediment

- source areas and future climate impact on soil erosion and sediment yield in a New York City water supply watershed, USA. *Geomorphology*, 183, 110-119.
- Mullan, D. (2013). Soil erosion under the impacts of future climate change: Assessing the statistical significance of future changes and the potential on-site and off-site problems. *Catena*, 109, 234-246.
- Müller-Nedebeck, D., Chivenge, P., and Chaplot, V. (2016). Selective organic carbon losses from soils by sheet erosion and main controls. *Earth Surface Processes and Landforms*, 41(10), 1399-1408.
- Nath, A. J. and Rattan, L. A. L. (2017). Effects of tillage practices and land use management on soil aggregates and soil organic carbon in the North Appalachian region, USA. *Pedosphere*, 27(1), 172-176.
- Nabben, T. and Nduli, N. (2000). International Landcare partnership between Australia and South Africa. In Proc. 1st International Landcare Conference.
- Nel, W., Hauptfleisch, A., Sumner, P. D., Booijhawon, R., Rughooputh, S. D., and Dhurmea, K. R. (2016). Intra-event characteristics of extreme erosive rainfall in Mauritius. *Physical Geography*, 37(3-4), 264-275.
- Nel, W. and Sumner, P. (2007). Intensity, energy, and erosivity attributes of rainstorms in the KwaZulu-Natal Drakensberg, South Africa. *South African Journal of Science*, 103, 398-402.
- Nel, W., Reynhardt, D., and Sumner, P. (2010). Effect of altitude on erosive characteristics of concurrent rainfall events in the KwaZulu-Natal Drakensberg. *Water SA*, 36(4).
- Neteler, M. and Mitasova, H. (2013). *Open source GIS: a GRASS GIS approach* (Vol. 689). Springer Science & Business Media.
- Niu, Z. H. , Wang, Z. L., and Huang, X. H. (2004). Advances of soil erosion research in Loess Plateau region of China. *Soil and Water Conservation Research*, 11(4), 169-173
- Oghenekome, M. E. (2012). *Sedimentary environments and provenance of the Balfour Formation (Beaufort Group) in the area between Bedford and Adelaide, Eastern Cape Province, South Africa*. Doctoral thesis, University of Fort Hare.
- Oldeman, L. R. (1997). Soil Degradation: A threat to food security?. In *International conference on time ecology: " Time for Soil Culture-Temporal Perspectives on Sustainable Use of Soil"*, April 6-9, 1997.

- Oroza, C. A., Bales, R. C., Stacy, E. M., Zheng, Z., and Glaser, S. D. (2018). Long-term variability of soil moisture in the southern Sierra: Measurement and prediction. *Vadose Zone Journal*, 17(1), 1-9.
- Osman, K. T. (2018). Degraded soil. In “Osman, K. T. (2018). Management of soil problems. Springer: Cham.
- Ouri, A. E., Golshan, M., Janizadeh, S., Cerdà, A., and Melesse, A. M. (2020). Soil erosion susceptibility mapping in Kozetopraghi Catchment, Iran: A mixed approach using rainfall simulator and data mining techniques. *Land*, 9(10), 1-18.
- Owolabi, S. T., Madi, K., and Kalumba, A. M. (2021). Comparative evaluation of spatio-temporal attributes of precipitation and streamflow in Buffalo and Tyume Catchments, Eastern Cape, South Africa. *Environment, Development and Sustainability*, 2, 4236–4251
- Owolabi, S. T., Madi, K., Kalumba, A. M., and Orimoloye, I. R. (2020). A groundwater potential zone mapping approach for semi-arid environments using remote sensing (RS), geographic information system (GIS), and analytical hierarchical process (AHP) techniques: a case study of Buffalo catchment, Eastern Cape, South Africa. *Arabian Journal of Geosciences*, 13(22), 1-17.
- Ozsahin, E., Duru, U., and Eroglu, I. (2018). Land use and land cover changes (LULCC), a key to understand soil erosion intensities in the Maritsa Basin. *Water*, 10(3), 335.
- Panagos, P., Borrelli, P., Meusburger, K., Alewell, C., Lugato, E., and Montanarella, L. (2015). Estimating the soil erosion cover-management factor at the European scale. *Land Use Policy*, 48, 38-50.
- Pandey, A., Himanshu, S. K., Mishra, S. K., and Singh, V. P. (2016). Physically based soil erosion and sediment yield models revisited. *Catena*, 147, 595-620.
- Parwada, C. and Van Tol, J. (2016). The nature of soil erosion and possible conservation strategies in Ntabelanga area, Eastern Cape Province, South Africa. *Acta Agriculturae Scandinavica, Section B—Soil & Plant Science*, 66(6), 544-552.
- Pei, T., Qin, C. Z., Zhu, A. X., Yang, L., Luo, M., Li, B., and Zhou, C. (2010). Mapping soil organic matter using the topographic wetness index: A comparative study based on different flow-direction algorithms and kriging methods. *Ecological Indicators*, 10(3), 610-619.

- Phinzi, K. and Ngetar, N. S. (2019). Land use/land cover dynamics and soil erosion in the Umzintlava catchment (T32E), Eastern Cape, South Africa. *Transactions of the Royal Society of South Africa*, 74(3), 223-237.
- Piguet, E., Pécoud, A., de Guchteneire, P., and Guchteneire, P. F. (Eds.). (2011). *Migration and climate change*. Cambridge University Press: London.
- Pimentel, D. (2010). Corn and cellulosic ethanol problems and soil erosion. *Soil quality and biofuel production*, 119-136. In *Soil quality and biofuel production*, R Lal and B. A. Stewart (Eds.). CRC Press, Boca Raton, 119– 135.
- Pimentel, D. and Burgess, M. (2013). Soil erosion threatens food production. *Agriculture*, 3(3), 443-463.
- Poesen, J., Nachtergaele, J., Verstraeten, G., and Valentin, C. (2003). Gully erosion and environmental change: importance and research needs. *Catena*, 50(2-4), 91-133.
- Pohlert T. (2016). Non-parametric trend tests and change-point detection. CC BY-ND. 2016 May 14, 4.
- Poesen, J. and de Vente, J. (2005). Predicting soil erosion and sediment yield at the basin scale: scale issues and semi-quantitative models. *Earth-Science Reviews*, 71, 95-125.
- Pomposi, C., Funk, C., Shukla, S., Harrison, L., and Magadzire, T. (2018). Distinguishing southern Africa precipitation response by strength of El Niño events and implications for decision-making. *Environmental Research Letters*, 13(7), 7-15.
- Pretorius, C. (2017). *Wetland diversity and ecosystem services in the Tlokwe Municipal Area*. Doctoral dissertation, North-West University (South Africa), Potchefstroom Campus.
- Radula, M. W., Szymura, T. H., and Szymura, M. (2018). Topographic wetness index explains soil moisture better than bioindication with Ellenberg's indicator values. *Ecological Indicators*, 85, 172-179.
- Rahman, M. R., Shi, Z. H., and Chongfa, C. (2009). Soil erosion hazard evaluation—an integrated use of remote sensing, GIS, and statistical approaches with biophysical parameters towards management strategies. *Ecological Modelling*, 220(13-14), 1724-1734.
- Rai, P. K., Mishra, V. N., and Mohan, K. (2017). A study of morphometric evaluation of the Son basin, India using the geospatial approach. *Remote Sensing Applications: Society and Environment*, 7, 9-20.

- Reitsma, K. D., Dunn, B. H., Mishra, U., Clay, S. A., DeSutter, T., and Clay, D. E. (2015). Land-use change impact on soil sustainability in a climate and vegetation transition zone. *Agronomy Journal*, 107(6), 2363-2372.
- Renard, K. G., Foster, G. R., Weesies, G. A., and Porter, J. P. (1991). RUSLE: Revised universal soil loss equation. *Journal of Soil and Water Conservation*, 46(1), 30-33.
- Riley, S. J., DeGloria, S. D. and Elliot, R. (1999). Index that quantifies topographic heterogeneity. *Intermountain Journal of Sciences*, 5(1-4), 23-27.
- Robb, L. J., Brandl, G., Anhaeusser, C. R., Poujol, M., Johnson, M. R., and Thomas, R. J. (2006). Archaean granitoid intrusions. *The Geology of South Africa*, 57-94.
- Różycka, M., Migoń, P., and Michniewicz, A. (2017). Topographic wetness index and terrain ruggedness index in geomorphic characterization of landslide terrains, on examples from the Sudetes, SW Poland. *Zeitschrift für geomorphologie, Supplementary Issue*, 61(2), 61-80.
- Russell, J. M., and Ward, D. (2016). Historical land-use and vegetation change in Northern Kwazulu-Natal, South Africa. *Land Degradation & Development*, 27(7), 1691-1699.
- Sachs, E. and Sarah, P. (2017). Effect of raindrop temperatures on soil runoff and erosion in dry and wet soils. A laboratory experiment. *Land Degradation & Development*, 28(5), 1549-1556.
- Sadhasivam, N., Bhardwaj, A., Pourghasemi, H. R., and Kamaraj, N. P. (2020). Morphometric attributes-based soil erosion susceptibility mapping in Dnyanganga watershed of India using individual and ensemble models. *Environmental Earth Sciences*, 79(14), 1-28.
- Salami, A. T. and Adepoju, K. A. (2012). Geo-Information System for land degradation evaluation in Nigeria. In *Technologies and innovations for development* (233-248). Springer, Paris.
- Santos, J. C. N. D., Andrade, E. M. D., Medeiros, P. H. A., Guerreiro, M. J. S., and Palácio, H. A. D. Q. (2017). Land use impact on soil erosion at different scales in the Brazilian semi-arid. *Revista Ciência Agronômica*, 48(2), 251-260.
- Sappington, J. M., Longshore, K. M., and Thompson, D. B. (2007). Quantifying landscape ruggedness for animal habitat analysis: a case study using bighorn sheep in the Mojave Desert. *The Journal of Wildlife Management*, 71(5), 1419-1426.

- Sato, C. F., Strong, C. L., Holliday, P., Florance, D., Pierson, J., and Lindenmayer, D. B. (2019). Environmental and grazing management drivers of soil condition. *Agriculture, Ecosystem, and Environment*, 276, 1–7.
- Schellenberg, G., Donnelly, C.R., Holder, C., and Ahsan, R. (2017). Dealing with sediment: effects on dams and hydropower generation. *Hydro Review Worldwide*.
- Schmidt, J. and Hewitt, A. (2004). Fuzzy land element classification from DTMs based on geometry and terrain position. *Geoderma*, 121(3-4), 243-256.
- Sen, P. K. (1968). Estimates of the regression coefficient based on Kendall's tau. *Journal Of The American Statistical Association*, 63(324), 1379-1389.
- Sharma, A., Tiwari, K. N., and Bhadoria, P. B. S. (2011). Effect of land use land cover change on soil erosion potential in an agricultural watershed. *Environmental Monitoring and Assessment*, 173(1-4), 789-801.
- Shengqiang, T. and Dongli, S. (2018). Synergistic effects of rock fragment cover and polyacrylamide application on erosion of saline-sodic soils. *Catena*, 171, 154-165.
- Shen, H., Zhenga, F., Wen, L., Han, Y., and Hu, W. (2016). Impacts of rainfall intensity and slope gradient on rill erosion processes at loessial hillslope. *Soil and Tillage Research*, 155, 429-436.
- Shi, Z. H., Fang, N. F., Wu, F. Z., Wang, L., Yue, B. J., and Wu, G. L. (2012). Soil erosion processes and sediment sorting associated with transport mechanisms on steep slopes. *Journal of Hydrology*, 454, 123-130.
- Shit, P. K., Nandi, A. S., and Bhunia, G. S. (2015). Soil erosion risk mapping using RUSLE model on Jhargram sub-division at West Bengal in India. *Modelling Earth Systems and Environment*, 1(3), 28.
- Singh, S. K., Srivastava, P. K., Gupta, M., Thakur, J. K., and Mukherjee, S. (2014). Appraisal of land use/land cover of mangrove forest ecosystem using support vector machine. *Environmental Earth Sciences*, 71(5), 2245-2255.
- Smith, M. W. (2014). Roughness in the earth sciences. *Earth-Science Reviews*, 136, 202-225.
- Smith, P., Calvin, K., Nkem, J., Campbell, D., Cherubini, F., Grassi, G., Korotkov, V., Le Hoang, A., Lwasa, S., McElwee, P., and Nkonya, E. (2020). Which practices co-deliver food security, climate change mitigation and adaptation, and combat land degradation and desertification? *Global Change Biology*, 26(3), 1532-1575.

- Sonneveld, M. P. W., Everson, T. M., and Veldkamp A. (2005). Multi-scale analysis of soil erosion dynamics in Kwazulu-Natal, South Africa. *Land degradation & Development*, 16, 287-301.
- Soto, J. and Navas, A. (2008). A simple model of Cs-137 profile to estimate soil redistribution in cultivated stony soils. *Radiation Measurements*, 43(7), 1285-1293.
- Soufi, M., Bayat, R., and Charkhabi, A. H. (2020). Gully erosion in IR Iran: Characteristics, processes, causes, and land-use. In “Gully Erosion Studies from India and Surrounding Regions. Springer: Cham, 357-368.
- Stocking, M. A. and Elwell, H. A. (1976). Rainfall erosivity over Rhodesia. *Institute of the British Geographers*. 1, 231-245.
- Streiner, D. L. and Cairney, J. (2007). What's under the ROC? An introduction to receiver operating characteristics curves. *The Canadian Journal of Psychiatry*, 52(2), 121-128.
- Stroosnijder, L. (2005). Measurement of erosion: is it possible? *Catena*, 64(2-3), 162-173.
- Sun, W., Shao, Q., Liu, J., and Zhai, J. (2014). Assessing the effects of land use and topography on soil erosion on the Loess Plateau in China. *Catena*, 121, 151-163.
- Sun, L., Zhang, G. H., Liu, F., and Luan, L. L. (2016). Effects of incorporated plant litter on soil resistance to flowing water erosion in the Loess Plateau of China. *Biosystems Engineering*, 147, 238-247. *Together in Excellence*
- Sutherland, R. A. and Ziegler, A. D. (2007). Effectiveness of coir-based rolled erosion control systems in reducing sediment transport from hillslopes. *Applied Geography*, 27(3-4), 150-164.
- Takahashi, T. and Das, D. K. (2014). Debris flow: mechanics, prediction and countermeasures. CRC press.
- Thornes, J. B. (2007). Modelling soil erosion by grazing: Recent developments and new approaches. *Geographical Research*, 45(1), 13-26.
- Troeh, F. R., Hobbs, J. A., and Donahue, R. L. (1991). *Soil and Water Conservation* Prentice Hall. Inc., Englewood Cliffs: NJ.
- Ullrich, A. and Volk, M. (2009). Application of the Soil and Water Assessment Tool (SWAT) to predict the impact of alternative management practices on water quality and quantity. *Agricultural Water Management*, 96(8), 1207-1217.

- UNCCD (2007). United Nations Convention to Combat Desertification. Official website of the United Nations Convention to Combat Desertification, <http://www.unccd.int/>.
- Van Oost, K., Cerdan, O., and Quine, T. A. (2009). Accelerated sediment fluxes by water and tillage erosion on European agricultural land. *Earth Surface Processes and Landforms*, 34(12), 1625-1634.
- Van Zyl, A. J. (2007). A knowledge gap analysis on multi-scale predictive ability for agriculturally derived sediments under South African conditions. *Water Science and Technology*, 55(3), 107-114.
- Vandanapu, R., Omer, J. R., and Attom, M. F. (2019). Three-dimensional finite element analyses of ground settlement and structural damage caused by irrigation of desert landscapes overlying collapsible soil strata. *International Journal of Geotechnical Engineering*, 1-13.
- Vanwalleghem, T., Gómez, J. A., Amate, J. I., de Molina, M. G., Vanderlinden, K., Guzmán, G., Laguna, A., and Giráldez, J. V. (2017). Impact of historical land use and soil management change on soil erosion and agricultural sustainability during the Anthropocene. *Anthropocene*, 17, 13-29.
- Verbakel, J. Y., Steyerberg, E. W., Uno, H., De Cock, B., Wynants, L., Collins, G. S., and Van Calster, B. (2020). ROC curves for clinical prediction models part 1. ROC plots showed no added value above the AUC when evaluating the performance of clinical prediction models. *Journal of Clinical Epidemiology*, 126, 207-216.
- Vos, H., Kuhn, N., Fister, W., and Greenwood, P. (2019). Experimental study on dust emission from soil crusts on croplands in the Free State, South Africa. *Geophysical Research Abstracts*, 21, 1.
- Wang, C., Deser, C., Yu, J. Y., DiNezio, P., and Clement, A. (2017). El Niño and Southern Oscillation (ENSO): a review. In *Coral reefs of the eastern tropical Pacific* (85-106). Springer, Dordrecht.
- Wang, Y., Ran, L., Fang, N., and Shi, Z. (2018). Aggregate stability and associated organic carbon and nitrogen as affected by soil erosion and vegetation rehabilitation on the Loess Plateau. *Catena*, 167, 257-265.
- Watson, A. and Evans, R. (1991). A comparison of estimates of soil erosion made in the field and from photographs. *Soil and Tillage Research*, 19(1), 17-27.

- Walling, D. E. and Quine, T. A. (1992). The use of caesium-137 measurements in soil erosion surveys. In *Erosion and sediment transport monitoring programmes in river basins, Proceedings of the Oslo Symposium, August 1992*. IAHS Publ. no. 210, 143-152.
- Wang, L. Y., Xiao, Y., Rao, E. M., Jiang, L., Xiao, Y., and Ouyang, Z. Y. (2018). An assessment of the impact of urbanization on soil erosion in Inner Mongolia. *International Journal of Environmental Research and Public Health*, 15(3), 550.
- Wang, X., Zhang, T., Cao, L., and Liang, Y. (2016). Erosion and global change. *Europe*, 93, 39.
- Wang, X., Zhao, X., Zhang, Z., Yi, L., Zuo, L., Wen, Q., and Liu, B. (2016). Assessment of soil erosion change and its relationships with land use/cover change in China from the end of the 1980s to 2010. *Catena*, 137, 256-268.
- Wiggs, G. and Holmes, P. (2011). Dynamic controls on wind erosion and dust generation on west-central Free State agricultural land, South Africa. *Earth Surface Processes and Landforms*, 36, 827– 838.
- Wilson, A., Flint, S., Payenberg, T., Tohver, E., and Lanci, L. (2014). Architectural styles and sedimentology of the fluvial lower Beaufort Group, Karoo Basin, South Africa. *Journal of Sedimentary Research*, 84(4), pp.326-348.
- Wilson, G. V., Wells, R., Kuhnle, R., Fox, G., and Nieber, J. (2018). Sediment detachment and transport processes associated with internal erosion of soil pipes. *Earth Surface Processes and Landforms*, 43(1), 45-63.
- Wischmeier, W. H. and Smith, D. D. (1978). *Predicting rainfall erosion losses: a guide to conservation planning* (No. 537). Department of Agriculture, Science, and Education Administration.
- Xia, J., Zong, Q., Deng, S., Xu, Q., and Lu, J. (2014). Seasonal variations in composite riverbank stability in the Lower Jingjiang Reach, China. *Journal of Hydrology*, 519, 3664-3673.
- Yang, S. and Jiang, X. (2014). Prediction of eastern and central Pacific ENSO events and their impacts on East Asian climate by the NCEP Climate Forecast System. *Journal of Climate*, 27(12), 4451-4472.
- Yang, S., Li, Z., Yu, J. Y., Hu, X., Dong, W., and He, S. (2018). El Niño–Southern Oscillation and its impact in the changing climate. *National Science Review*, 5(6), 840-857.

- Yang, J. and Chu, X. (2015). A new modeling approach for simulating microtopography-dominated, discontinuous overland flow on infiltrating surfaces. *Advances in Water Resources*, 78, 80-93.
- Yuan, Y. and Yang, S. (2012). Impacts of different types of El Niño on the East Asian climate: Focus on ENSO cycles. *Journal of Climate*, 25(21), 7702-7722.
- Yue, S., Pilon, P., and Cavadias, G. (2002). Power of the Mann–Kendall and Spearman's rho tests for detecting monotonic trends in hydrological series. *Journal of Hydrology*, 259(1-4), 254-271.
- Zare, M., Panagopoulos, T., and Loures, L. (2017). Simulating the impacts of future land-use change on soil erosion in the Kasilian watershed, Iran. *Land Use Policy*, 67, 558-572.
- Zelege, G. and Hurni, H. (2001). Implications of land use and land cover dynamics for mountain resource degradation in the Northwestern Ethiopian highlands. *Mountain Research and Development*, 21(2), 184-191.
- Zhai, H., Cui, B., Hu, B., and Zhang, K. (2010). Prediction of river ecological integrity after cascade hydropower dam construction on the mainstream of rivers in Longitudinal Range-Gorge Region (LRGR), China. *Ecological Engineering*, 36(4), 361-372.
- Zuazo V. H. D. and Pleguezuelo C.R.R. (2009) Soil-erosion and runoff prevention by plant covers: A review. In: Lichtfouse E., Navarrete M., Debaeke P., Véronique S., Alberola C. (eds) *Sustainable Agriculture*. Springer, Dordrecht.